AD-A138 049 PATTERN NULLING BY REFLECTOR SHAPING(U) AIR FORCE INST 1/2
OF TECH WRIGHT-PATTERSON AFB OH SCHOOL OF ENGINEERING
D A HAVENS DEC 83 AFIT/GE/EE/83D-26

UNCLASSIFIED F/G 20/14 NL

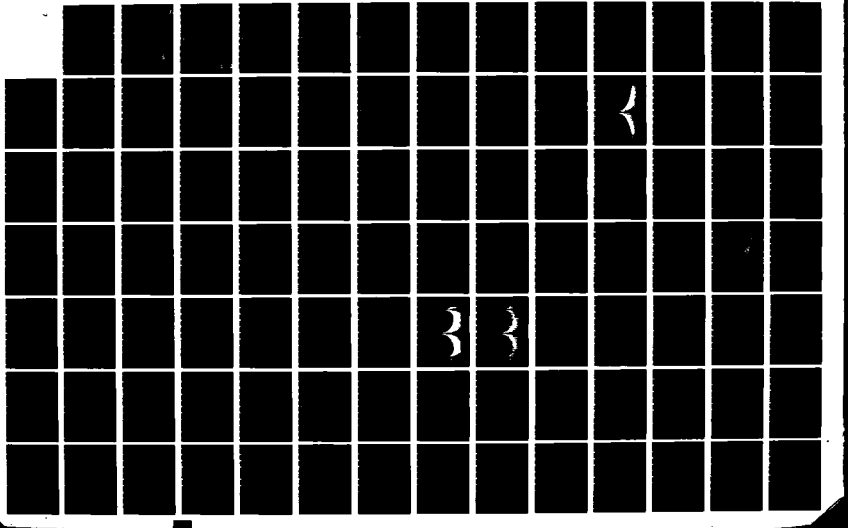

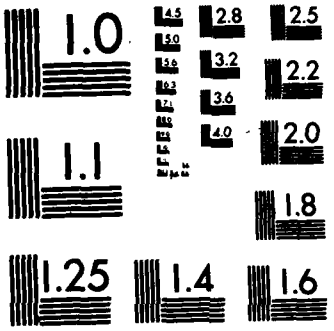

PATTERN NULLING BY REFLECTOR SHAPING

THESIS

Douglas A. Havens
Second Lieutenant, USAF

AFIT/GE/EE/83D-26

DEPARTMENT OF THE AIR FORCE
AIR UNIVERSITY
AIR FORCE INSTITUTE OF TECHNOLOGY

Wright-Patterson Air Force Base, Ohio

PATTERN NULLING BY REFLECTOR SHAPING

THESIS

Douglas A. Havens
Second Lieutenant, USAF

AFIT/GE/EE/83D-26

AFIT/GE/EE/83D-26

PATTERN NULLING BY REFLECTOR SHAPING

THESIS

Presented to the Faculty of the School of Engineering

of the Air Force Institute of Technology

Air University

In Partial Fulfillment of the

Requirements for the Degree of

Master of Science in Electrical Engineering

Douglas A. Havens, B.S.

Second Lieutenant, USAF

December, 1983

Table of Contents

Abstract

The applicability of adaptive array concepts to continuous aperture antennas was studied and appropriate aperture field distributions for pattern nulling were found from them. The adaptive array weights were found to be useful as discrete points in a continuous distribution. This distribution could then be used in an aperture integration scheme to produce a nulled pattern.

Also studied was the use of geometrical optics to calculate the aperture field distribution of an arbitrarily shaped reflector. Under some restrictions, geometrical optics can provide a useful approximation. Constructing the aperture field of a reflector defined by a discrete grid of points using a numerical ray tracing scheme was also investigated. Certain numerical problems were identified.

Finally, an attempt was made to implement the nulled pattern by a well known beamshaping method based on geometrical optics principles. This technique was found to be inadequate. More promising techniques for implementing the aperture distributions were suggested but not pursued in this work.

I Introduction

The Problem

Many systems which use antennas must contend with the possibility of jamming by hostile transmitters. System designers often attempt to deal with noise by devising signal processing schemes to improve the signal-to-noise ratio of the system. This may be the only way for most types of noise, such as thermal noise in the receiver. However, one often has a little more information about hostile jammers. Using this information presents the system designer with yet another tool for raising the signal-to-noise ratio of his creation.

Thoughts like these have led to the development of adaptive antenna systems. Such an antenna modifies its radiation pattern according to some predetermined criterion through feedback control (Reference 1). What does this accomplish? Basically, an adaptive antenna improves the signal-to-noise ratio of the system it serves by rejecting interference. Some adaptive antennas use knowledge of the desired signal to track that signal and reject all else. If instead, one has knowledge of the spatial distribution of noise sources (Ref 1), he might configure the adaptive antenna to place pattern nulls on those particular directions. Either way, one seeks to maximize the signal-to-noise ratio by rejecting the interference with the antenna itself.

To date, adaptive antenna designers have confined their attention primarily to array type antenna (Reference 1). Controlling the radiation pattern of an array antenna is easily accomplished by varying the amplitude and phase of the input signals which drive each array element

(Reference 1). Since such control is strictly electronic, the system does not require mechanical assistance; hence, the interest in array antennas. To control the radiation pattern of a reflector antenna with a continuous aperture, one would have to devise some scheme to distort the reflector from its equilibrium shape in a well controlled manner.

Such a scheme requires as a foundation, some knowledge of which reflector geometries are capable of generating radiation pattern nulls in predetermined locations. One must know if such shapes exist and if these shapes are physically realized. Clearly, a reflector with a loop in it simply will not do. This work attempts to address the problem of finding shapes that place nulls in the radiation pattern at specified locations.

Only the simplest techniques were used in this preliminary work. Principles of geometrical optics were applied to reflector surfaces to generate approximate aperture field distributions. Geometrical optics assumes that reflector dimensions are much greater than the wavelength (Ref 12:454). Furthermore, the radius of curvature of the reflector surface at any point must also remain much greater than the wavelength (Ref 9: 123). This all means that consideration here is confined to large reflectors that are not too "bumpy". Once the aperture distribution was determined, simplified aperture integration generated the radiation pattern. These approximations mean that the results are really only qualitative; but they do give some idea of the location of nulls in the radiation pattern, at least for angles not far from boresight. The analyses were also limited to the two dimensional case, in the interest of simplicity.

In the work that follows, a brief description of Applebaum adaptive array antenna concepts will be presented in order to familiarize the

reader with the adaptive array ideas which are later applied to apertures. In Section II, the aperture integration technique used in this work is described along with proposed aperture field distributions that generate pattern nulls. Section III deals with geometrical optics as applied to large reflectors. The algorithm used to trace the ray path from feed to aperture is presented also. Section IV attempts to implement a nulled pattern using well known beam-shaping techniques also based on geometrical optics. Section V attempts to find reflectors which implement the aperture distributions found in Section II. A summary of the results rounds out this document.

Possible Antenna for Reflector Distortion

At this point, the reader might wonder about the feasibility of a reflector that changes shape after construction is completed. Jeffrey H. Lang, et al have proposed an antenna which might offer a possible solution to this problem. They have suggested a reflector constructed from a thin membrane whose shape is controlled electronically (Ref 5,6,7).

Figure 1.1 illustrates the Lang concept (Ref 5: 655). An electron beam controls the shape of the reflector (Ref 5: 655). Referring to Figure 1.1, the command surface is pulled into a roughly parabolic shape by guy wires and the reflector is pulled toward the command surface by application of a bias potential resulting in an approximately parabolic reflector (Ref 5: 655). The computer uses optical measurements to determine if the reflector shape meets tolerances. If not, it instructs the electron beam to scan the command surface in such a way that the modified charge distribution and resulting electrostatic force refine the reflector shape (Ref 6: 992). This results in a parabola which meets some predetermined tolerance.

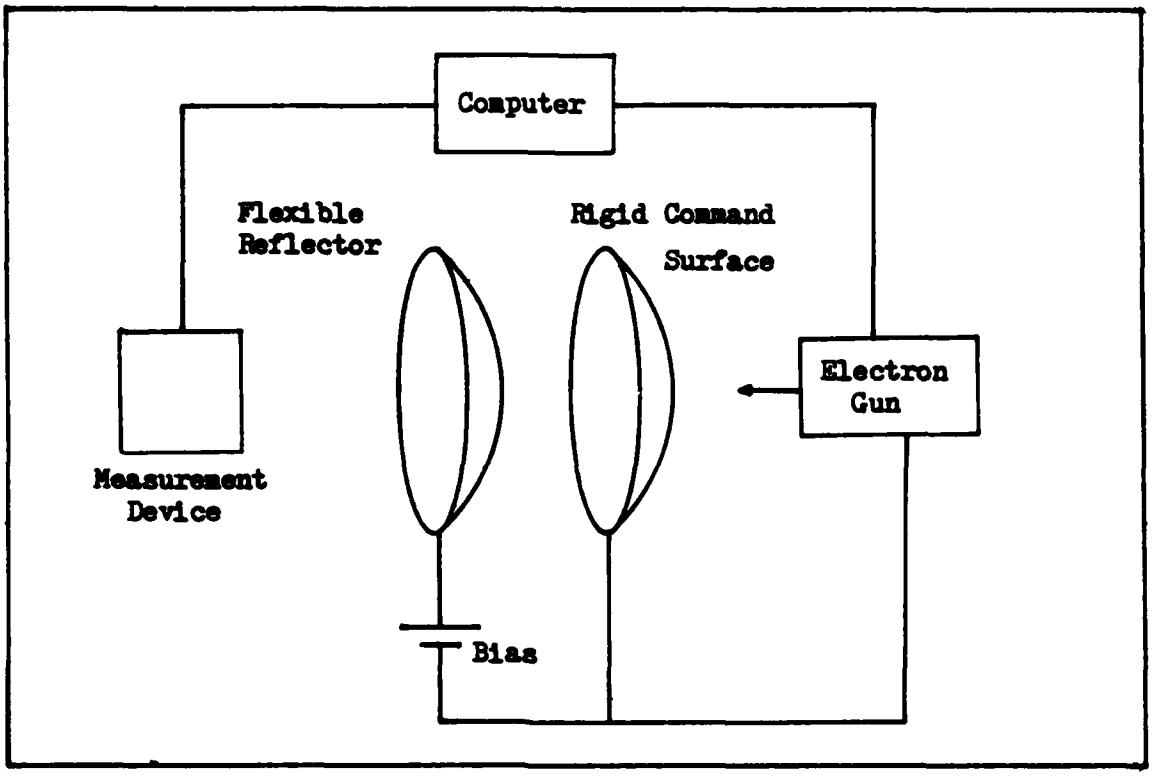

Fig 1-1. Lang Concept

If such an antenna were perfected, it might prove useful in the reflector distortion problem. Instead of warping the membrane into a parabolic shape, perhaps the charge distribution could be altered to form null generating shapes. Such a scheme would be superior to purely mechanical means especially for large reflectors. J. H. Lang, et al envision reflectors up one kilometer in diameter (Ref 7). A mechanical scheme for such an antenna must be clever indeed. However, an investigation of the electrostatic reflector's applicability to the nulling problem is beyond the scope of this work and will not be considered further.

Applebaum Adaptive Array

Applebaum devised an adaptive array scheme which maximized the single-to-noise ratio (Ref 1). It accomplishes this by placing nulls

in the radiation pattern on the angular positions of any jamming transmitter. Applebaum assumed that the angles of jammers was known when he developed his control law for array weights.

Figure 1.2 (Ref 1: 585) provides a starting point for the description of Applebaum's array. The array in question has K elements. The desired input signal at element i is x_i and the undesirable noise input at element i is n_i. Actually, these are the complex envelopes of the desired signal and noise. The output desired signal v_s is the sum of the x_i weighted by the appropriate w_i. The output noise signal v_n is the sum of the n_i similarly weighted by the w_i.

One knows from probability and communication theory that $\rho_{ij} = E[n_i^* n_j]$ gives the covariance of noise signals n_i and n_j. In developing his array concept, Applebaum assumed that the ρ_{ij} are known. They depend only on receiver noise and the angular distribution of the noise sources (Ref 1: 585). He then defined the noise covariance matrix as $M = [\rho_{ij}]$ where i and j both vary from one to K (Ref 1: 586).

Applebaum further assumed that the desired signals were narrowband. In general, the interelement phase shift in an array is frequency dependent (Reference 1). However, if the desired signal has narrowbandwith, the interelement phase shift is essentially constant and depends only on interelement spacing and angle of incidence. This enabled Applebaum to write the desired signals x_i as $x_i = \alpha s_i$ where α is the complex envelope of the desired signal incident on the array and the s_i is a phase factor depending on angle of incidence, interelement spacing, and element pattern. Assuming isotropic elements, the total phase shift at the i^{th} element referenced to the first element is $\beta L(i-1)$ where $\beta = 2\pi/\lambda$ and $L = d \sin \theta$ as shown in Figure 1.3. Therefore, the s_i are given by

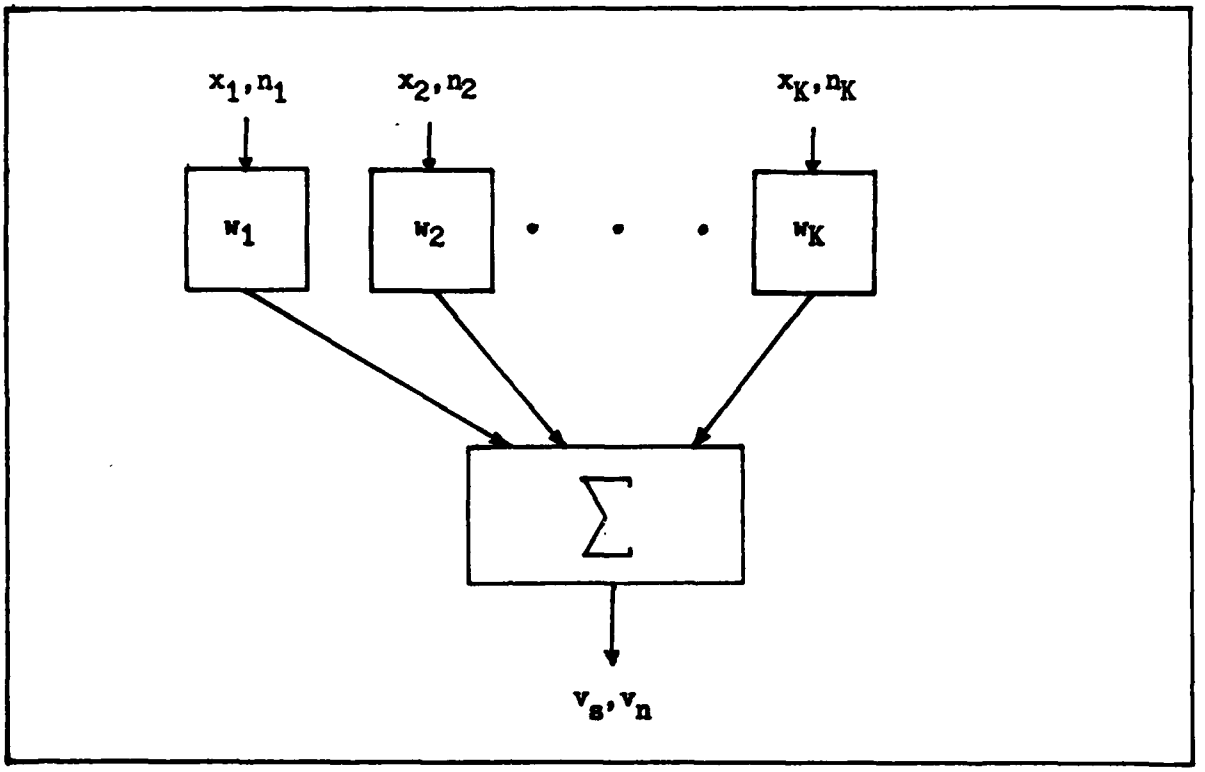

Fig 1-2. Linear Array

(Ref 1: 586):

$$s_i = \exp(j\beta d i \sin\theta) \qquad (1\text{-}1)$$

With these definitions in hand, Applebaum determined that the optimum weights which maximized signal-to-noise ratio are given by (Ref 1: 586):

$$MW = \mu S^* \qquad (1\text{-}2)$$

where M is the noise covariance matrix defined previously, W is the vector of array weights, S* is the vector of S_i* with S_i give by Eq (1-1). The star denotes the complex conjugate. The μ is an arbitrary constant. The reader should refer to Appendix A for verification of this result.

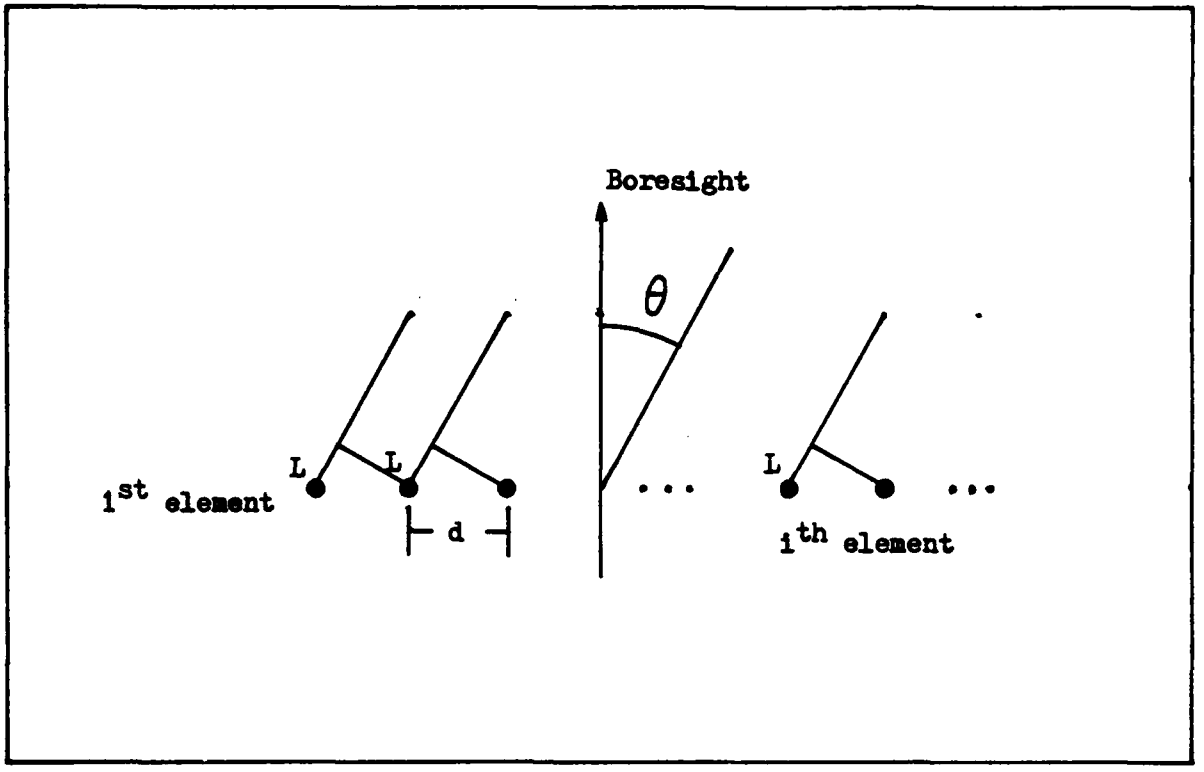

Fig 1-3. s_i Determination

Applebaum then generalized this result. If no noise is incident, then the noise covariance matrix reflects only receiver noise which is equal in all channels and uncorrelated between channels. This defines the quiescent noise covariance matrix as $M_q = \rho_q I_k$ where ρ_q is quiescent noise power and I_k is a K x K identity matrix (Ref 1: 589). Since $Mq^{-1} = \frac{1}{\rho_q} I_k$, the quiescent weights are $W_q = \mu Mq^{-1} S = \frac{\mu}{\rho_q} S^*$. Thus W_q and S^* are scalar multiples and $S = \frac{\rho_q}{\mu} W_q^*$ is a measure of the quiescent weights and hence quiescent pattern (Reference 1). In fact, S corresponds to uniform quiescent weights. If one wants different quiescent weights, he merely defines $T = \frac{\rho_q}{\mu} W_q^*$ with the new weights and using $MW = MT^*$ comes up with the modified control law (Ref 1: 588):

$$MW = M_q W_q \qquad (1\text{-}3)$$

This accepts some degredation of optimal signal-to-noise ratio in order to achieve control over the quiescent pattern (Refel: 587).

According to Applebaum, Equation (1-3) gives weights that place a pattern null on a jammer. To illustrate this, and see what the array weights are, consider a K element array whose mainbeam is angle θ_s from mechanical boresight. The quiescent noise covariance matrix is $M_q = \rho_q I_k$ as stated before. The quiescent weights are given by:

$$Wq = \begin{bmatrix} a_1 \\ a_2 \; e^{-j\beta d \sin \theta_s} \\ a_3 \; e^{-j2\beta d \sin \theta_s} \\ \vdots \\ a_k \; e^{-j(K-1)\beta d \sin \theta_s} \end{bmatrix} \qquad (1\text{-}4)$$

The a_i are the real number amplitude weights and if the a_i are all equal, the quiescent pattern is just the familiar sin(Kx)/sin(x) (Ref 1: 589). From fundamental antenna theory, the quiescent pattern is (Ref 1: 589):

$$F_q(\theta) = \sum_{i=1}^{K} a_i \; e^{j(i-1)\beta d(\sin \theta - \sin \theta_s)} \qquad (1\text{-}5)$$

where θ is the angle of observation referenced to the mechanical boresight. Vector notation greatly simplifies the task. Therefore, defining the vector B for the sake of convenience as (Ref 1: 589):

$$B = \begin{bmatrix} 1 \\ e^{j\beta d \sin \theta} \\ e^{j2\beta d \sin \theta} \\ \vdots \\ e^{j(K-1)\beta d \sin \theta} \end{bmatrix} \qquad (1\text{-}6)$$

permits the quiescent radiation pattern to be rewritten as:

$$F_q(\Theta) = B^T W_q \tag{1-7}$$

With this preliminary out of the way, one must now seek an expression for W. From Eq (1-3) and $Mq = \rho_q I_k$, the W is (Ref 1: 590):

$$W = \rho_q M^{-1} W_q \tag{1-8}$$

One must now find the noise covariance matrix and hence M^{-1}.

Define the jamming signal in the first array element as J(t). Then the jamming signal in the i^{th} element is $J_i(t) = J(t) \exp [j(i-1)\beta d \sin \theta j]$. The covariance between $J_i(t)$ and $J_k(t)$ is:

$$\begin{aligned} E [J_i^*(t)J_k(t)] &= E[J^*(t)e^{-j(i-1)\beta d \sin \theta j} J(t) e^{j(K-1)\beta d \sin \theta j}] \\ &= E[J^*(t)J(t)]\, e^{-j(i-k)\beta d \sin \theta j} \\ &= E[|J(t)|^2]\, e^{-j(i-k)\beta d \sin \theta j} \\ &= \rho_j\, e^{-j(i-k)\beta d \sin \theta j} \end{aligned} \tag{1-9}$$

Consequently, the covariance matrix of the jamming signal is $M_j = \rho_j(\exp[-j(i-k)\beta d \sin \Theta j])$ for i and k from one to K. M_j is Hermitian with all elements on the same diagonal equal. Its simple structure permits a further modification (Ref 1: 590). Defining the matrix (Ref 1: 590):

$$H = \begin{bmatrix} 1 & & & \\ & e^{j\beta d \sin \theta j} & & \\ & & e^{j2\beta d \sin \theta j} & \\ & & & \ddots \\ & & & e^{j(k-1)\beta d \sin \theta j} \end{bmatrix} \tag{1-10}$$

and also defining U as a KxK matrix of ones leads to (Ref 1: 590):

$$M_j = \rho\, H^* U H \tag{1-11}$$

Since the receiver and jammer noise are uncorrelated, the total noise covariance matrix is (Ref 1: 590):

$$M = M_q + M_j = \rho_q I_k + \rho_j H^*UH \tag{1-12}$$

Applebaum gives M^{-1} as (Ref 1: 590):

$$M^{-1} = \frac{1}{\rho_q} \left[I_k - \left(\frac{\rho_j}{\rho_q + \rho_j} \right) H^*UH \right] \tag{1-13}$$

Applying this expression to Eq (1-8) leads to the following equation defining the weights (Ref 1: 590):

$$W = W_q - \left(\frac{\rho_j}{\rho_q + K\rho_j} \right) H^*UHW_q \tag{1-14}$$

Some further simplification is in order (Ref 1: 590):

$$HW_q = \begin{bmatrix} a_1 \\ a_2\, e^{j\beta d\,(\sin \theta j - \sin \theta s)} \\ a_3\, e^{j\beta d\,(\sin \theta j - \sin \theta s)} \\ \vdots \\ a_k\, e^{j(K-1)\,\beta d\,(\sin \theta j - \sin \theta s)} \end{bmatrix} \tag{1-15}$$

$$UHW_q = F_q(\theta j) \begin{bmatrix} | \\ | \\ | \\ \vdots \\ | \end{bmatrix} \tag{1-16}$$

$$H^*UHW_q = F_q(\theta j) \begin{bmatrix} | \\ e^{-j\beta d \sin \theta j} \\ e^{-j2\beta d \sin \theta j} \\ \vdots \\ e^{-j(K-1)\,\beta d \sin \theta j} \end{bmatrix} \tag{1-17}$$

Defining the vector in Eq (1-17) as B_j^* allows one to write Eq (1-17) as (Ref 1: 590):

$$H^*UHW_q = F_q(\theta j)\, B_j^* \tag{1-18}$$

Substituting Eq (1-18) into Eq (1-14) results in (Ref 1: 590):

$$W = W_q - \left(\frac{\rho_j}{\rho_q + K\rho_j}\right) F_q(\theta j) B_j^* \tag{1-19}$$

To get the nulled pattern, one multiplies Eq (1-19) by B^T where B is defined in Eq (1- 6) (Ref 1: 590):

$$F(\theta) = F_q(\theta) - \left(\frac{\rho_j}{\rho_q + K\rho_j}\right) F_q(\theta j) B^T B_j^* \tag{1-20}$$

$$B^T B_j^* = 1 + e^{j\beta d\,(\sin\theta - \sin\theta j)} + \cdots + e^{j(K-1)\beta d\,(\sin\theta - \sin\theta j)}$$

$$= \sum_{K=1}^{K} e^{j(K-1)\beta d\,(\sin\theta - \sin\theta j)}$$

$$= \sum_{K=1}^{K} \left[e^{j\beta d\,(\sin\theta - \sin\theta j)}\right]^{(K-1)} \tag{1-21}$$

Eq (1-21) is a geometrical progression and simplifies to:

$$B^T B_j^* = e^{j(K-1)\,\frac{\beta d}{2}\,(\sin\theta - \sin\theta j)} \frac{\sin\left[K\frac{\beta d}{2}\,(\sin\theta - \sin\theta j)\right]}{\sin\left[\frac{\beta d}{2}\,(\sin\theta - \sin\theta j)\right]} \tag{1-22}$$

Since $\left(\frac{\rho_j}{\rho_q + K\rho_j}\right) F_q(\theta j)$ is just a number, the second term in Eq (1-20) is a sin(Kx)/sin(x) pattern with its main beam at θj (Ref 1: 590). This comprises the nulling mechanism.

Eqs (1-20) and (1-22) provide an expression for a pattern with a null at θj. However, the expression for the weights should be broken down for use in Section II. Using Eq (1-14), the i^{th} weight is:

$$W_i = (W_q)_i - \frac{\rho_j}{\rho_q + K\rho_j} \sum_{K=1}^{K} e^{-j(i-k)\beta d \sin \theta j} (W_q)_k$$

$$= (W_q)_i - \frac{\rho_j}{\rho_q + K\rho_j} e^{-j\beta di \sin \theta j} \sum_{K=1}^{K} [e^{j\beta d \sin \theta j}]^k (W_q)_k \qquad (1\text{-}23)$$

Substituting $(W_q)_i = 1$ into Eq (1-23) for uniform quiescent weighting gives:

$$W_i = 1 - \frac{\rho_j}{\rho_q + K\rho_j} e^{-j\beta di \sin \theta j} \sum_{K=1}^{K} [e^{j\beta d \sin \theta j}]^k \qquad (1\text{-}24)$$

Employing geometrical progression and some algebra gives:

$$W_i = 1 - \frac{\rho_j}{\rho_q + K\rho_j} \frac{\sin\left(K \frac{\beta d}{2} \sin \theta j\right)}{\sin\left(\frac{\beta d}{2} \sin \theta j\right)} e^{j(1+K-2i) \frac{\beta d}{2} \sin \theta j} \qquad (1\text{-}25)$$

Eq (1-25) will figure prominently in Section II while Eqs (1-20) and (1-22) will be important in Section IV.

II Pattern Calculations

Aperture Integration

All the radiation patterns in this work were computed by integrating an aperture electric field distribution over an aperture plane. For simplicity, calculations involved only two dimensional geometrics; therefore, only one dimensional, single integrations were involved.

The expression for radiation pattern follows from the following definition for an electric vector potential:

$$\bar{E} = -\bar{\nabla} \times \bar{F} \tag{2-1}$$

where $\bar{E}$ is electric field and $\bar{F}$ is electric vector potential. The $\bar{F}$ solves a vector wave equation with a magnetic current source term (Ref 4: 56). It is given by (Ref 4: 56):

$$\bar{F} = \bar{M}_s(\bar{r}^1) \frac{e^{-j\beta R}}{4\pi R} ds^1 \tag{2-2}$$

where

$R = |\bar{r}-\bar{r}^1|$

$\bar{r}$ = Observation Point Position Vector.

$\bar{r}^1$ = Source Point Position Vector.

$\bar{M}_s(\bar{r}^1)$ = Magnetic Surface Current.

Σ = Surface on which $\bar{M}_s(\bar{r}^1)$ exists.

The far-field approximation for this is (Ref 12: 379):

$$\bar{F} = \frac{e^{-j\beta r}}{4\pi r} \int_{\Sigma} \bar{M}_s(\bar{r}^1) e^{j\beta \hat{r}\cdot\bar{r}^1} ds^1 \tag{2-3}$$

where $\overline{r}$ is the spherical coordinate radial unit vector and r is the radial distance to the observation point.

In aperture integration problems, the magnetic surface current density on surface Σ is an equivalent current derived from the electric field on the surface (Ref 12:376). The expression is (Ref 12:376):

$$\overline{M}_s = \overline{E} \times \hat{n} \tag{2-4}$$

where $\overline{E}$ is the electric field on surface Σ and $\hat{n}$ is the outward normal unit vector to Σ. If one selects a planar Σ, then $\hat{n}$ remains constant on the surface of integration. Substituting Eq (2-4) into Eq (2-3) yields (Ref 12: 382):

$$\overline{F} = \frac{e^{-j\beta r}}{4\pi r} \left[\int_{\Sigma} \overline{E}\, e^{j\beta \hat{r} \cdot \overline{r}^1}\, ds^1 \right] \times \hat{n} \tag{2-5}$$

The aperture surface Σ is often chosen to lie in the xy-plane. The aperture electric field $\overline{E}_a$ is also assumed to be everywhere tangential to the aperture plane (Ref 12:381). Under these conditions, $\hat{n}$ is simply the z-directed unit vector and ds^1 is just $dx^1 dy^1$ where the primes refer to points in the aperture plane. For convenience, the bracketed term in Eq (2-5) will be called $\overline{P}$ (Ref 12:382).

Since $\overline{E}_a$ has only x and y components, the $\overline{P}$ vector has only x and y components. Identifying these components as Px and Py and substituting into Eq (2-5) results in (Ref 12:382):

$$\overline{F} = \frac{e^{-j\beta r}}{4\pi r} (Py\, \hat{x} - Px\, \hat{y}) \tag{2-6}$$

where $\hat{x}$ and $\hat{y}$ are the x and y directed unit vectors respectively.

Given the magnetic vector potential, defined by $\overline{H} = \overline{\nabla} \times \overline{A}$, the far zone electric field is $\overline{E} = j\omega\mu\overline{A}$ less the $\hat{r}$ component, where ω is radian

frequency and μ is the magnetic permeability (Ref 12: 25). Since $\overline{F}$ is the dual of $\overline{A}$, the far zone $\overline{H}$ field is simply $\overline{H} = j\omega\epsilon\overline{F}$ less its $\hat{r}$ component, where ϵ is the permittivity (Ref 12:379). The far zone fields exhibit plane wave behavior; therefore, $\overline{E} = \sqrt{\frac{\mu}{\epsilon}}\ \overline{H} \times \hat{r} = -j\omega\sqrt{\mu\epsilon}\ \overline{F} \times \hat{r}$. Since $\omega\sqrt{\mu\epsilon} = 2\pi f/c$, where c is the speed of light, we have $\omega\sqrt{\mu\epsilon} = 2\pi/\lambda = \beta$. This gives the far zone electric field as (Ref 12: 383):

$$\overline{E} = j\beta\hat{r} \times F \tag{2-7}$$

Substituting Eq (2-6) into Eq (2-7) yields the expressions for far zone electric field (Ref 12: 383):

$$E\theta = j\beta\frac{e^{-j\beta r}}{4\pi r}\ (Px \cos \phi + Py \sin \phi) \tag{2-8}$$

$$E\phi = j\beta\frac{e^{-j\beta r}}{4\pi r} \cos\theta\ (Py \cos \phi - Px \sin \phi) \tag{2-9}$$

To develop the pattern equation, one must consider the geometry illustrated in Figure 2-1. The geometry is assumed to be completely symmetrical in the x direction. The aperture plane lies on the y axis and extends from y_{amin} to y_{amax}. In this situation, $\phi = \pi/2$. The feed is an electric line source along the x axis in the positive direction. This results in an x directed aperture field given by $\overline{Ea} = \hat{x}\ \delta(x)\ Eax(y)$. Feeding this information into Eq (2-9) gives:

$$E\phi = -j\beta\frac{e^{-j\beta r}}{4\pi r} \cos\theta \int_{y_{amin}}^{y_{amax}} Eax(y^1)\ e^{\,j\beta y^1 \sin\theta}\ dy^1 \tag{2-10}$$

where $\hat{r}\cdot\overline{r}^1$ was executed using $\overline{r}^1 = \hat{y}y^1$.

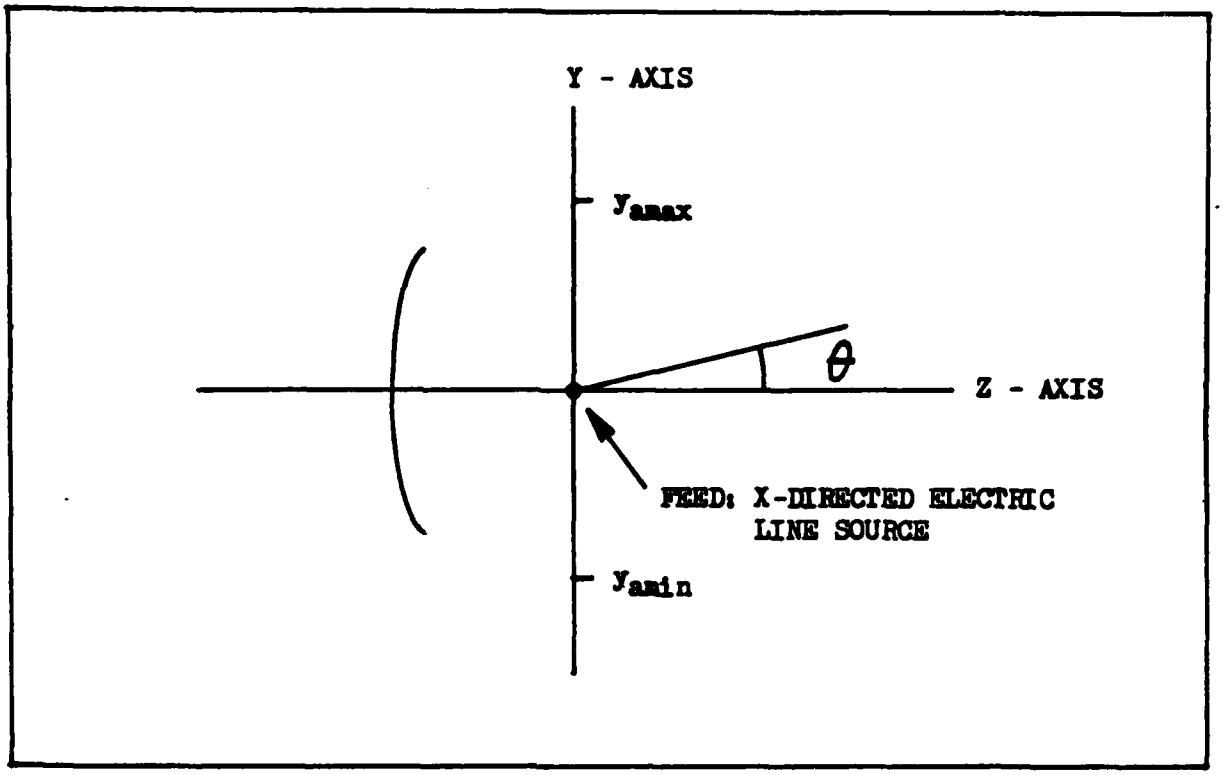

Fig 2-1. Aperture

When pattern calculations are made, the radial distance remains constant and terms involving it are eliminated along with other constant terms by normalization. The resulting for field pattern is given by:

$$G(\theta) = \frac{\left| \cos\theta \int_{y_{amin}}^{y_{amax}} Eax(y^1)\ e^{j\beta y^1 \sin\theta}\ dy^1 \right|}{\max \left| \cos\theta \int_{y_{amin}}^{y_{amax}} Eax(y^1)\ e^{j\beta y^1 \sin\theta}\ dy^1 \right|} \qquad (2\text{-}11)$$

When using aperture integration, one normally confines his attention to angles near boresight where cost will remain close to unity. Consequently, the final expression for pattern used in this work is:

$$G(\theta) = \frac{\left| \int_{y_{amin}}^{y_{amax}} Eax(y^1)\ e^{j\beta y^1 \sin\theta}\ dy^1 \right|}{\max \left| \int_{y_{amin}}^{y_{amax}} Eax(y^1)\ e^{j\beta y^1 \sin\theta}\ dy^1 \right|} \qquad (2\text{-}12)$$

Figure 2-2 shows Eq (2-12) applied to a uniform distribution over a 100 wavelength aperture. Figure 2-3 shows the results from a 10 wavelength aperture. Analytic integration results in:

$$G(\theta) = \left| \frac{\sin\left(\frac{\beta L}{2} \sin\theta\right)}{\frac{\beta L}{2} \sin\theta} \right| \qquad (2\text{-}13)$$

For the 10 wavelength aperture, the first null occurs at $\sin\theta = 0.1$ corresponding to $\theta = 5.7$ degrees.

In the preceding discussion, the aperture fields were assumed tangential to the aperture plane, that is the field vectors lie completely in the plane. For non-uniform phase distributions, however, this is not the case (Ref 10: 162). The direction of propogation of the reflected wavefront is normal to the eikonal surfaces. Since in the geometrical optics approximation the fields exhibit plane wave behavior, the $\overline{H}$ field will not lie in the aperture plane for the x directed $\overline{E}$ field considered previously if the phase distribution varies over the aperture.

If one considers the effect of non-uniform phase distributions, he must employ an alternative expression such as in Reference ten. The expression for far-zone electric field is (Ref 10: 161):

$$\overline{E} = -j\beta \frac{e^{-j\beta r}}{4\pi r}\ \hat{r} \times \int_{\Sigma} \{\hat{n} \times \overline{Ea} - [\hat{r} \cdot (\hat{s} \times \overline{Ea})\ n - (\hat{s} \times \overline{Ea})(\hat{n} \cdot \hat{r})]\} e^{j\beta \hat{r} \cdot \overline{r}^1}\, ds^1 \qquad (2\text{-}14)$$

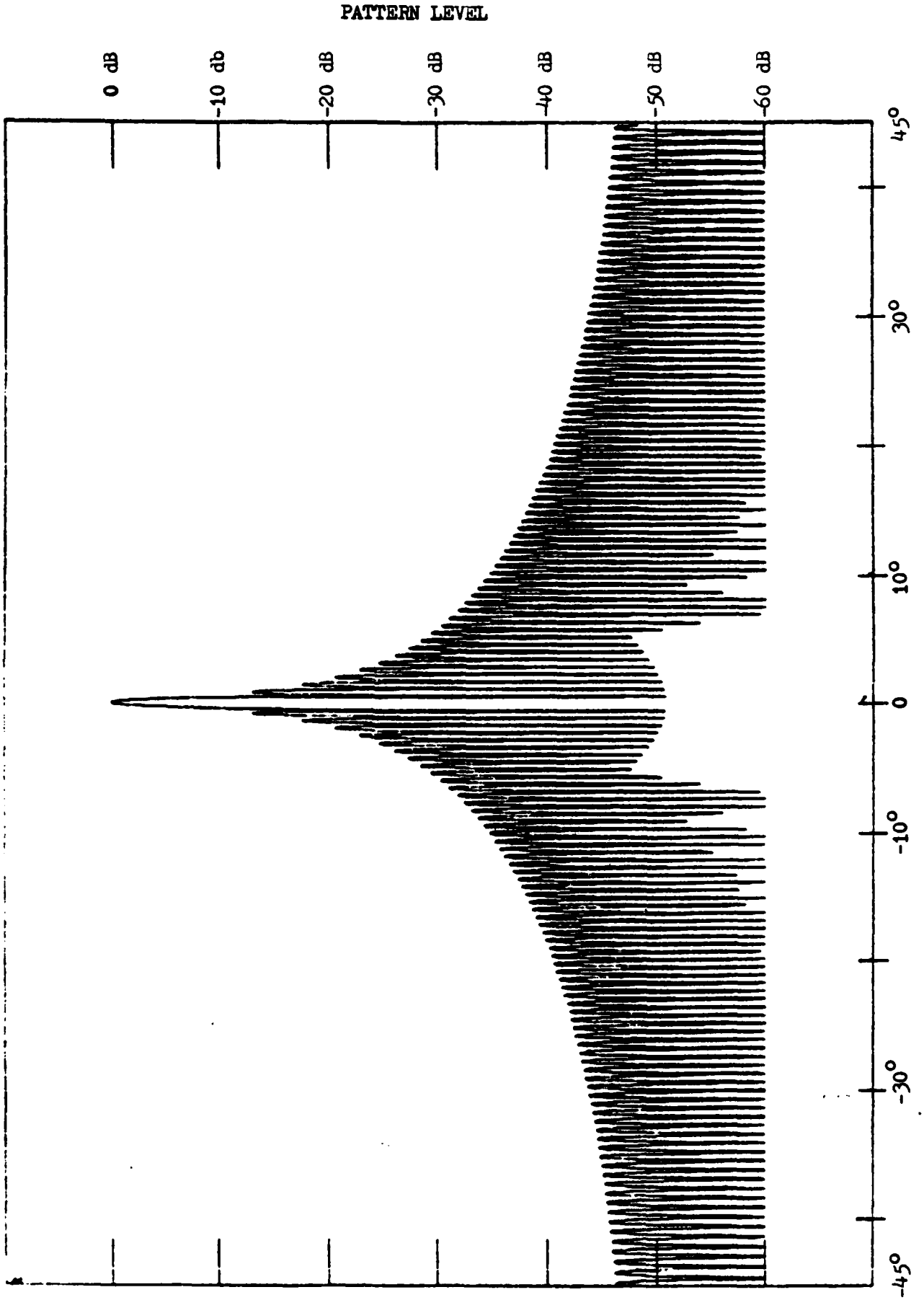
PATTERN LEVEL
0 dB
-10 db
-20 dB
-30 dB
-40 dB
-50 dB
-60 dB
45°
30°
10°
0
-10°
-30°
-45°

Fig 2-2.

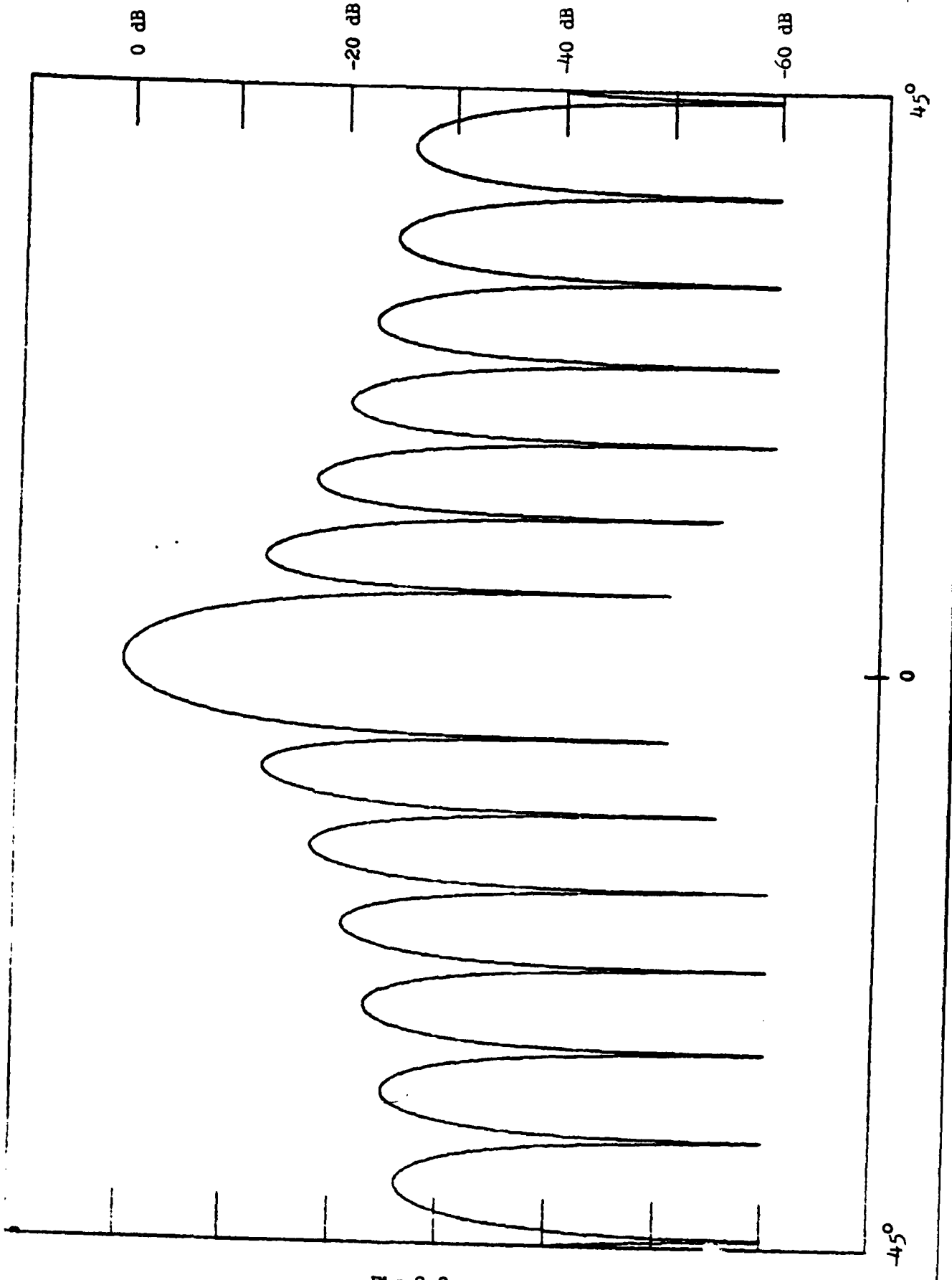

Fig 2-3.

where

Σ = plane aperture surface

$\hat{n}$ = outward normal to Σ

$\hat{r}$ = unit vector pointing from origin to field point

$\bar{r}^1$ = vector from origin to ds^1 in aperture

$\hat{s}$ = unit vector along ray through aperture

Eq (2-14) reduces to Eq (2-12) if the two dimensional assumptions are applied and the phase deviation from uniform are assumed small giving $\hat{s}$ approximately equal to $\hat{n}$ (Ref 10: 162). Ignoring the phase error is not really correct but is frequently done to simplify calculations; however, the results have primarily qualitative value (Ref 10: 173).

Applebaum Weights and Patterns

One reason for using the simplified aperture integration formula is its similarity to the summation expression found in array calculations. This suggests that one might use the Applebaum array weights as discrete points in an aperture distribution. Since the aperture integral is analogous to the array summation, such a distribution should produce a similarly nulled pattern. This is in fact the case.

To illustrate this Eq (1-25) from Section I was applied with K = 201 and d = 0.05 on a ten wavelength aperture. Figure 2-4 shows the aperture magnitude distribution and Figure 2-5 shows the phase distribution for creating a null in Figure 2-3 at two degrees. Similarly Figures 2-6 and 2-7 show aperture magnitude and phase respectively for a null at seven degrees, while figures 2-8 and 2-9 correspond to a null at ten degrees. Figures 2-10 through 2-12 show the patterns resulting from the appropriate distributions for two, seven, and ten degrees respectively.

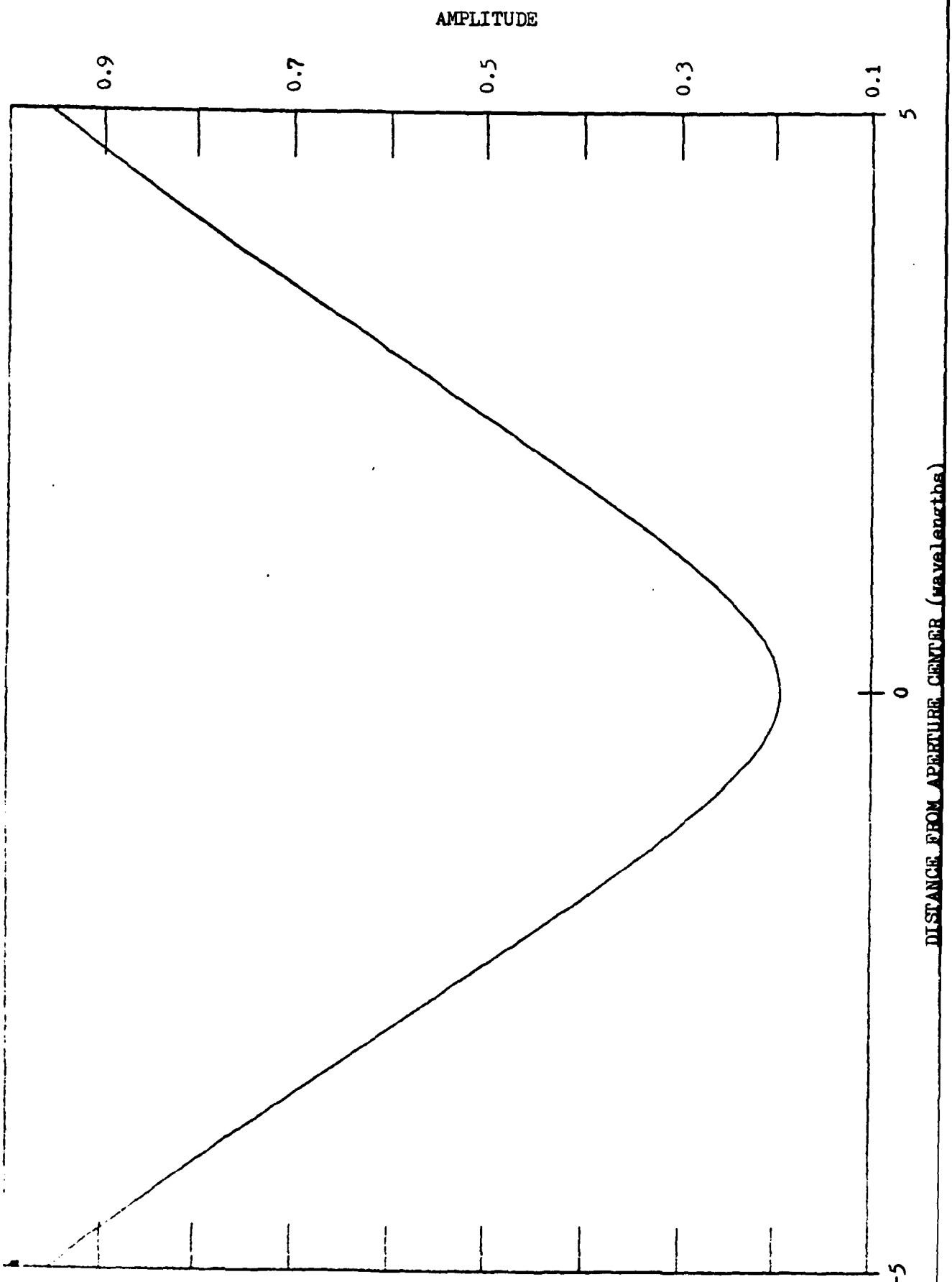
AMPLITUDE
0.9
0.7
0.5
0.3
0.1
5
0
-5
DISTANCE FROM APERTURE CENTER (wavelengths)

Fig 2-4.

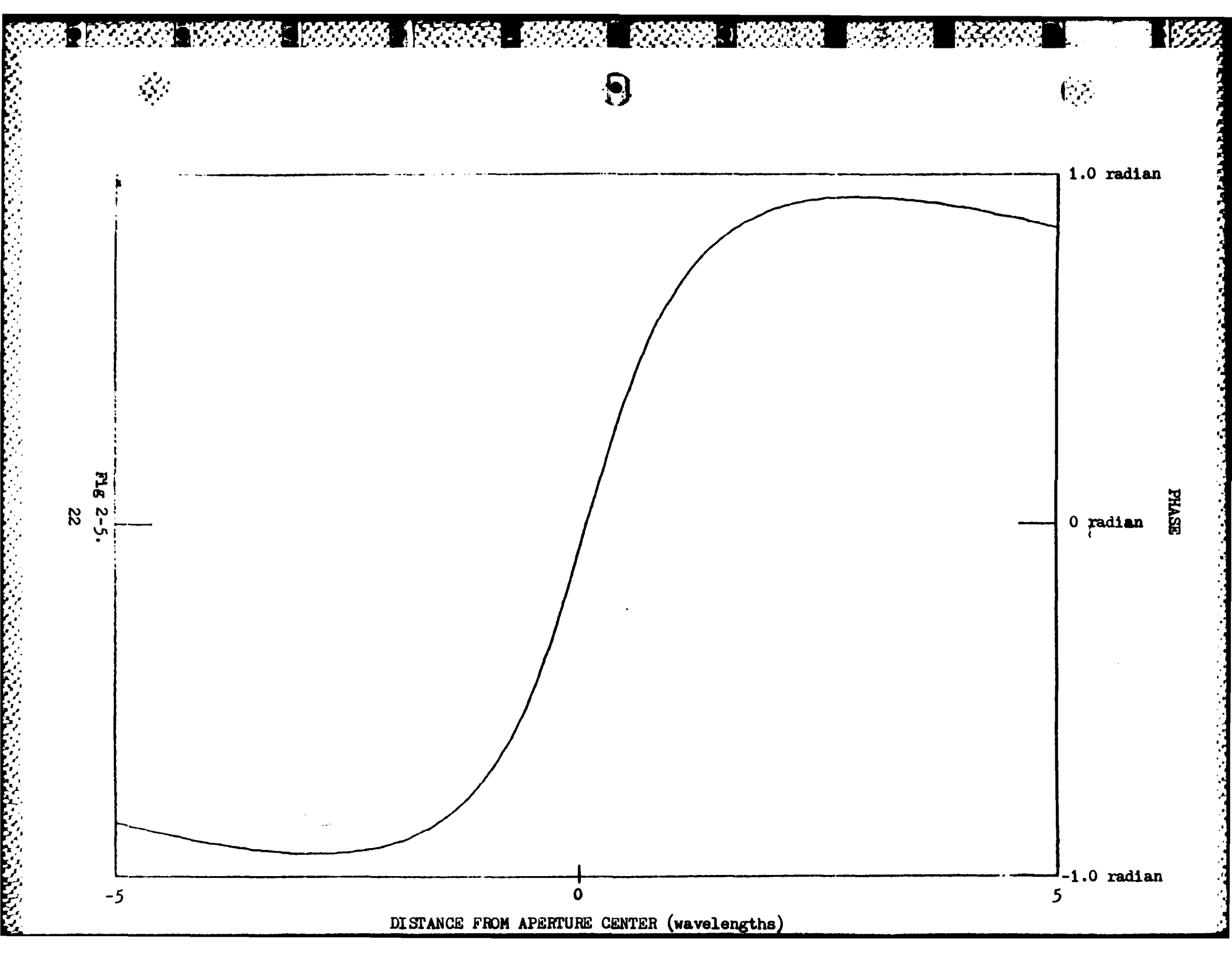
1.0 radian
0 radian
-1.0 radian
PHASE
-5
0
5
DISTANCE FROM APERTURE CENTER (wavelengths)

Fig 2-5.

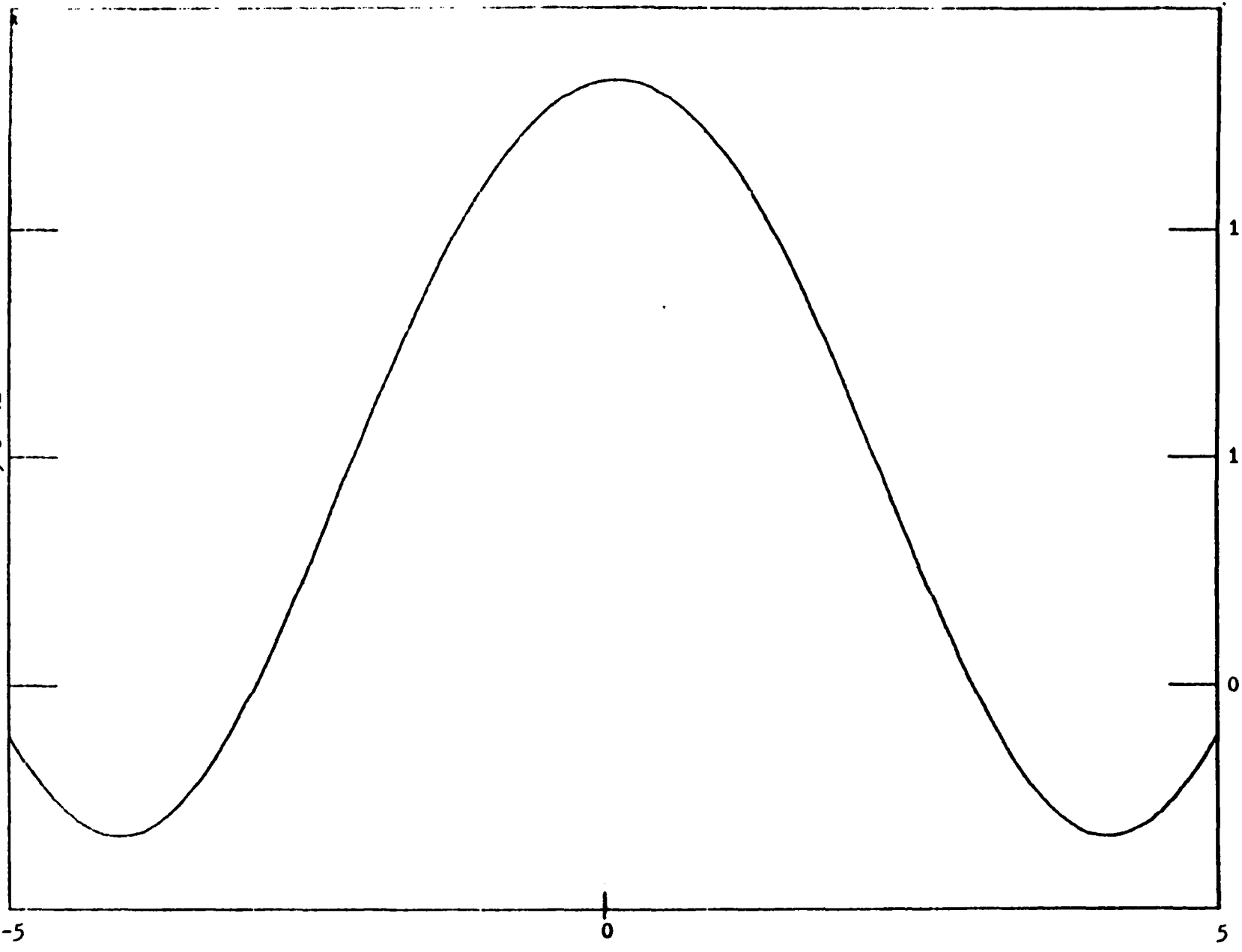
1.1
1.0
0.9
AMPLITUDE
-5
0
5
DISTANCE FROM APERTURE CENTER (wavelengths)

Fig 2-6.

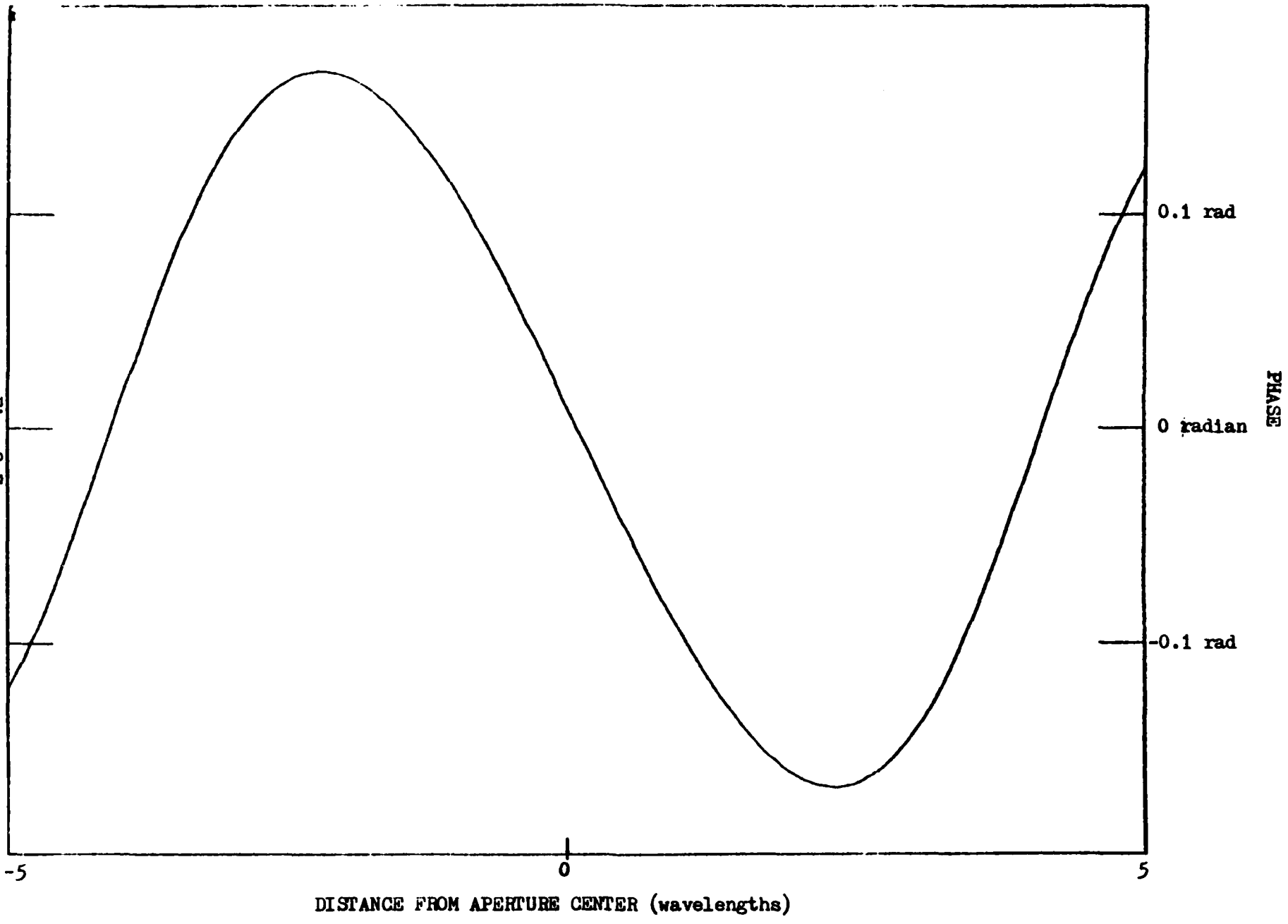
0.1 rad
0 radian
-0.1 rad
PHASE
-5
0
5
DISTANCE FROM APERTURE CENTER (wavelengths)

Fig 2-7.

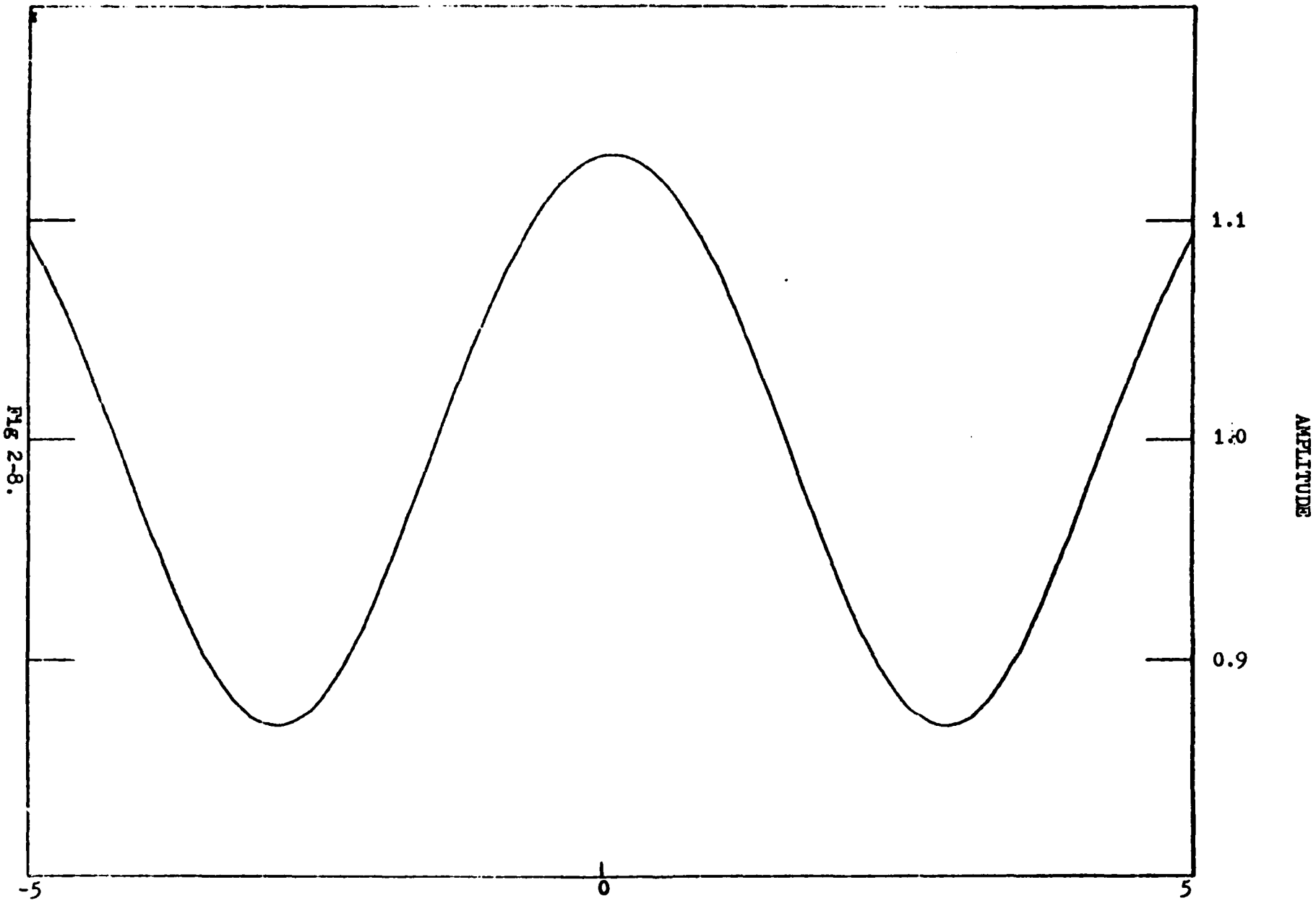
1.1
1.0
0.9
AMPLITUDE
-5
0
5
DISTANCE FROM APERTURE CENTER (wavelengths)

Fig 2-8.

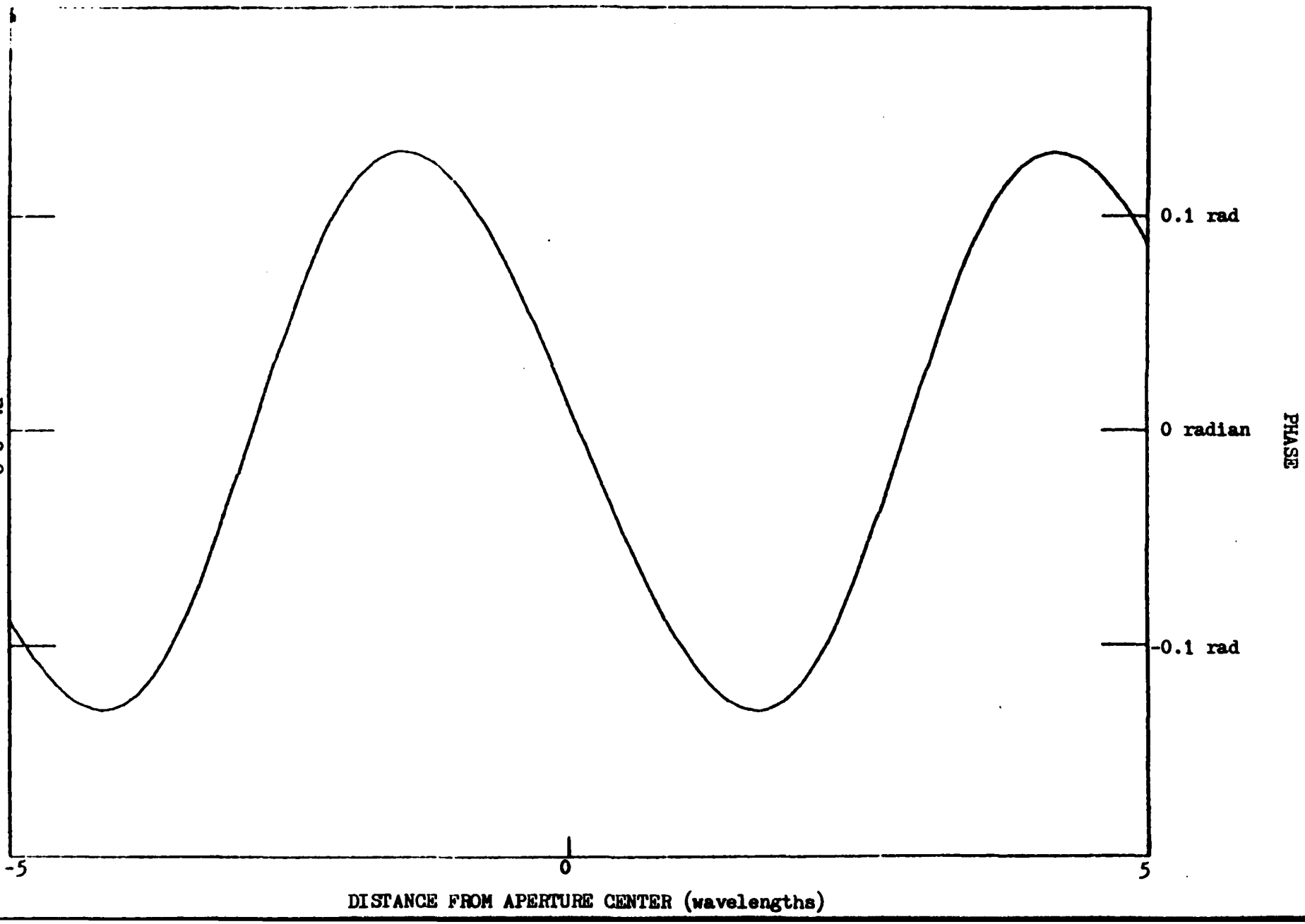
0.1 rad
0 radian
-0.1 rad
PHASE
-5
0
5
DISTANCE FROM APERTURE CENTER (wavelengths)

Fig 2-9.
26

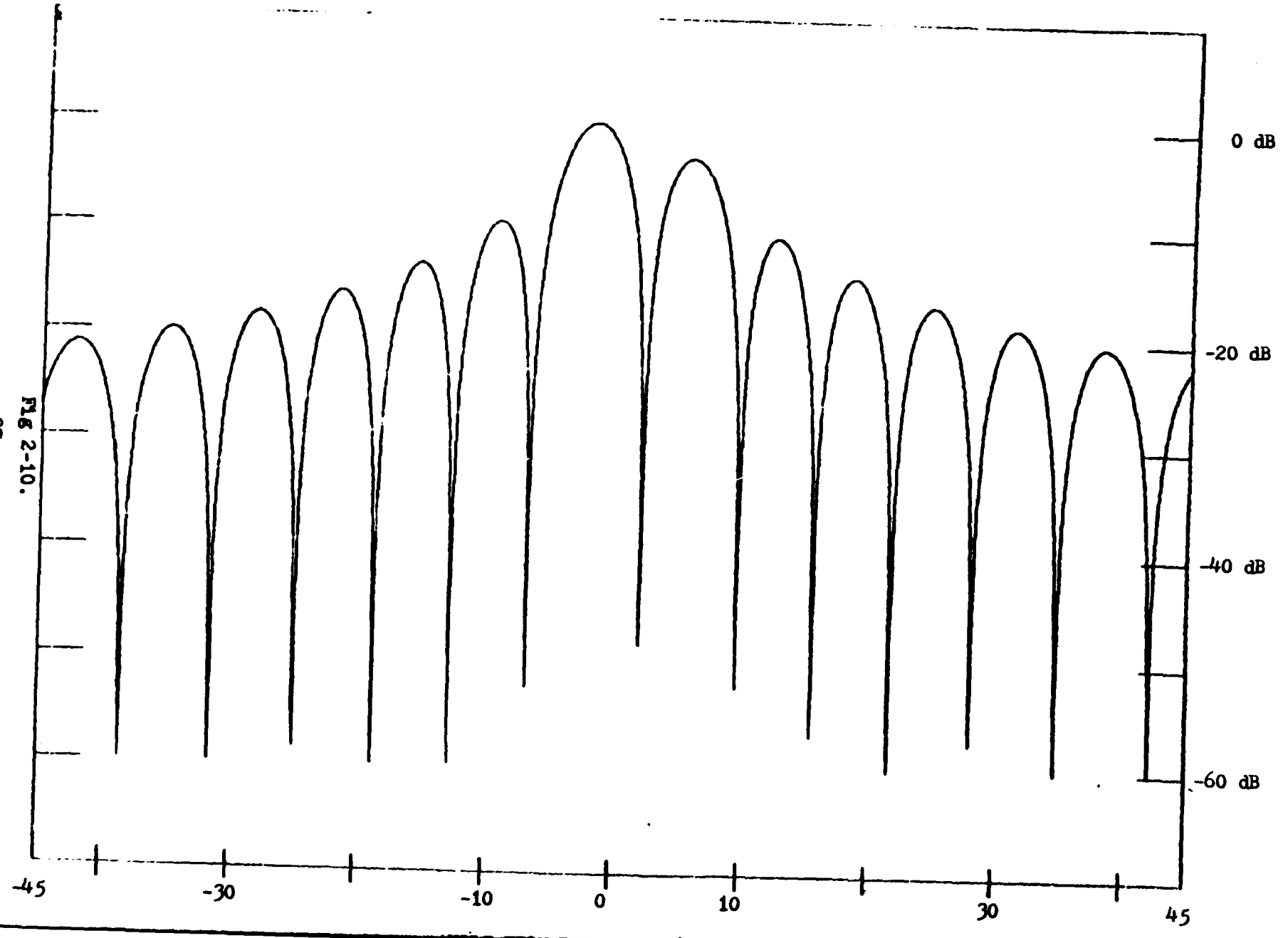

Fig 2-10.

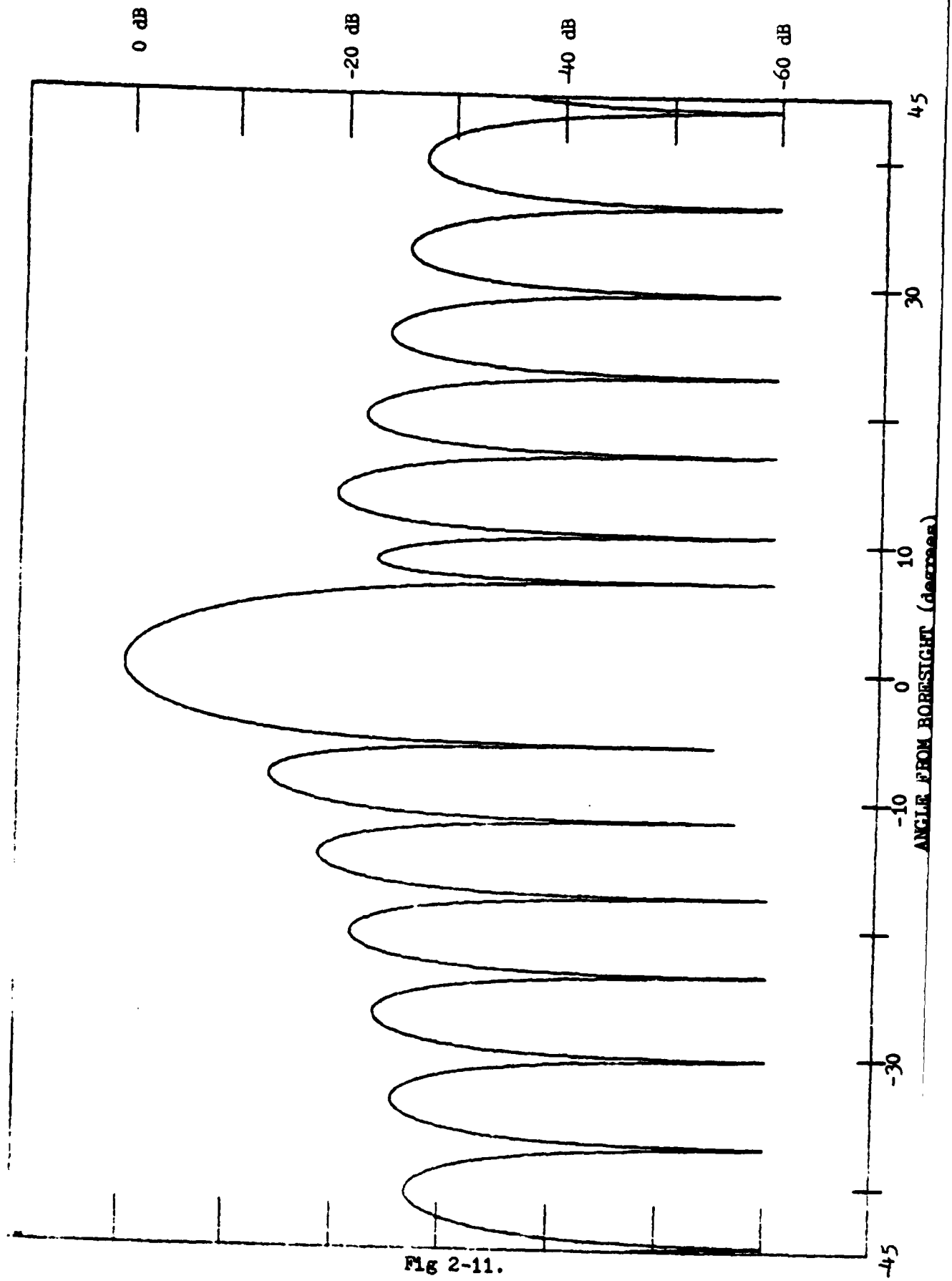
0 dB
-20 dB
-40 dB
-60 dB
45
30
10
0
-10
-30
-45
ANGLE FROM BORESIGHT (degrees)

Fig 2-11.

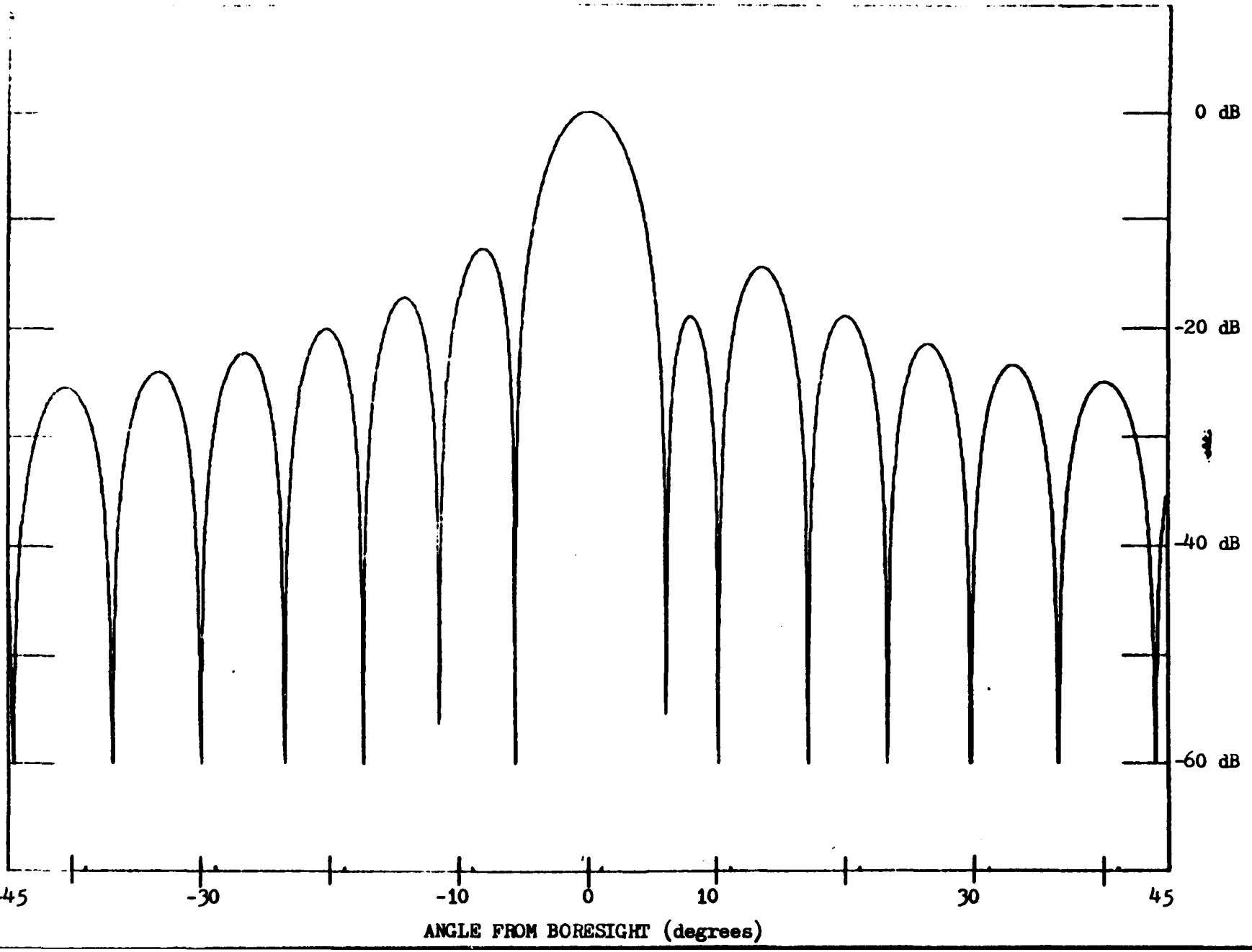
0 dB
-20 dB
-40 dB
-60 dB
-45
-30
-10
0
10
30
45
ANGLE FROM BORESIGHT (degrees)

Fig 2-12.

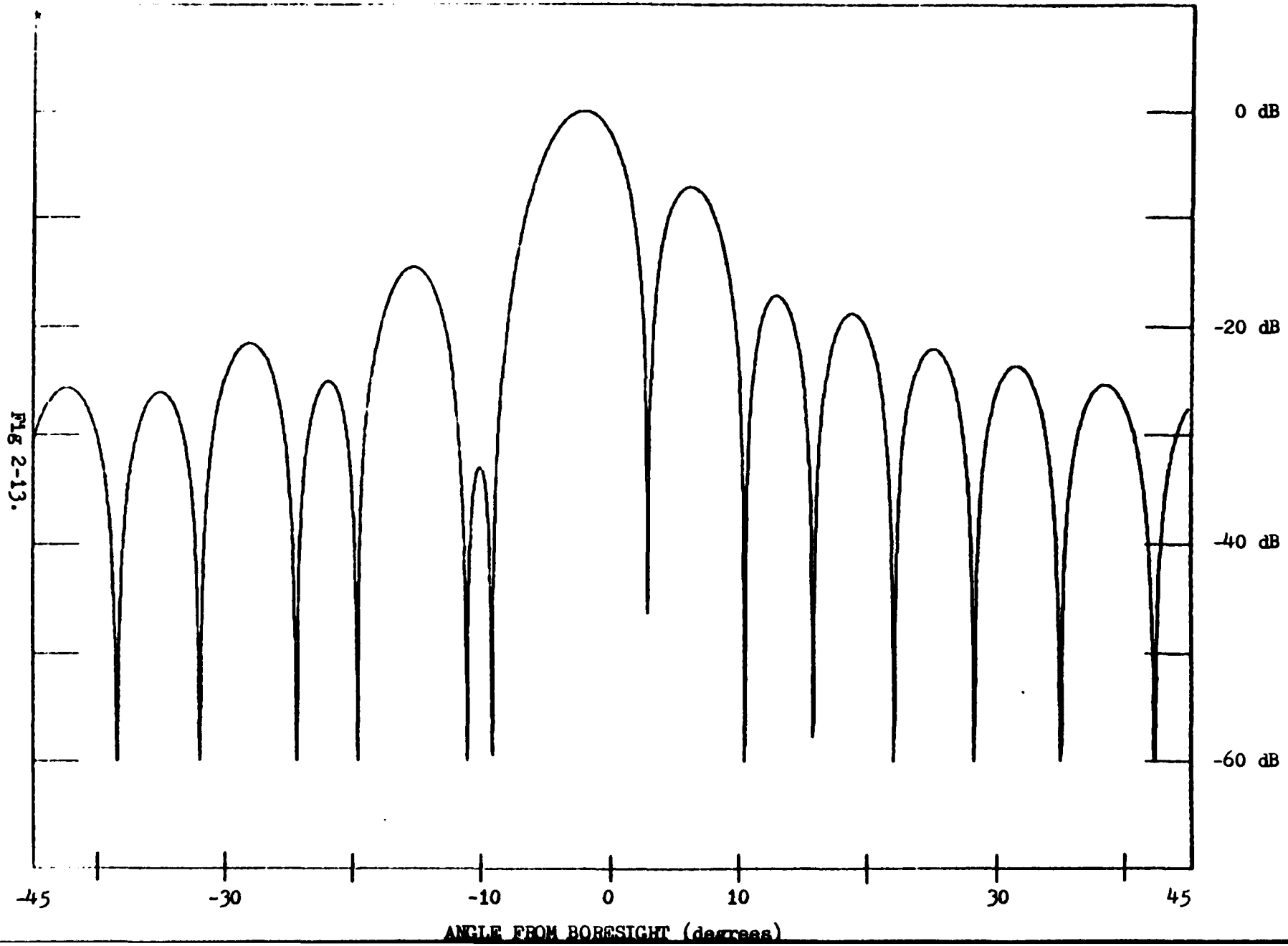
0 dB
-20 dB
-40 dB
-60 dB
-45
-30
-10
0
10
30
45
ANGLE FROM BORESIGHT (degrees)

Fig 2-13.

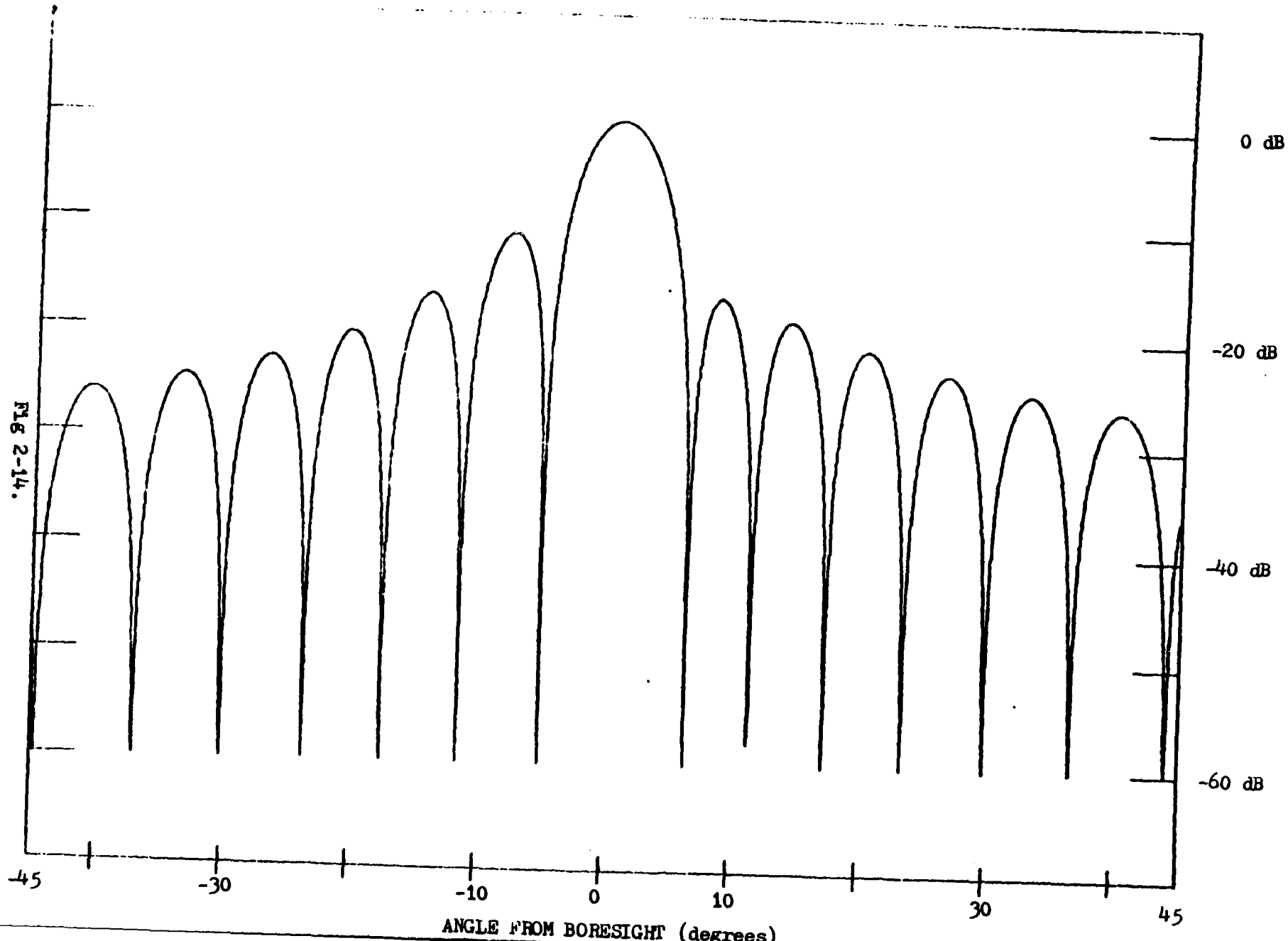
0 dB
-20 dB
-40 dB
-60 dB
-45
-30
-10
0
10
30
45
ANGLE FROM BORESIGHT (degrees)

Fig 2-14.

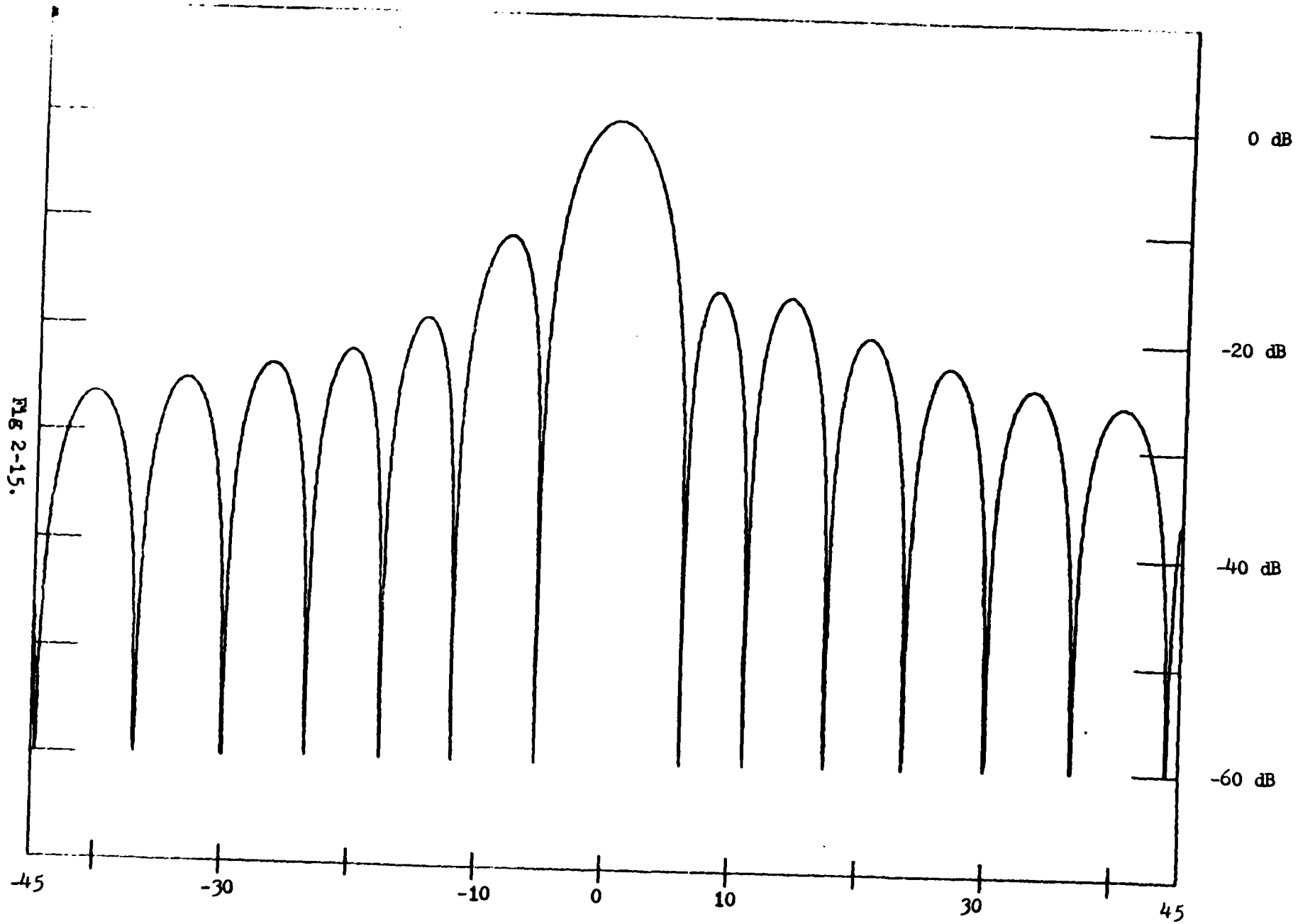
0 dB
-20 dB
-40 dB
-60 dB
-45
-30
-10
0
10
30
45
ANGLE FROM BORESIGHT (degrees)

Fig 2-15.

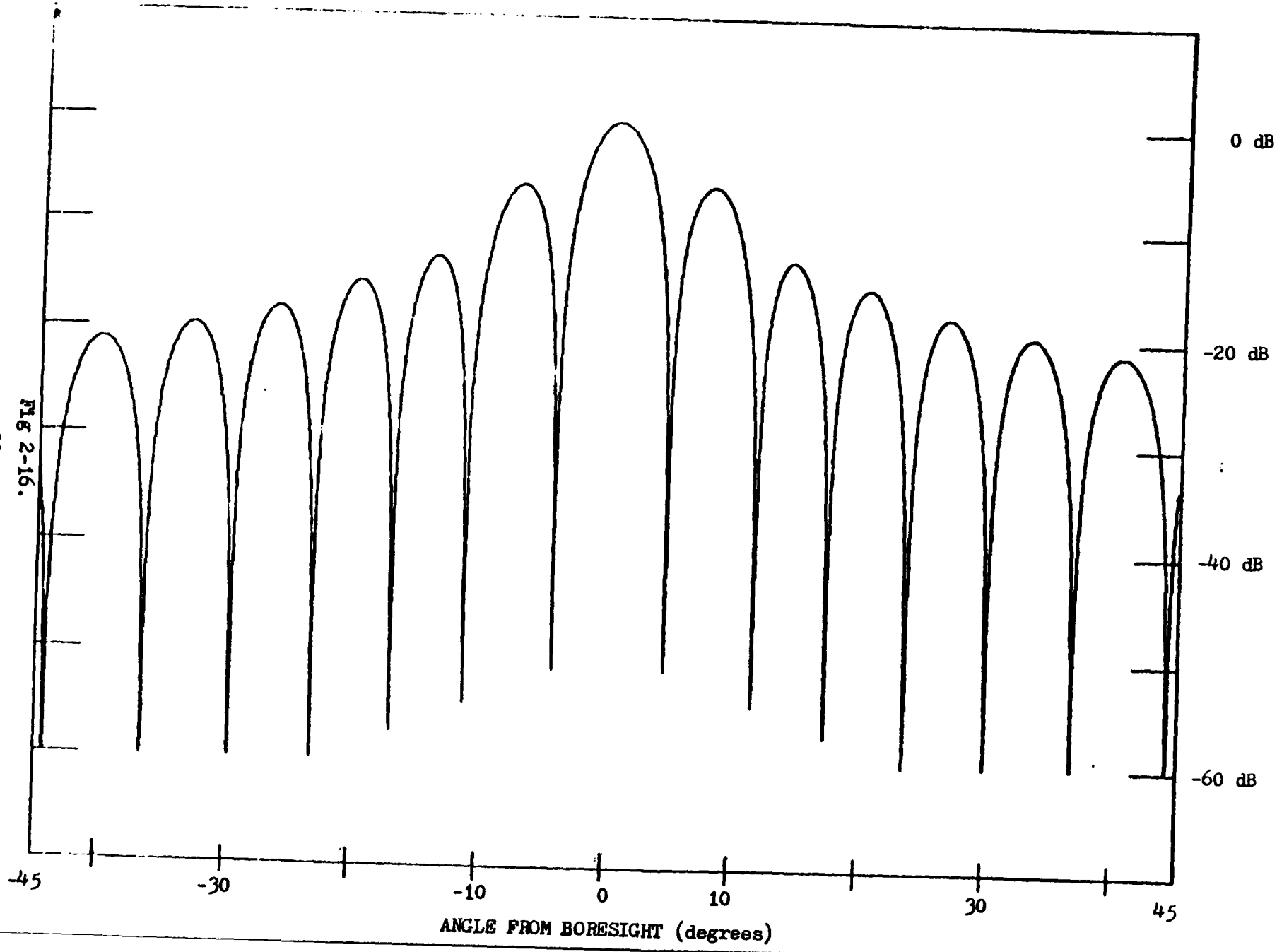
0 dB
-20 dB
-40 dB
-60 dB
-45
-30
-10
0
10
30
45
ANGLE FROM BORESIGHT (degrees)

Fig 2-16.

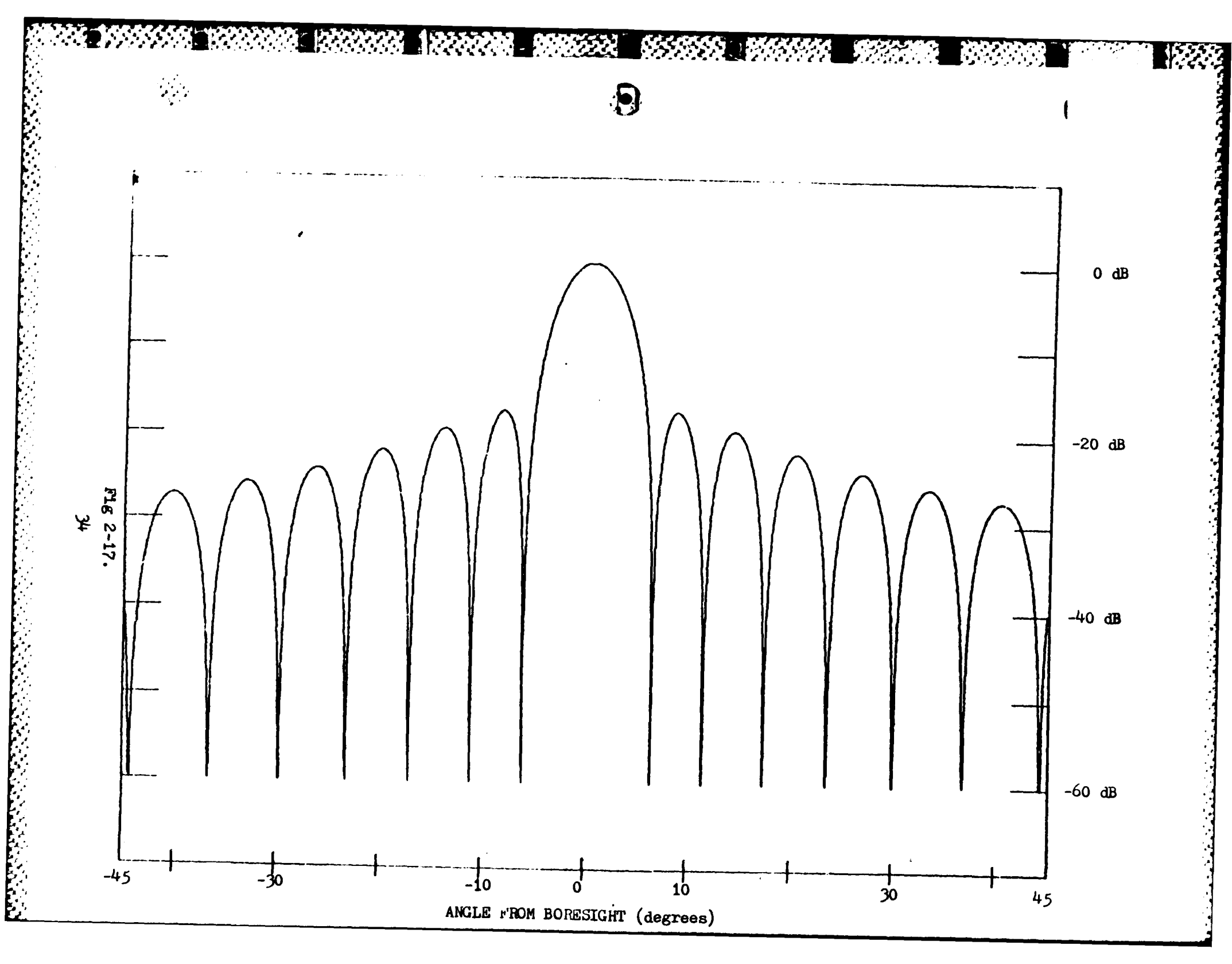
0 dB
-20 dB
-40 dB
-60 dB
-45
-30
-10
0
10
30
45
ANGLE FROM BORESIGHT (degrees)
FIG 2-17.
34

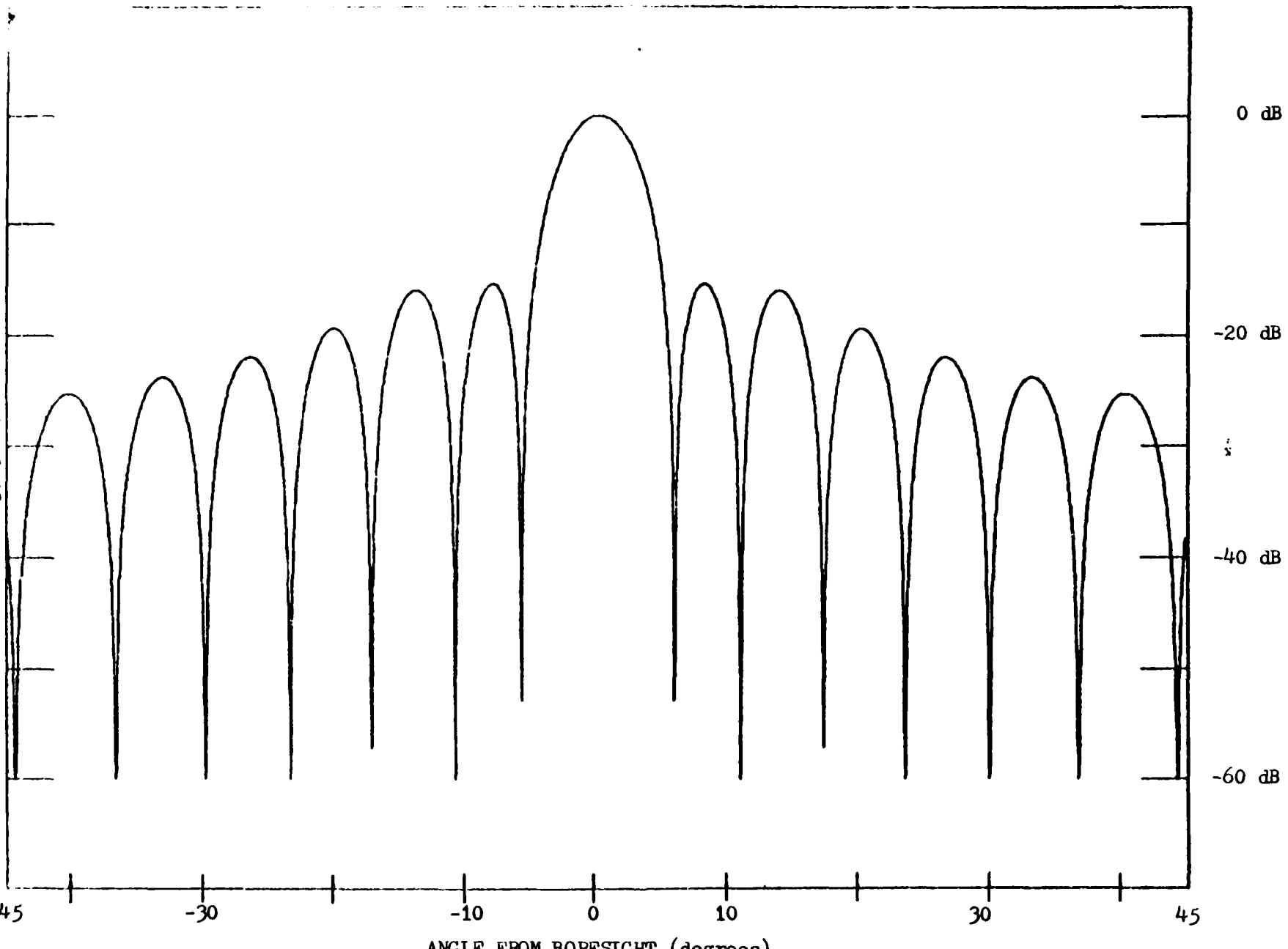
0 dB
-20 dB
-40 dB
-60 dB
-45
-30
-10
0
10
30
45
ANGLE FROM BORESIGHT (degrees)

Fig 2-18.

Further experimentation indicates that the phase distribution is the dominant factor in determining null location. Figure 2-13 shows that aperture integrating the phase distribution of Figure 2-5 with a uniform amplitude distribution creates a null at 2.7 degrees. Similarly, Figures 2-7 and 2-9 integrated with uniform amplitude distributions yield nulls at 6.7 degrees and 10.7 degrees as shown in Figures 2-14 and 2-15. Implementing the amplitude distributions with flat phase does not consistently come as close. Such calculations result in nulls at 4.5, 6.3, and 10.9 degrees for the three respective cases. Especially in the two degree null case, the flat phase patterns do not deviate much from the quiescent pattern with nulls at 5.7 and 11.5 degrees as shown in Figures 2-16, 2-17, and 2-18. This implies that the phase distribution should receive priority in any attempt to implement the aperture distributions shown in Figures 2-4 to 2-9. Using only the phase distribution, however, results in an as yet undetermined error which deserves further study.

III Secondary Pattern Calculation

Geometrical Optics

In order to approximate the field distribution in the aperture, geometrical optics principles were applied to the reflector shapes in question. The use of geometrical optics requires that the dimensions of the scattering surface be large compared to a wavelength (Ref 12:454). It also places a constraint on the smoothness of the surface, since the radius of curvature of the surface must always be large compared to a wavelength (Ref 9: 123). Even if these requirements are met, however, the approximation is still rather crude. All diffraction effects have been ignored. Thus, the reader should interpret the results qualitatively. The null positions and the effect of reflector shape on them are the points to watch.

Specialized to the two-dimensional case, the geometrical optics expression for amplitude is (Ref 12: 450):

$$|E| = |E_o| \sqrt{\frac{r_{cw}}{r_{cw}+\rho}} \tag{3-1}$$

where $|E_o|$ is the magnitude of the field at the reference location and r_{cw} is the radius of curvature of the wavefront at the reference point. The ρ denotes the distance from the reference point to the field point. To include phase, one simply applies a phase factor determined by ρ. The resultant expression is (Ref 12:451):

$$E = |E_o| \sqrt{\frac{r_{cw}}{r_{cw}+\rho}} \; e^{-j\beta\rho} \; e^{j\phi_o} \tag{3-2}$$

where β is simply $2\pi/\lambda$ and $\emptyset_0$ is the reference phase at the reference point.

In order to compute the aperture field contribution of a single ray, one must first determine the field radiated from the feed at the point of impact for that ray on the reflector. In this work, the feed is assumed to be a line source at the origin. Placing the reference point one wavelength from the feed and choosing $|E_0| = 1$, $\emptyset_0 = -\beta$ in Eq 3-2 yields:

$$E = \sqrt{\frac{1}{1+\rho}}\ e^{-j\beta(1+\rho)} \tag{3-4}$$

for the field phasor at the point of reflection. But $1 + \rho$ is simply the distance from feed to reflection point, so letting $1 + \rho = r_1$ gives:

$$E = \frac{1}{\sqrt{r_1}}\ e^{-j\beta r_1} \tag{3-5}$$

To calculate the field phasor in the aperture, one must compute 2 , the distance from the reflection point to the point where the ray in question intersects the aperture. Then using $|E_0| = 1/\sqrt{r_1}$ and $\emptyset_0 = -\beta r_1$ in Eq 3-2 gives:

$$E = \frac{1}{\sqrt{r_1}} \sqrt{\frac{r_{cw}}{r_{cw} + r_2}}\ e^{-j\beta r_2}\ e^{-j\beta r_1} \tag{3-6}$$

All that remains in finding r_{cw}, the radius of curvature of the reflected wavefront. This is given by (Ref 12:452):

$$\frac{1}{r_{cw}} = \frac{1}{r_1} + \frac{2}{r_c \cos\theta_0} \tag{3-7}$$

where r_c is the physical radius of curvature of the reflector at the reflection point and θ_0 is the angle of incidence of the incoming ray with respect to the surface normal. If the surface is convex when

viewed from the line source feed, r_c is greater than zero. If the surface is concave, the r_c is less than zero. Thus, given a ray, Eq 3-6 determines the aperture field due to it.

Ray Tracing

Before one can compute the aperture field approximation, he must first trace given rays from the feed through their points of reflection to their aperture intersection points. Figure 3-1 illustrates the geometry. The θ is the angle the incident ray makes with the horizontal axis. The reflector surface is described by a discrete grid of equi-spaced points.

The first step is to find the (x_i, y_i) impact point from θ_i and the grid. The line $y = kx$ represents the incident ray in this two dimensional geometry, where $k = \tan\theta_i$. To determine the impact point, one must define a miss function (Ref 11:1449) $g_n = kx_n - y_n$. Testing each grid point will yield same (x_{n-1}, y_{n-1}) and $(x_{n1}y_n)$ between which the miss function changes sign, because $g_{n-1}g_n < 0$. The impact point lies on the reflector surface between these two points. This impact point is determined by (Ref 11:1449):

$$x_i = y_n(1-F) + x_{n-1}F$$
$$y_i = y_n(1-F) + y_{n-1}F \qquad (3\text{-}8)$$

where $F = g_n / (g_n - g_{n-1})$.

To determine the point of impact in the aperture plane, one must consider Figure 3-2. The ϕ and the ψ are the angles made by the surface normal and the reflected ray respectively with the horizontal axis. Snell's Law at the impact point, valid for the smooth surfaces in question,

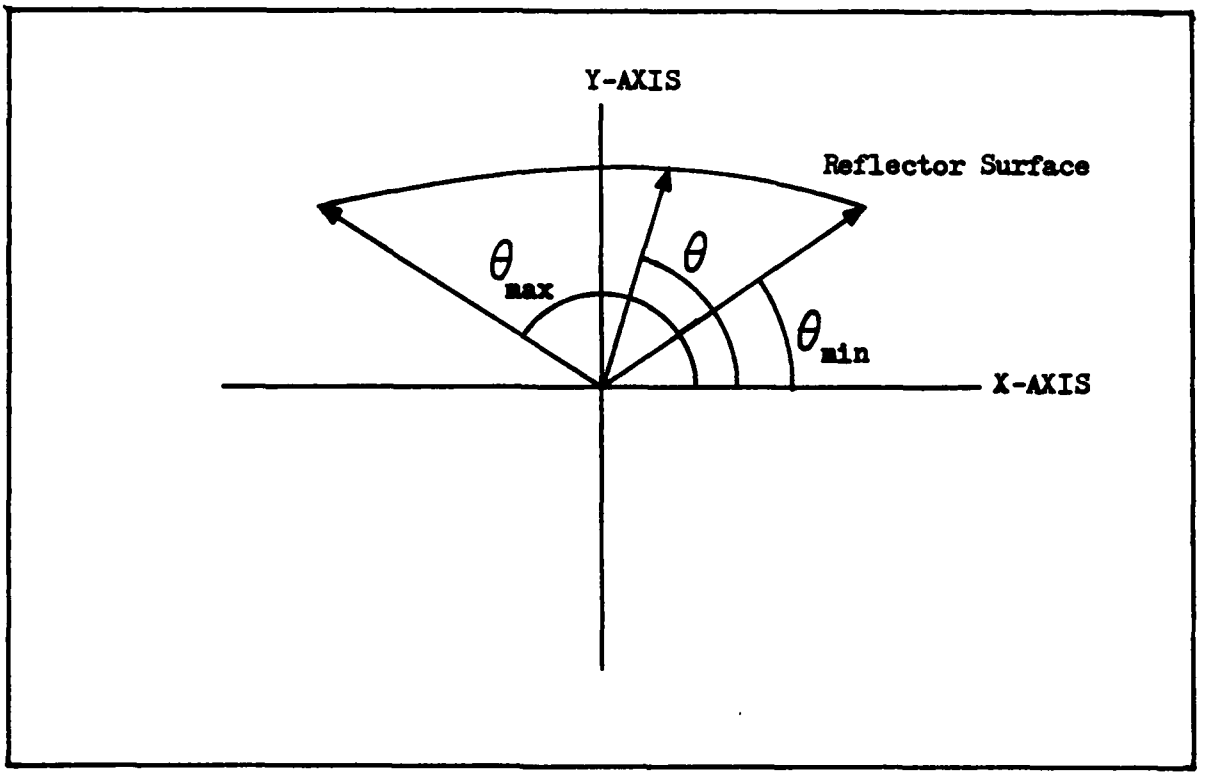

Fig 3-1. Incident Rays

dictates that the angle of incidence and angle of reflection with respect to the surface normal be the same (Ref 11:1449). This angle is denoted by δ in Figure 3-2. Simple geometry then yields:

$$x = 2\emptyset - \Theta \tag{3-9}$$

Determining $\emptyset$ requires approximation of the first derivative of the reflector surface at the impact point. Calculating it at (x_{n-1},y_{n-1}) and (x_n,y_n) by a well established finite difference formula, then using linear interpolation to (x_i,y_i) yields acceptable results. Once this derivative is determined, $\emptyset$ can be found. The tangent unit vector to the surface at (x_i,y_i) is given by $\hat{t} = \cos\alpha\,\hat{x} + \sin\alpha\,\hat{y}$, where α is the

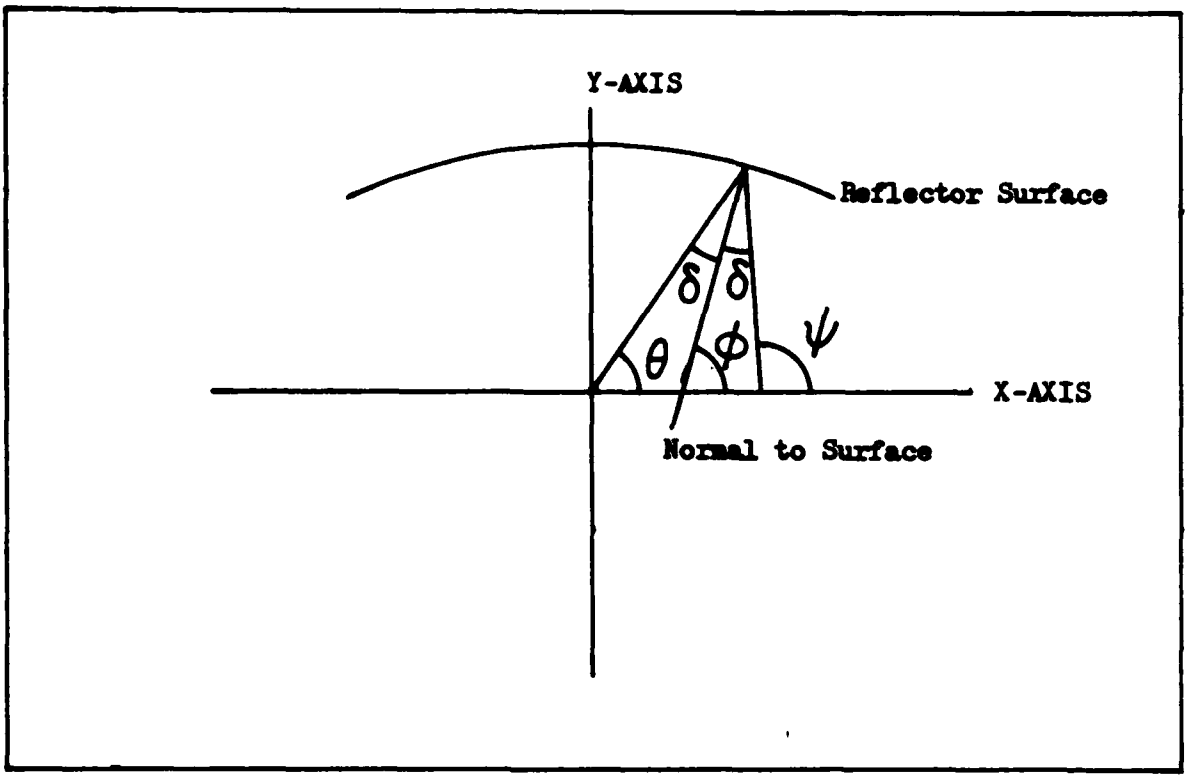

Fig 3-2. Angle Definitions

angle made by $\hat{t}$ and the horizontal. The slope of the line determined by $\hat{t}$ is $\tan\alpha$ and since this line is the tangent line to the curve at (x_i,y_i):

$$\tan\alpha = \frac{dy}{dx}\Big|_{x = x_i} \tag{3-10}$$

where $dy/dx|x=x_i$ was already discussed. The normal vector at (x_i,y_i) is $n = d\hat{t}/d\alpha = \sin\alpha\hat{x} + \cos\alpha\hat{y}$. The slope of the line determined by the normal is $\tan\phi$; hence, $\tan\phi = \cos\alpha/(-\sin\alpha) = -\cot\alpha$ which implies that $\tan\alpha = -\cot\phi$. Substituting back into Eq 3-20 yields ϕ in terms of a known quantity (Ref 11:1449):

$$-\cot\phi = \frac{dy}{dx}\Big|_{x = x_i} \tag{3-11}$$

One must consider some computational points before actually using Eq 3-11 to find ϕ. The range of ϕ is limited to $0 \leq \phi \leq \pi$. If $dy/dx|x=x_i > 0$, then $\phi > \pi/2$. If $dy/dx|x=x_i < 0$, then $\phi < \pi/2$. The case $dy/dx|x=x_i = 0$ implies that $\phi = \pi/2$. Any scheme to compute ϕ should reflect this. Since arctangent implementations on computers generally range only from $-\pi/2$ to $\pi/2$, one must exercise care in the computation. A suitable scheme is Eq (3-12).

$$\phi = \begin{cases} \tan^{-1}\left[\left|\left(\frac{dy}{dx}\Big|_{x=x_i}\right)^{-1}\right|\right] & \frac{dy}{dx}\Big|_{x=x_i} < 0 \\ \frac{\pi}{2} & \frac{dy}{dx}\Big|_{x=x_i} = 0 \\ \pi - \tan^{-1}\left[\left(\frac{dy}{dx}\Big|_{x=x_i}\right)^{-1}\right] & \frac{dy}{dx}\Big|_{x=x_i} > 0 \end{cases} \tag{3-12}$$

Using ϕ in Eq 3-9 gives ψ. From Figure 3-3, the point of intersection of the reflected ray with the aperture $(x_a,0)$ is given by:

$$x_a = \begin{cases} x_i - y_i/\tan\psi & x < \frac{\pi}{2} \\ x_i & x = \frac{\pi}{2} \\ x_i + y_i/\tan(\pi-\psi) & x > \frac{\pi}{2} \end{cases} \tag{3-13}$$

To compute the field contribution, one simply applies Eq 3-6 along with Eq 3-7. The physical radius of curvature at (x_i,y_i) of the reflector surface is simply:

$$r_c = \frac{\left[1 + \left(\frac{dy}{dx}\Big|_{x=x_i}\right)^2\right]^{3/2}}{\frac{d^2y}{dx^2}\Big|_{x=x_i}} \tag{3-14}$$

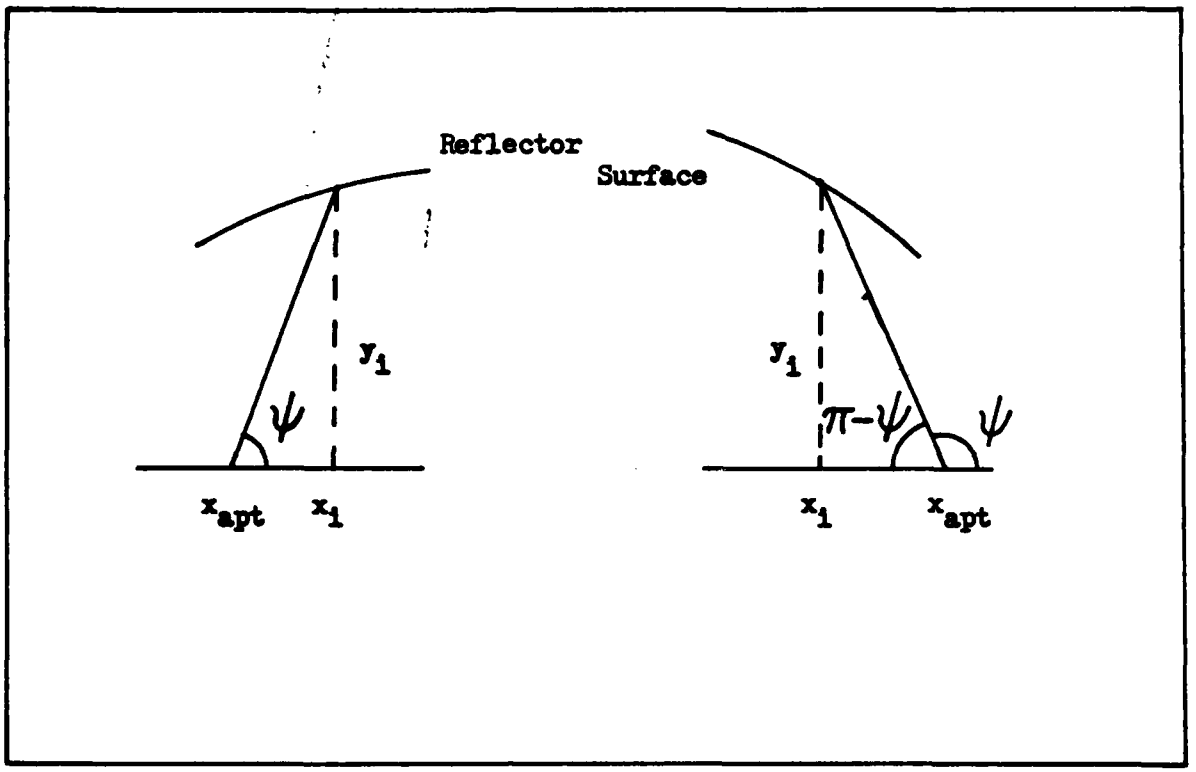

Fig 3-3. x_{apt} from Angle PSI

where the sign of the second derivative is preserved in order to make r_c appropriately positive or negative based on convexity or concavity.

The process of approximating the second derivative exhibits an inherent instability which defied efforts at eliminating it. The effect of the instability will show up graphically in the spherical reflector example. Appendix B describes the problem.

Aperture Field

After defining an aperture, usually centered on the reflector's boresight and wide enough to include all reflected ray intersection points, one selects a set of discrete points in the aperture at which he wishes to compute the field. Taking each point in turn, one determines which rays intersect the aperture at that point and adds the field

contributions of these rays. For most relatively smooth reflectors, only one ray will strike the point in question.

To find the right ray, one steps through possible values of θ until he finds θ_1 and θ_2 such that $x_{a2} < x_a < x_{a1}$ where x_a is the desired aperture point. Then one computes x_{a3} from $\theta_3 = (\theta_1 + \theta_2)/2$. Then one uses a bisection algorithm to close in on the correct value of θ. If $x_a - x_{a3} < 0$, then the correct θ is between θ_3 and θ_2. If $x_a - x_{a3} > 0$, then the θ is between θ_1 and θ_3. The bisection process is then repeated. When $x_a - x_{a3}$ is sufficiently close to zero, the process terminates. When completed, the process yields a discrete grid of aperture field points.

Parabolic Example

The scheme described before will now be tested on a parabola. Figure 3-4 shows the parabola. Its diameter is 100λ where λ is the wavelength. The focal length is 50λ with focus at the origin. The feed is an $\hat{x}$ directed electric line source at the origin. The aperture electric field will also be $\hat{x}$ directed, by application of Snells Law (Ref 12:426).

Analyzing the parabola, one notes that the phase will be constant on an aperture centered on boresight and 100λ wide. Thus, the wave front incident on this aperture is a plane wave. Since a plane wave has constant amplitude, attenuation occurs only between the feed and the reflector. Using this in Eq 3-6 yields:

$$E = \frac{1}{\sqrt{r_1}} \qquad (3\text{-}15)$$

A little analytic geometry shows that $r_1 = 50[1 + (\frac{y}{100})^2]$. Normalizing this to a unity maximum gives:

$$E = \frac{1}{\sqrt{1 + (\frac{y}{100})^2}} \qquad (3\text{-}16)$$

Figure 3-5 shows the amplitude distribution generated by the method of this section. The method duplicates the analytic geometrical optics analysis. It also duplicates the constant phase, but the flat line has not been plotted. Figure 3-6 shows the Section II pattern result.

Figures 3-7 through 3-9 correspond to Figures 3-4 through 3-6, but with diameter 10λ and focal length 5λ. For such a reflector, the validity of geometrical optics is questionable, since diffraction effects are present. However, for angles near boresight, the pattern results are still useful.

Spherical Example

Figure 3-10 shows the test surface. The radius of curvature is 200λ. The diameter of the reflector is 100λ. The feed is situated on the boresight 50λ from the center of the reflector and coincides with the origin. The aperture is centered on a feed and is 100λ wide to include all rays.

Figures 3-11 and 3-12 show the amplitude and phase calculated by the methods of this section with analytic determination of the second derivative. Figures 3-13 and 3-14 shows the results using the final second derivative approximation in Appendix B. While the phase result is good, the amplitude exhibits a messy error distribution.

The net effect of the error is not overly drastic. The messy amplitude distribution seems to cluster about the correct one. Also, phase is

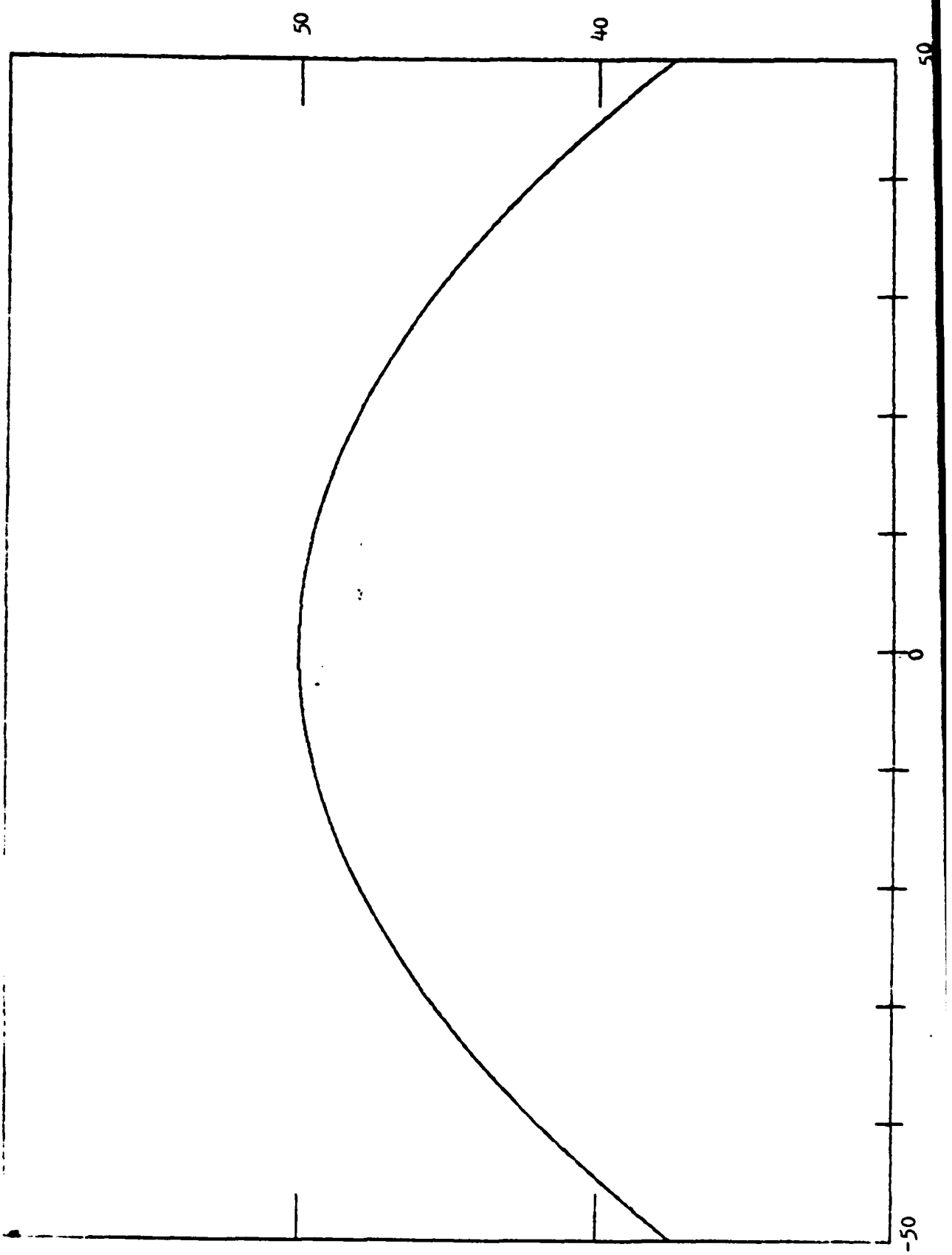

Fig 3-4.

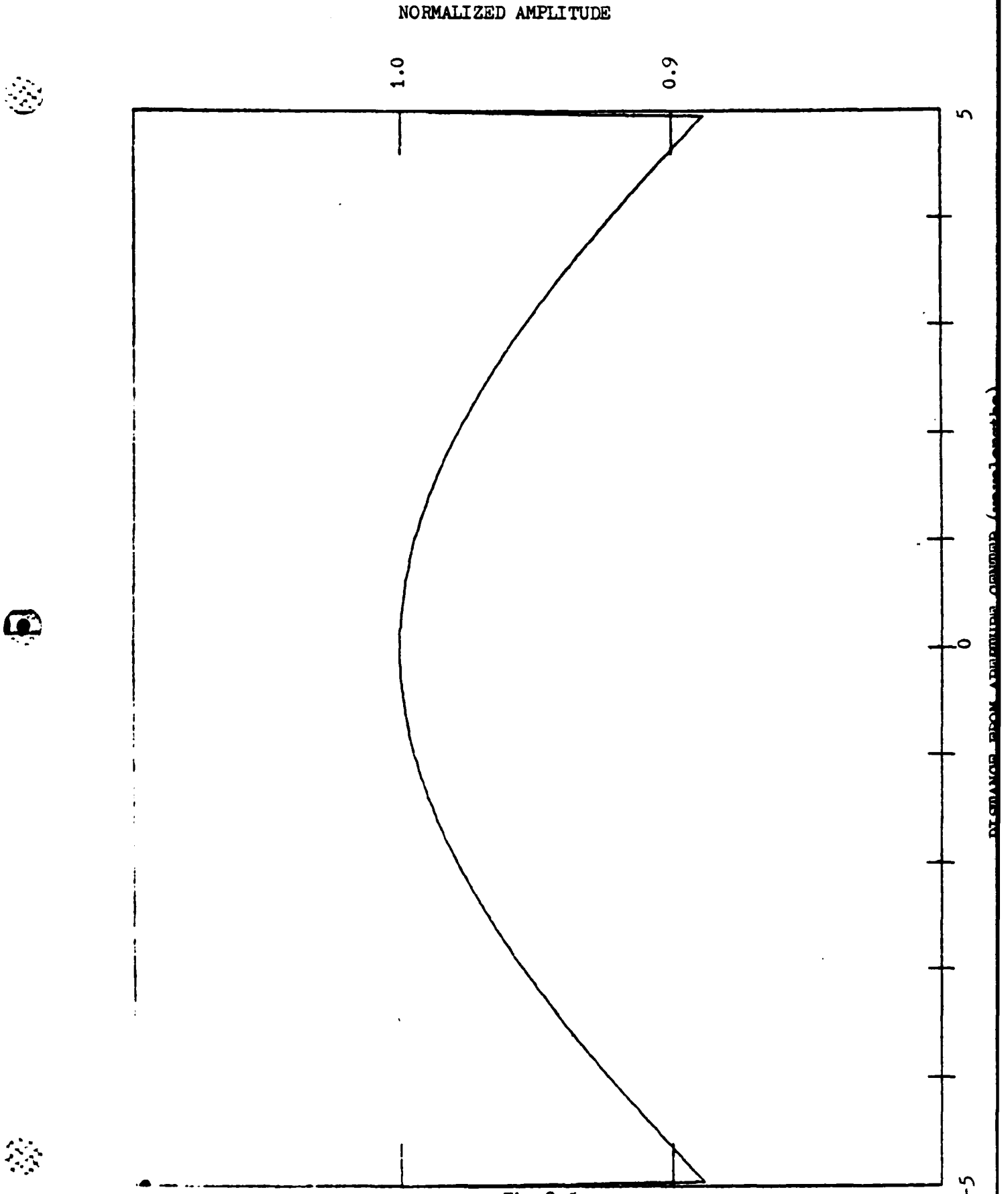
NORMALIZED AMPLITUDE
1.0
0.9
5
0
-5
DISTANCE FROM ARRAY CENTER (wavelengths)

Fig 3-5.

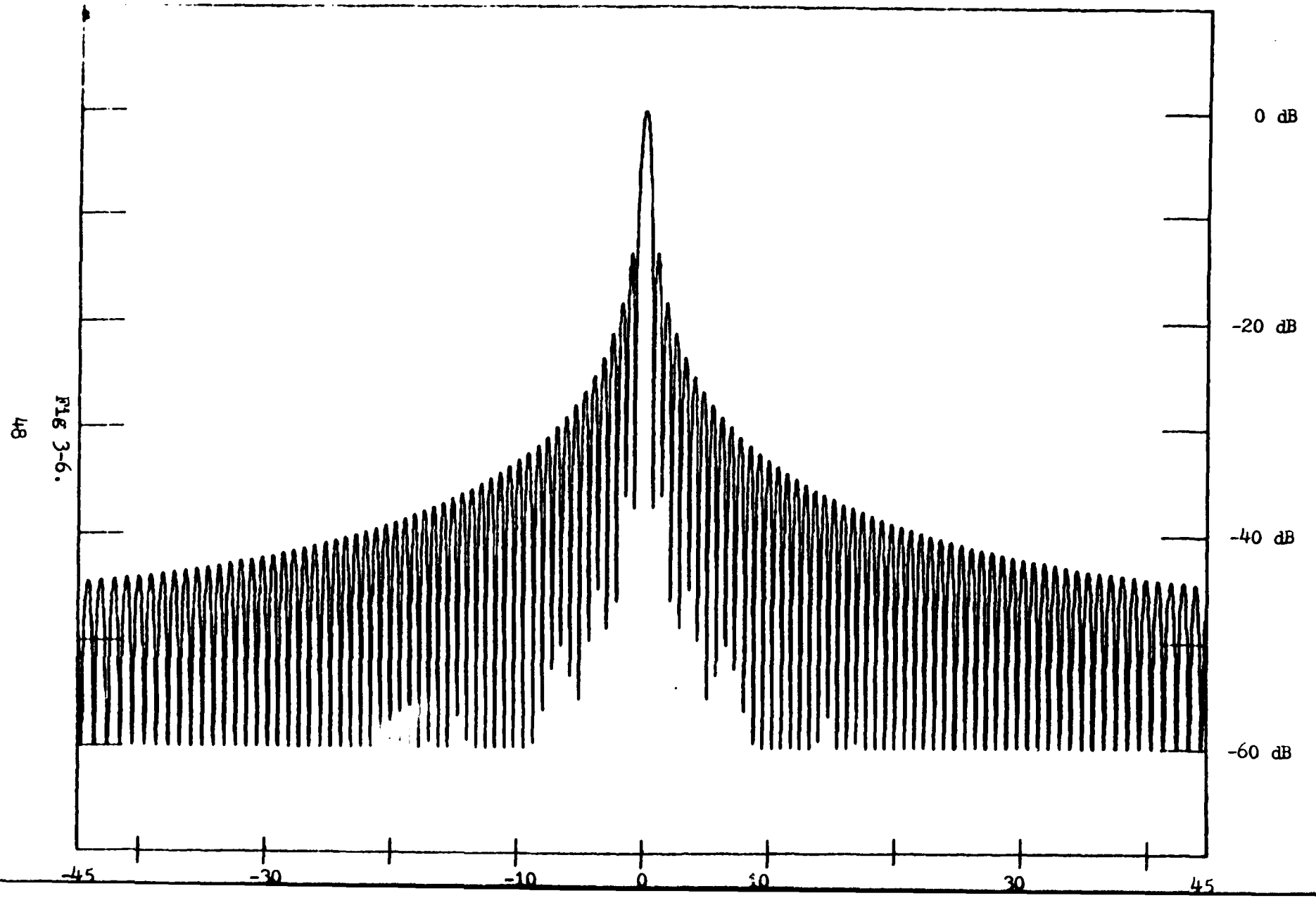

dB

Fig 3-6.

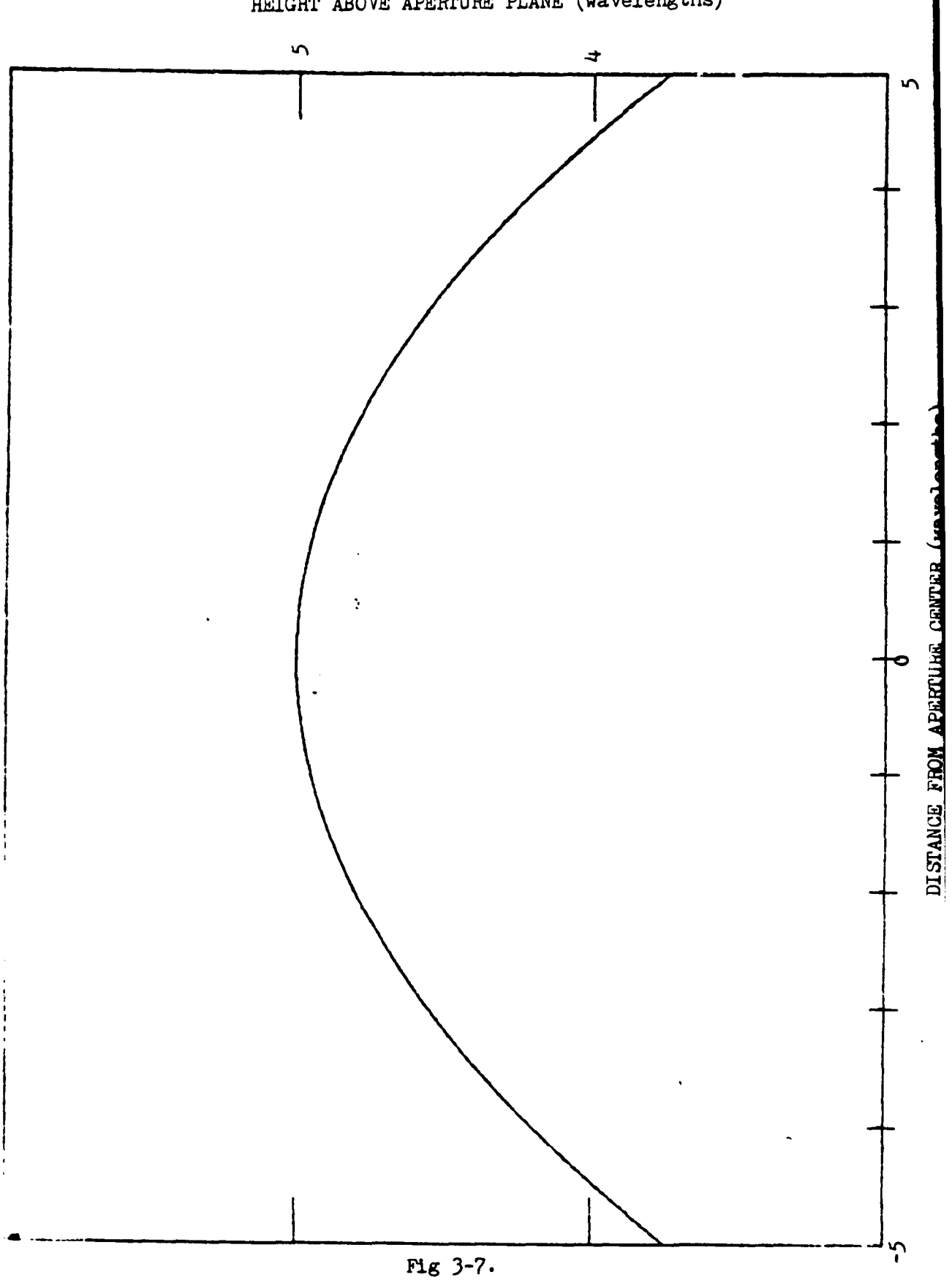
HEIGHT ABOVE APERTURE PLANE (wavelengths)
5
4
5
0
-5
DISTANCE FROM APERTURE CENTER (wavelengths)

Fig 3-7.

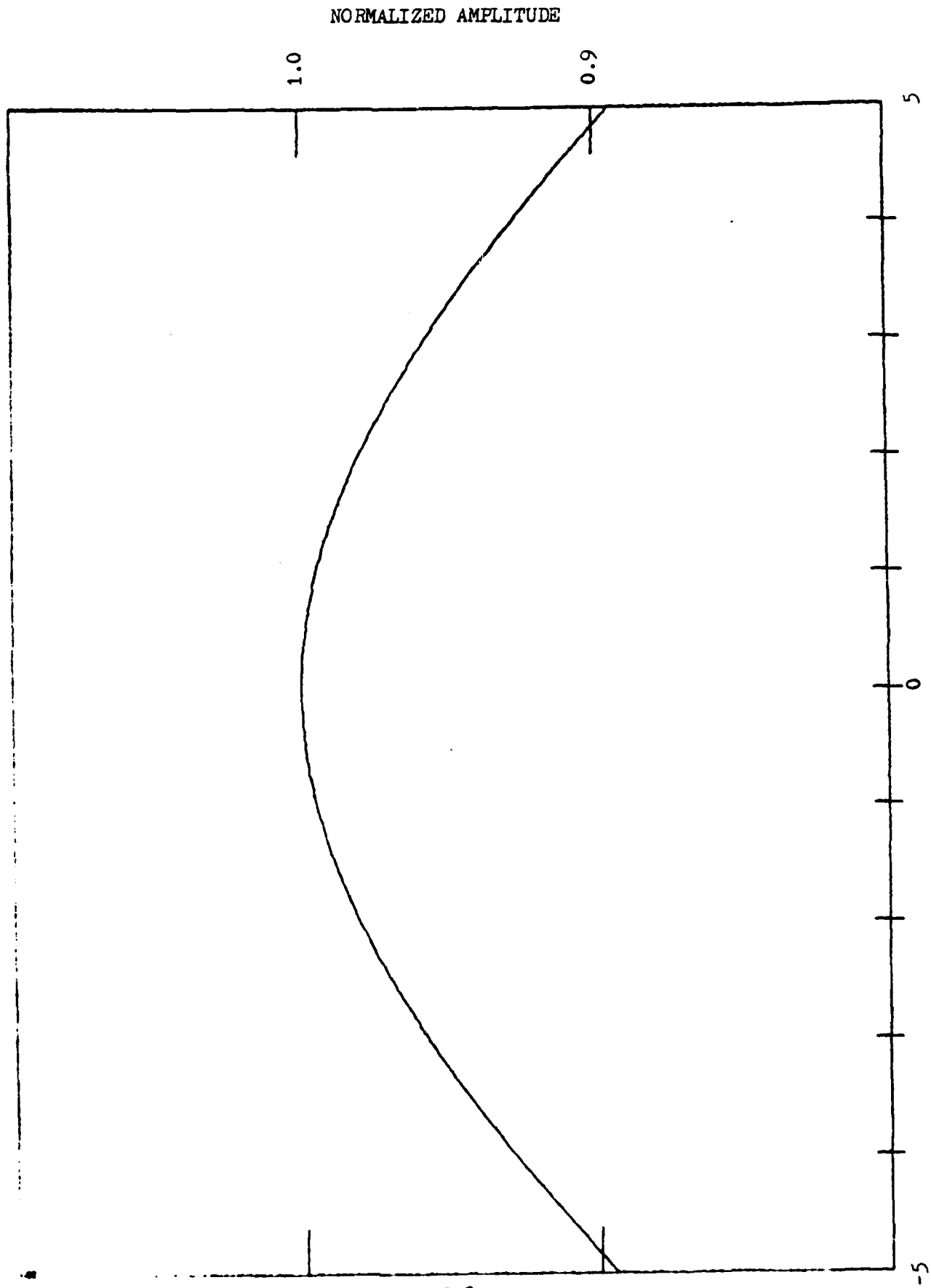

Fig 3-8.

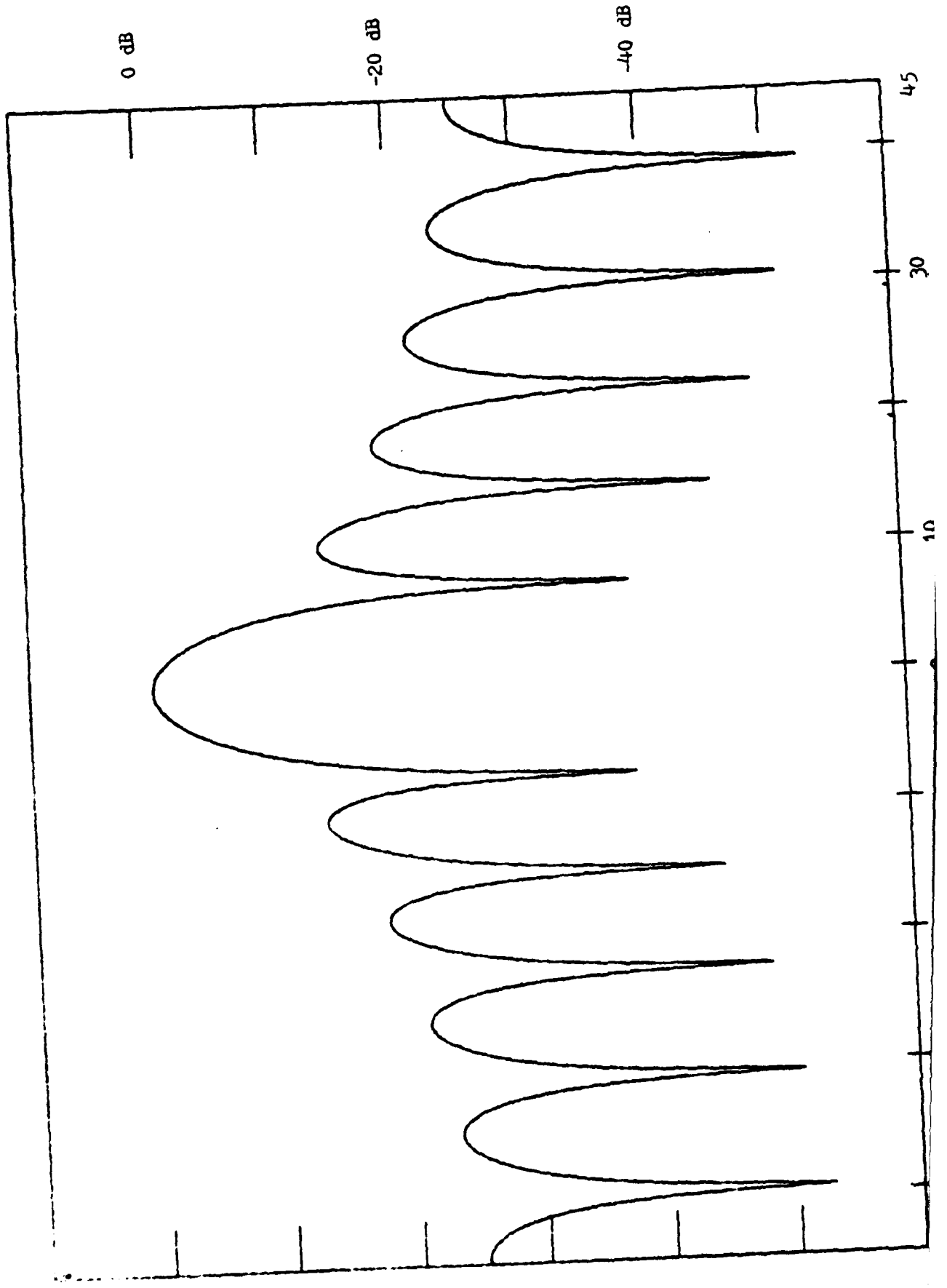

Fig 3-9.

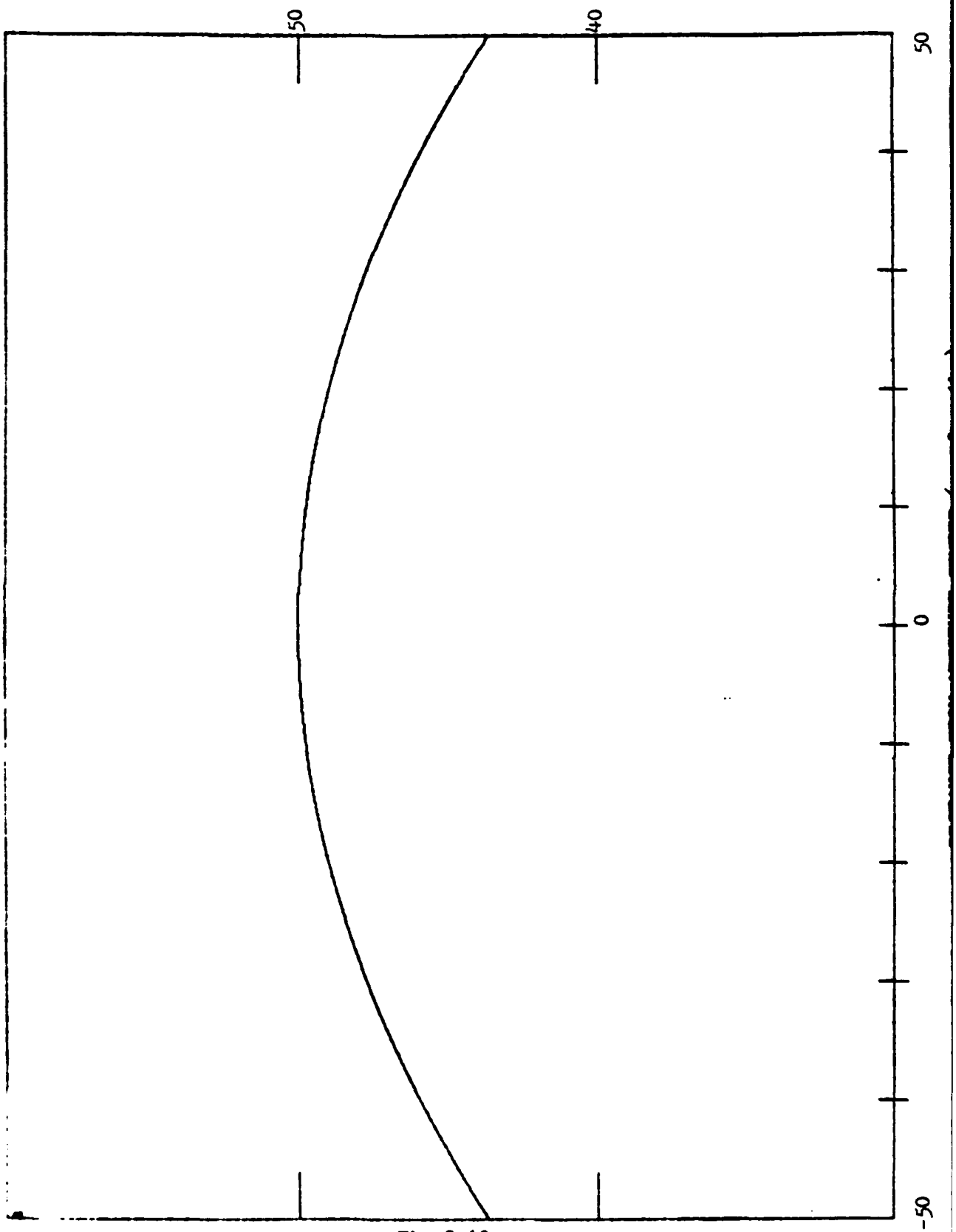

Fig 3-10.

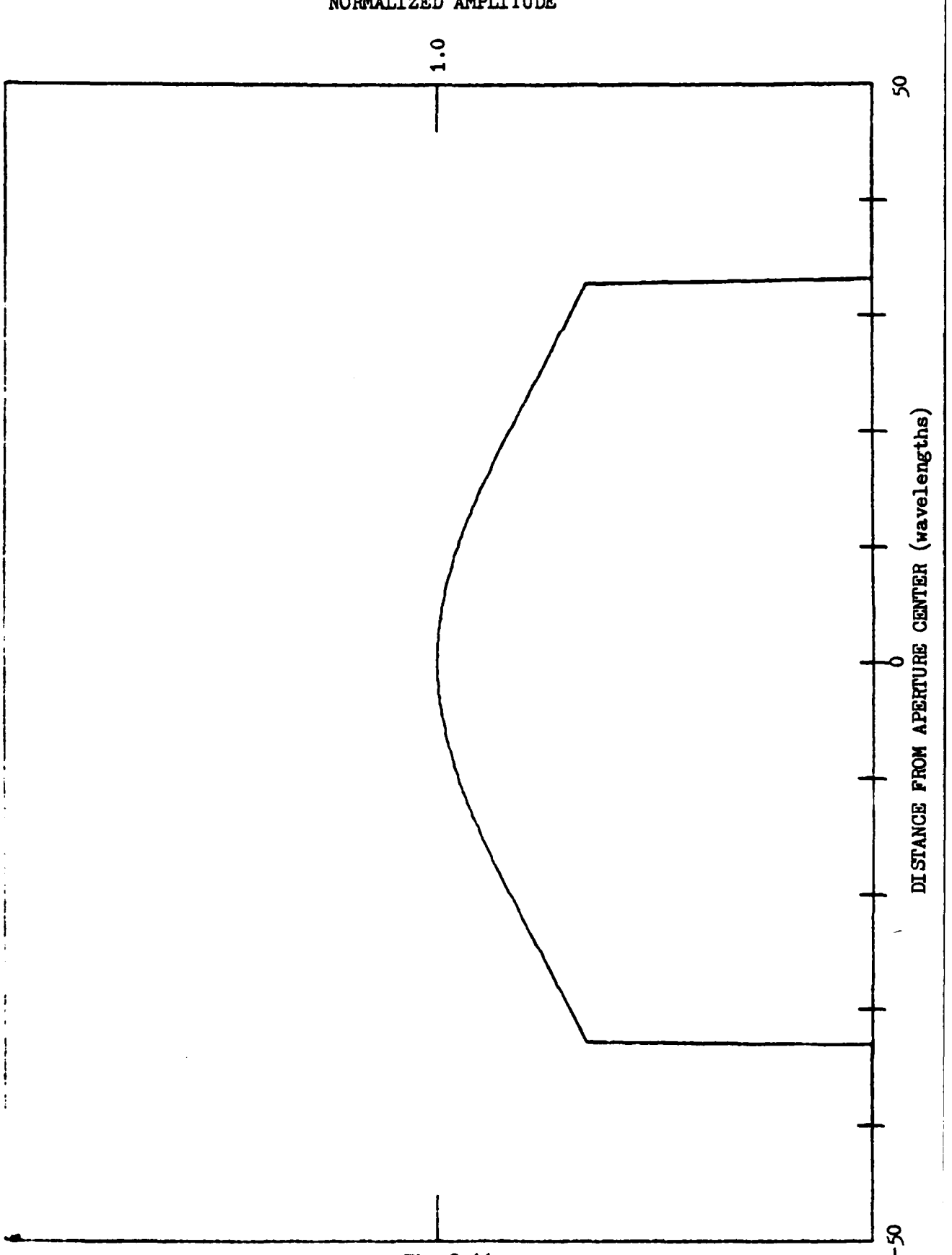
NORMALIZED AMPLITUDE
1.0
50
0
-50
DISTANCE FROM APERTURE CENTER (wavelengths)

Fig 3-11.

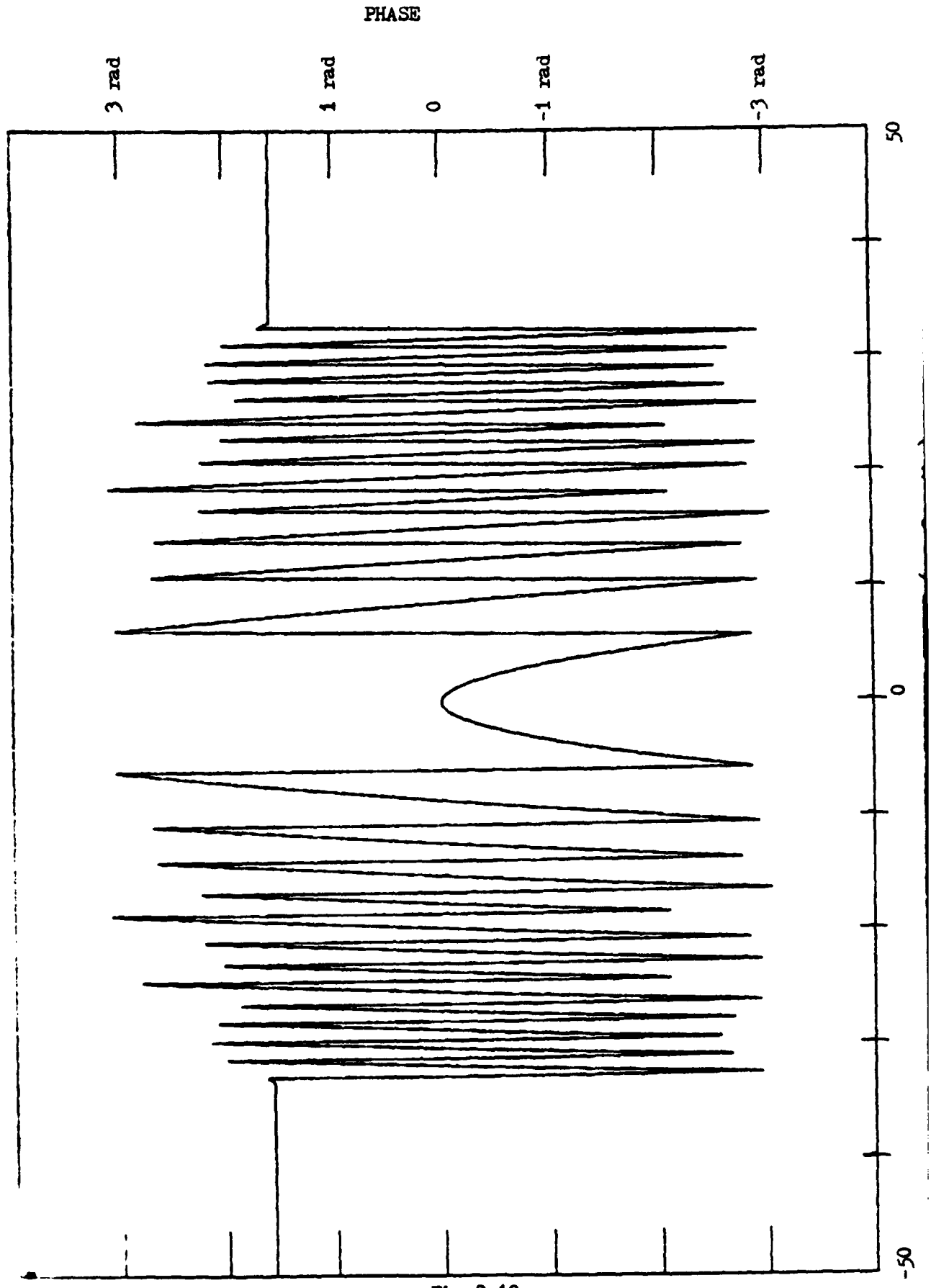

Fig 3-12.

NORMALIZED AMPLITUDE

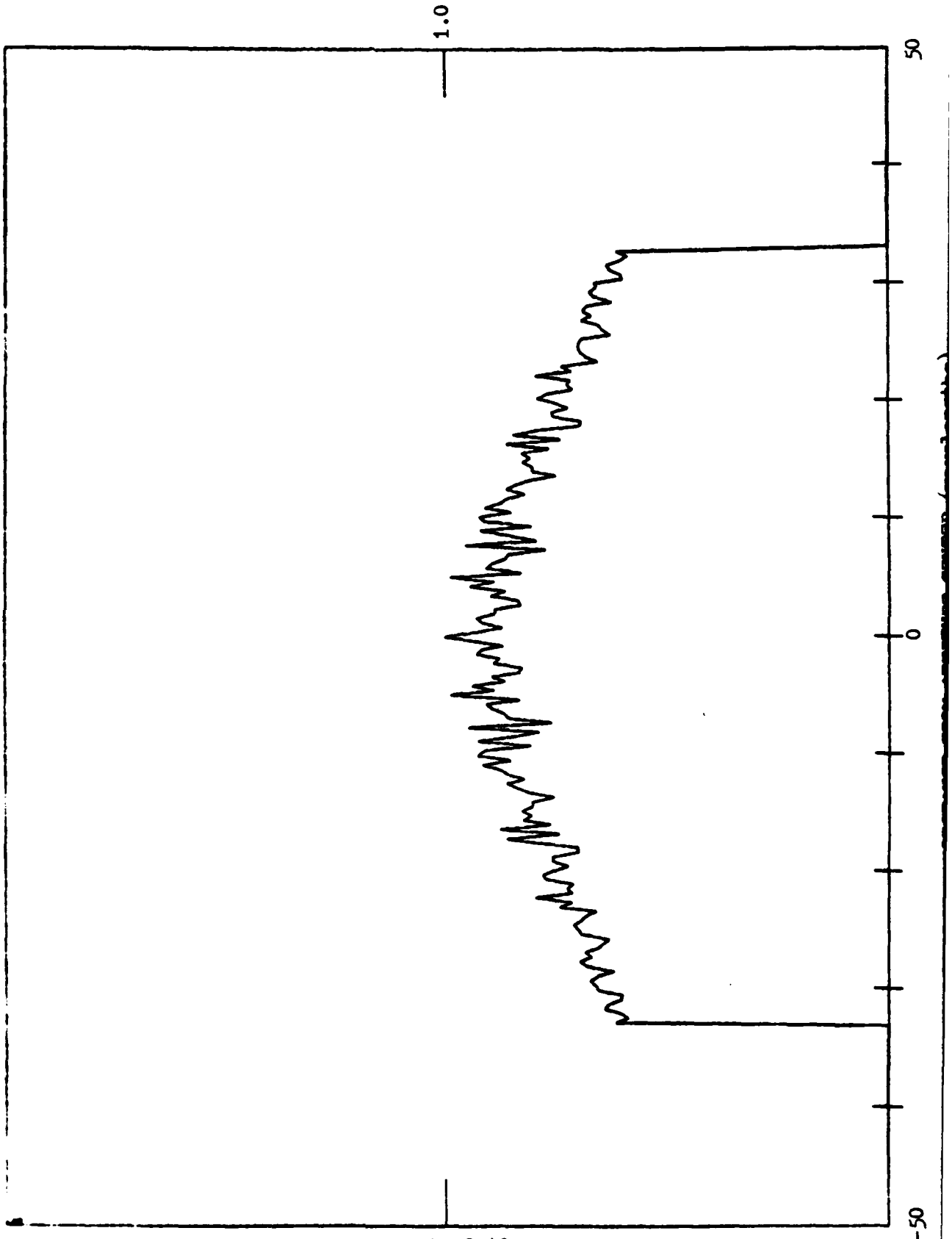

Fig 3-13.

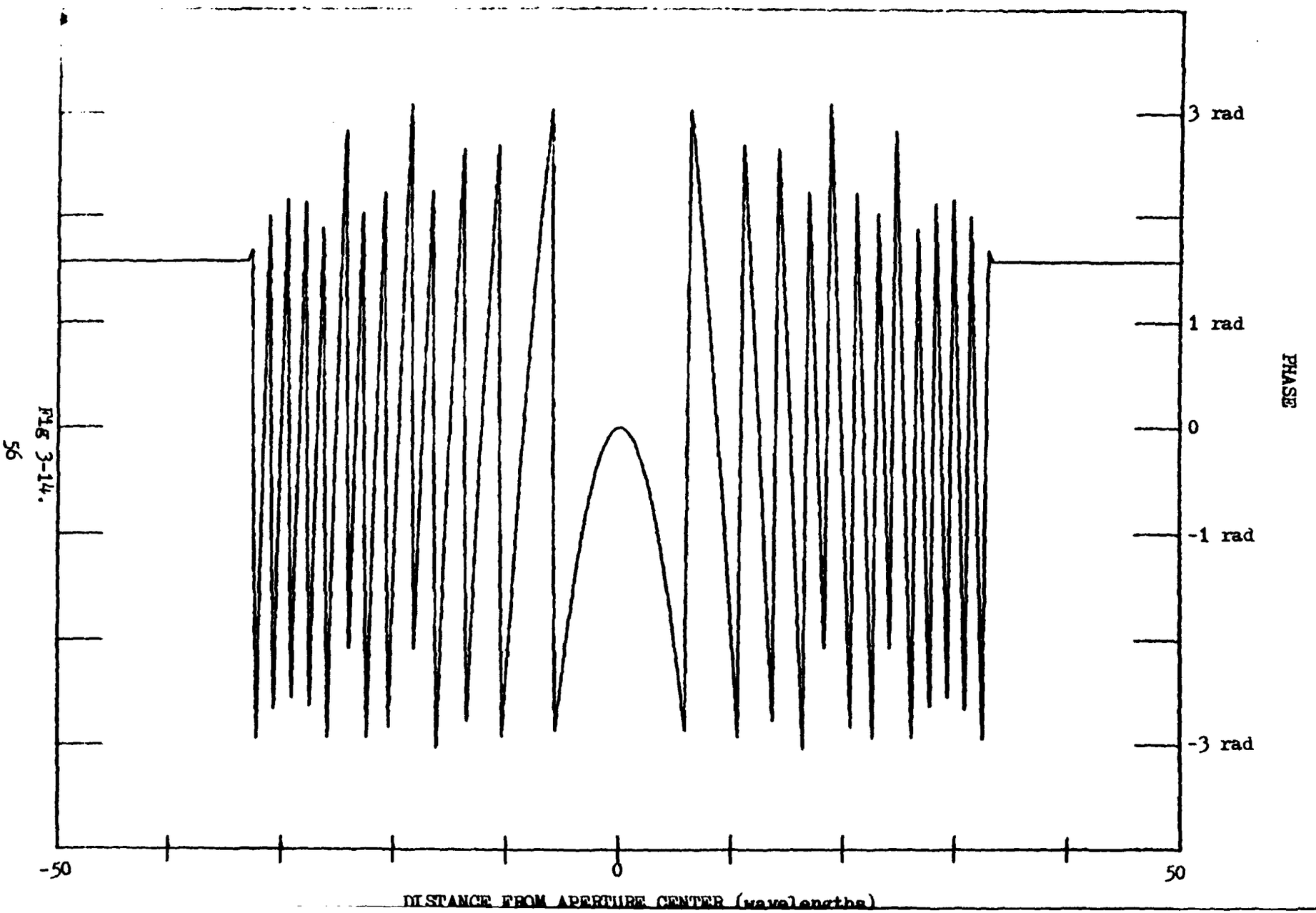
3 rad
1 rad
0
-1 rad
-3 rad
PHASE
-50
0
50
DISTANCE FROM APERTURE CENTER (wavelengths)

Fig 3-14.

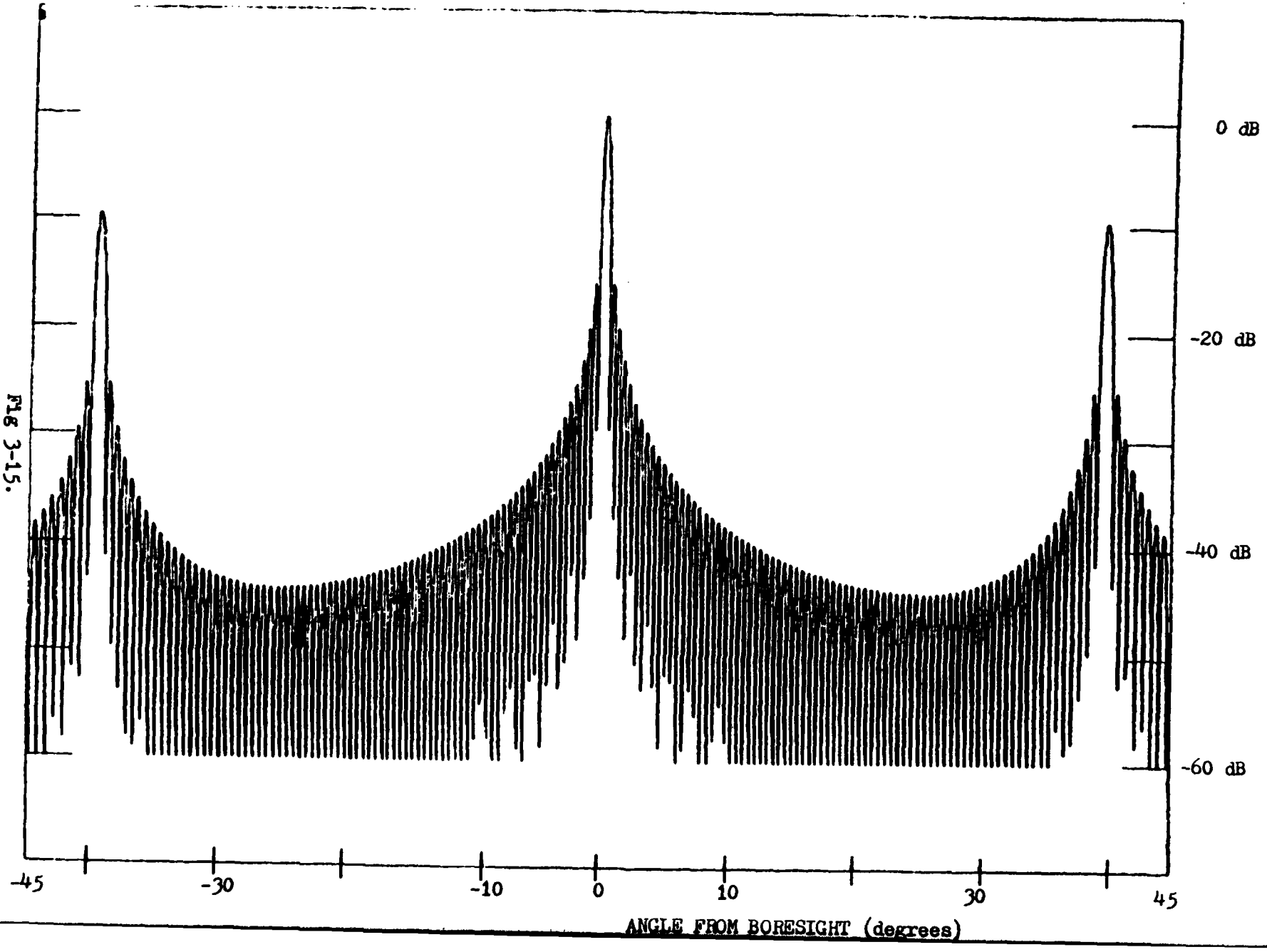
0 dB
-20 dB
-40 dB
-60 dB
-45
-30
-10
0
10
30
45
ANGLE FROM BORESIGHT (degrees)

Fig 3-15.

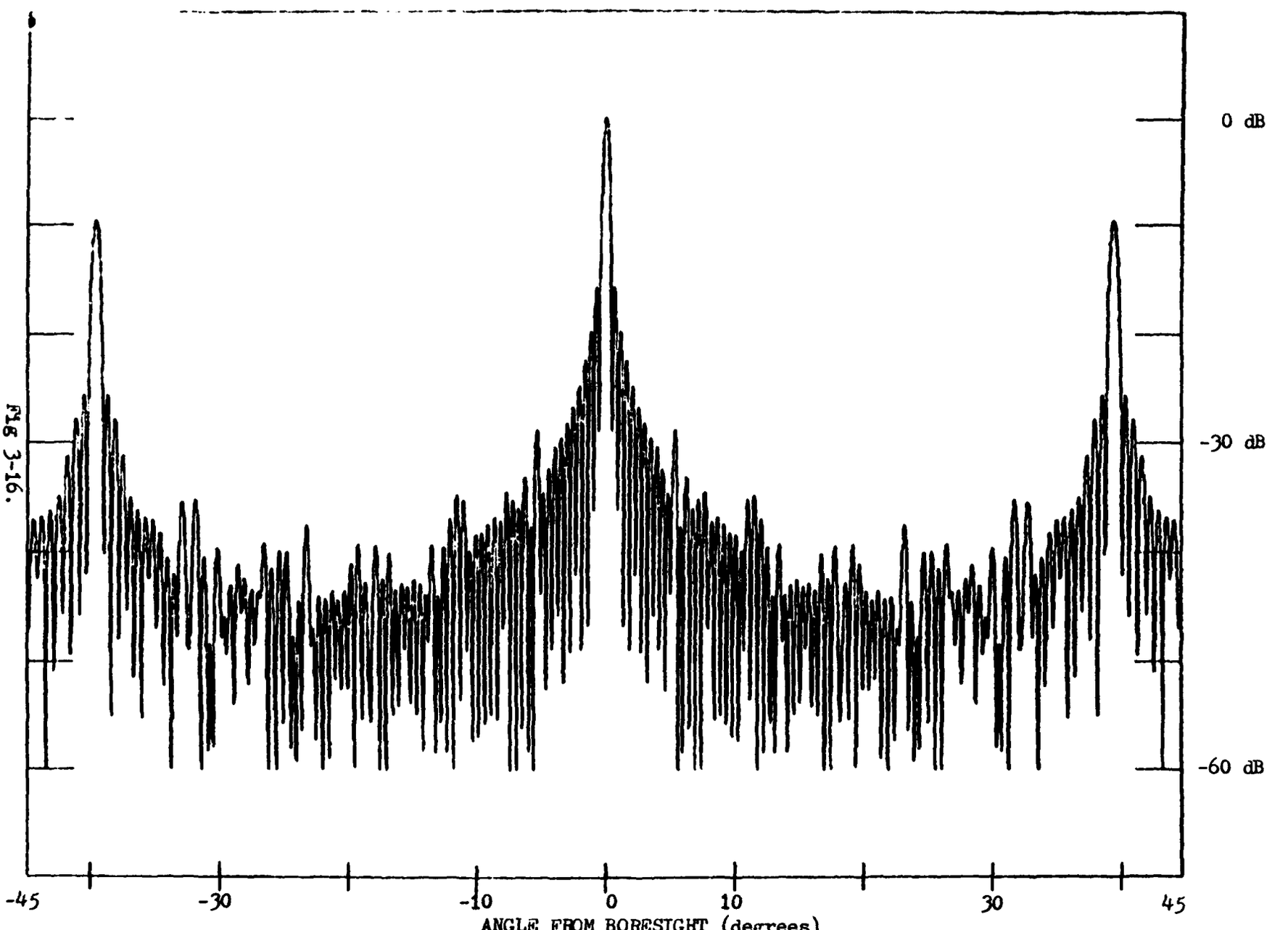

Fig 3-16.

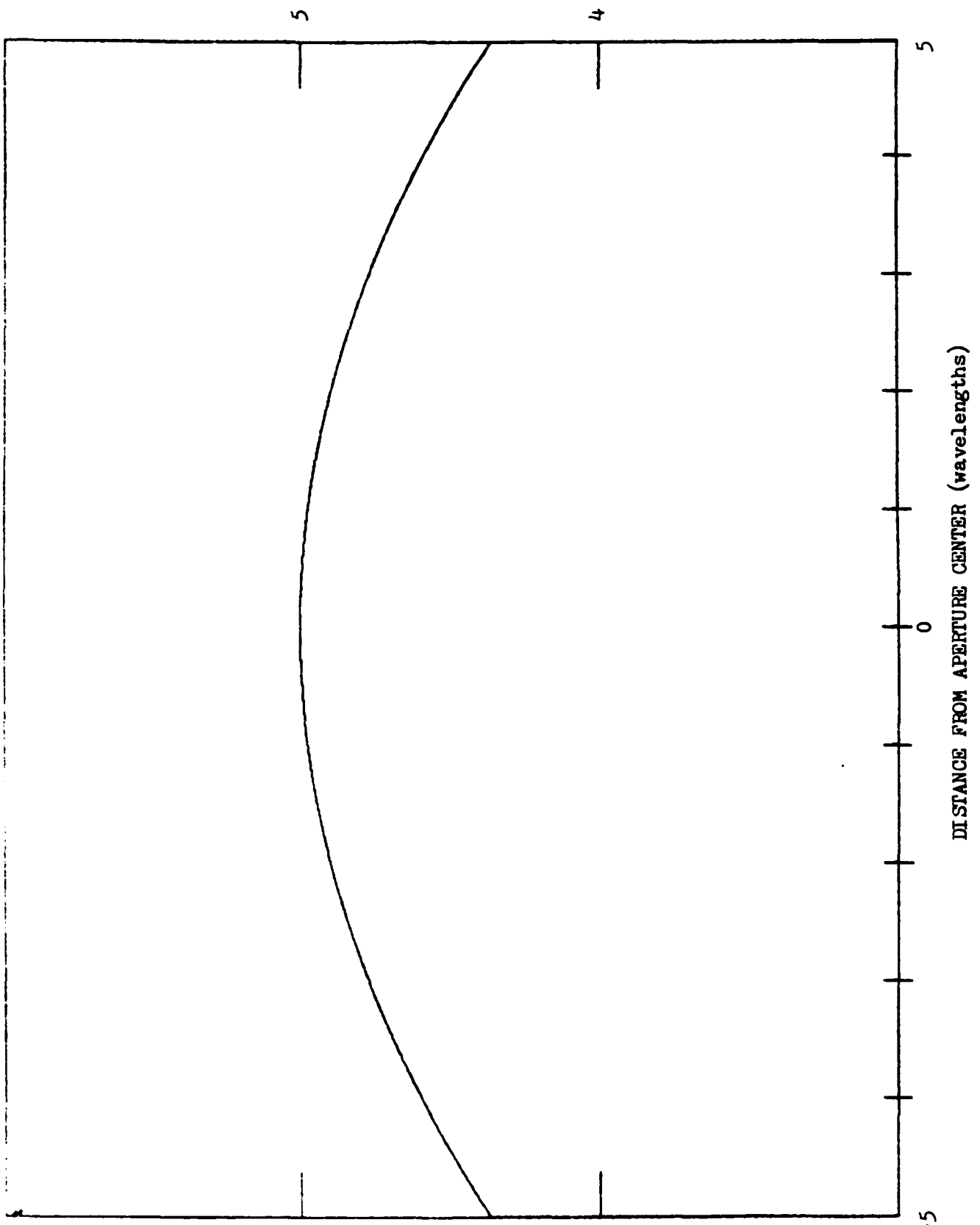
HEIGHT ABOVE APERTURE PLANE (wavelengths)
5
4
5
0
-5
DISTANCE FROM APERTURE CENTER (wavelengths)

Fig 3-17.

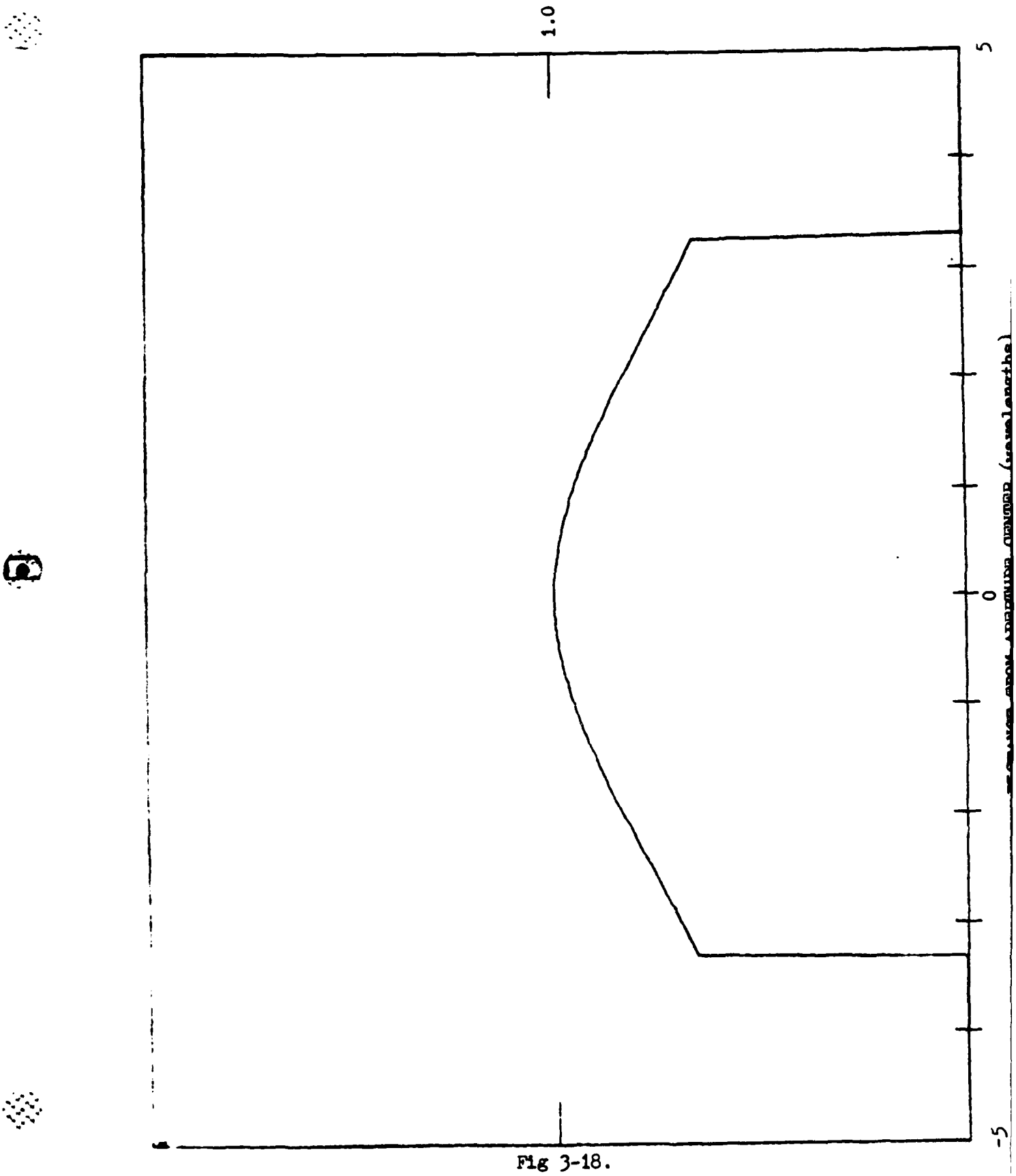

Fig 3-18.

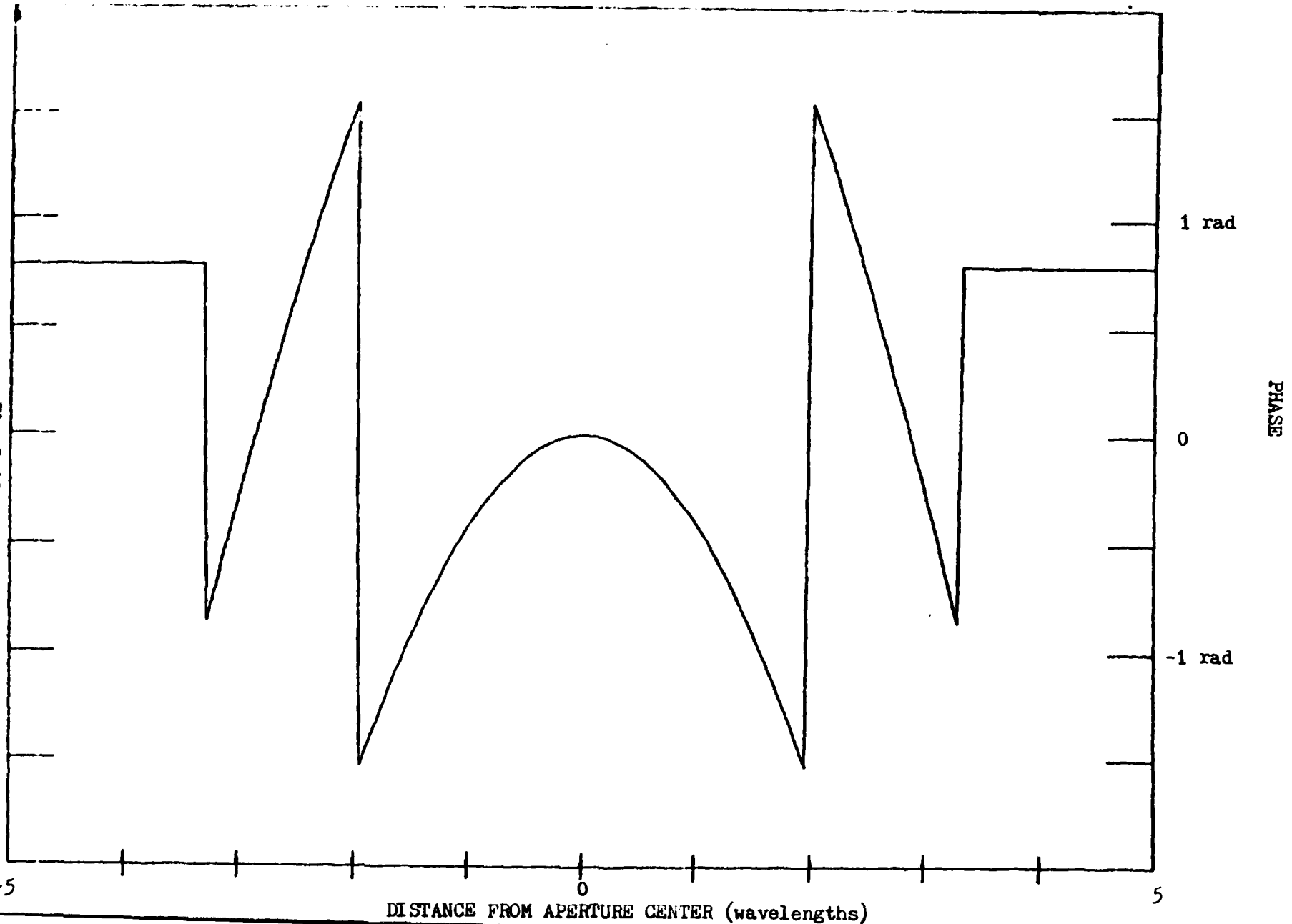
1 rad
0
-1 rad
PHASE
-5
0
5
DISTANCE FROM APERTURE CENTER (wavelengths)

Fig 3-19.

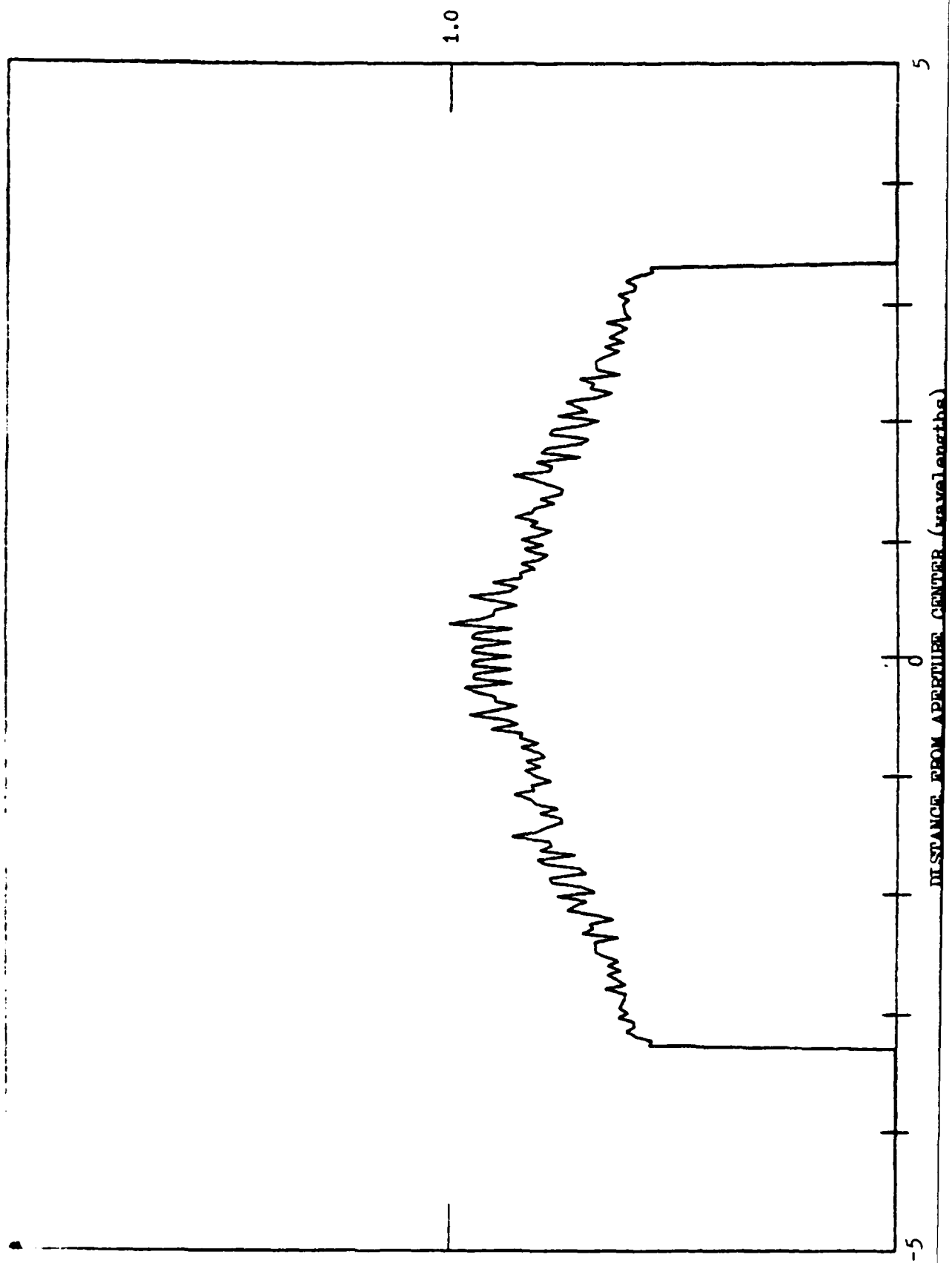
NORMALIZED AMPLITUDE
1.0
5
0
-5
DISTANCE FROM APERTURE CENTER (wavelengths)

Fig 3-20.

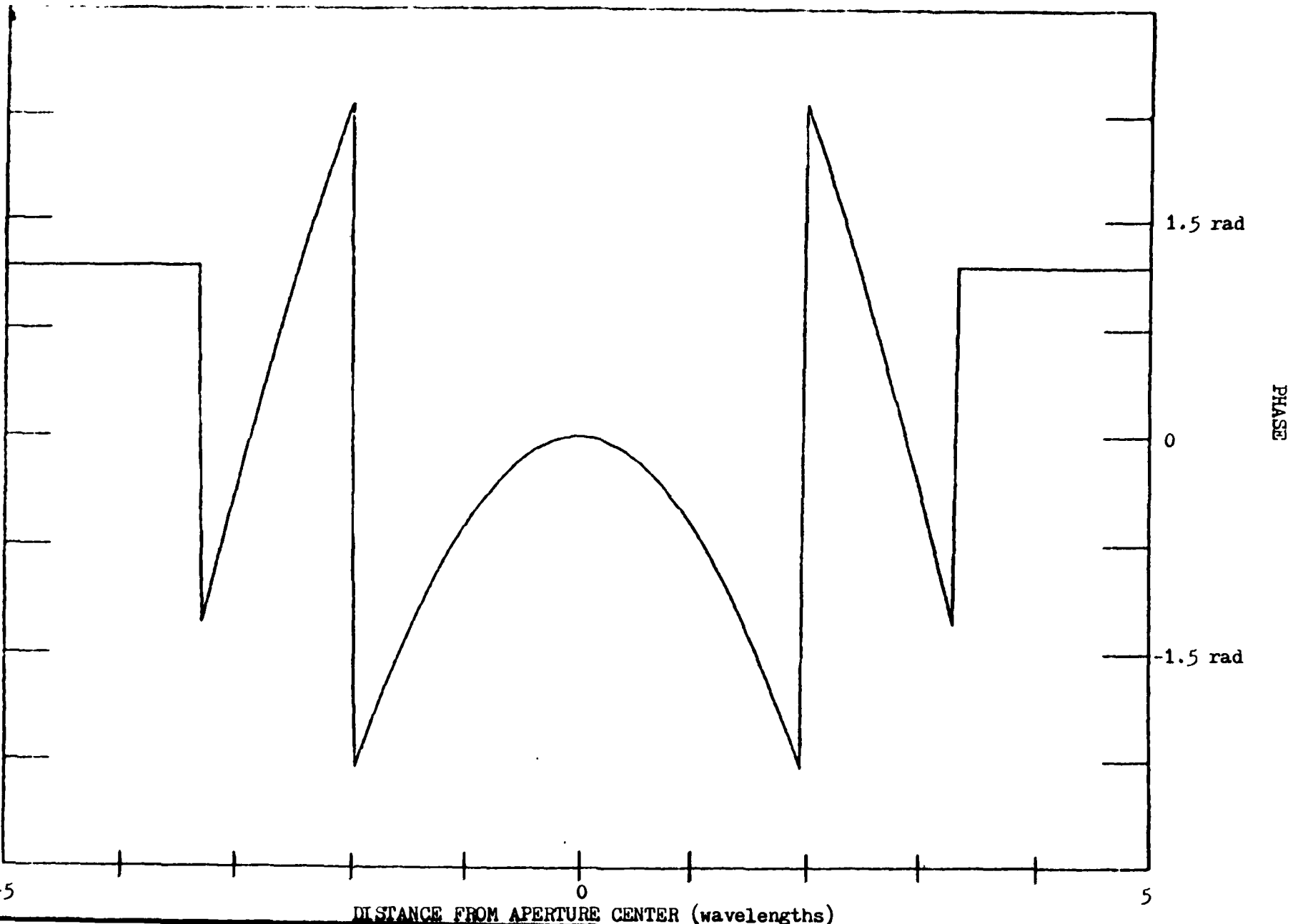
1.5 rad
0
-1.5 rad
PHASE
-5
0
5
DISTANCE FROM APERTURE CENTER (wavelengths)

Fig 3-21.

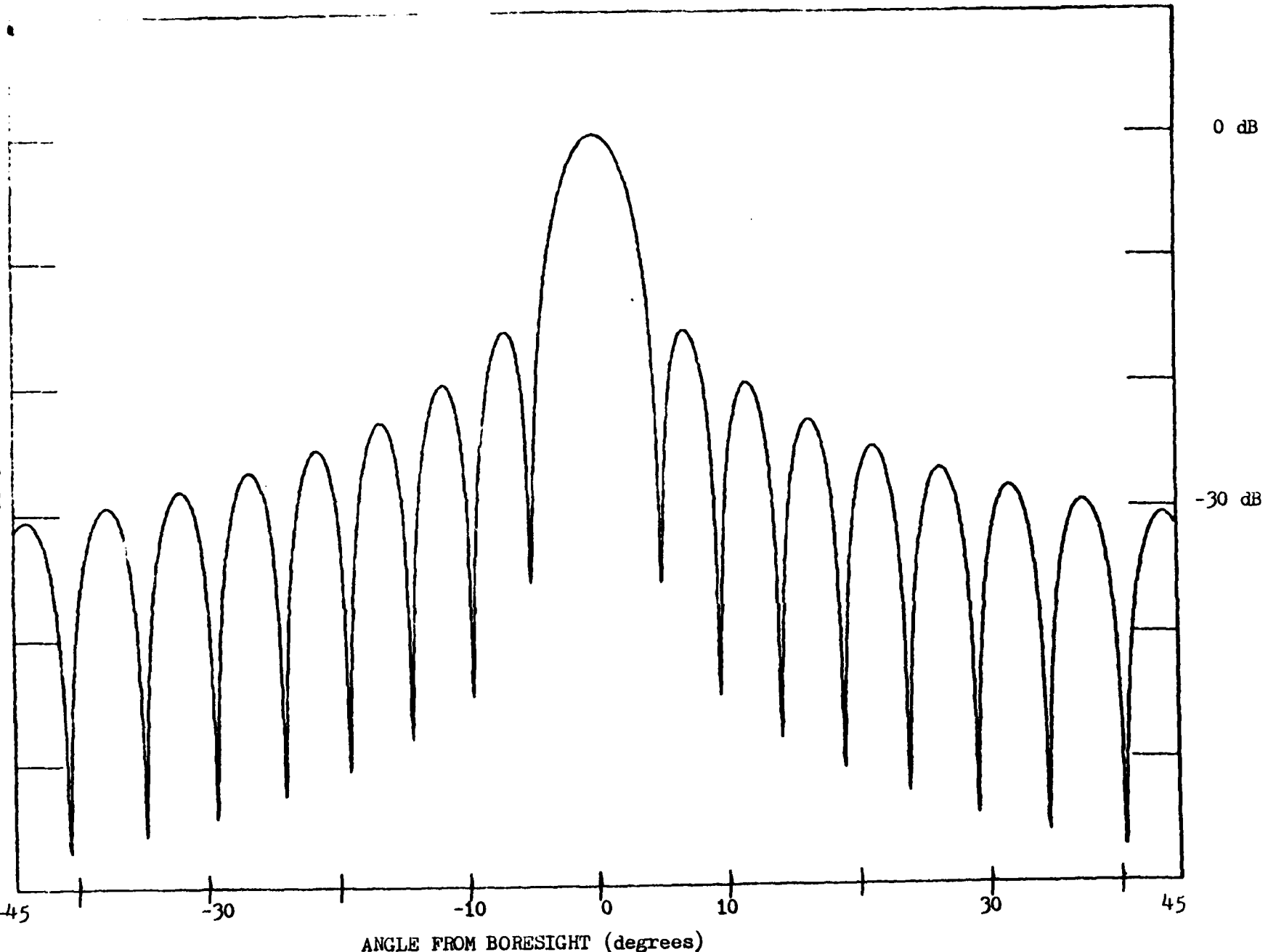

Fig 3-22.

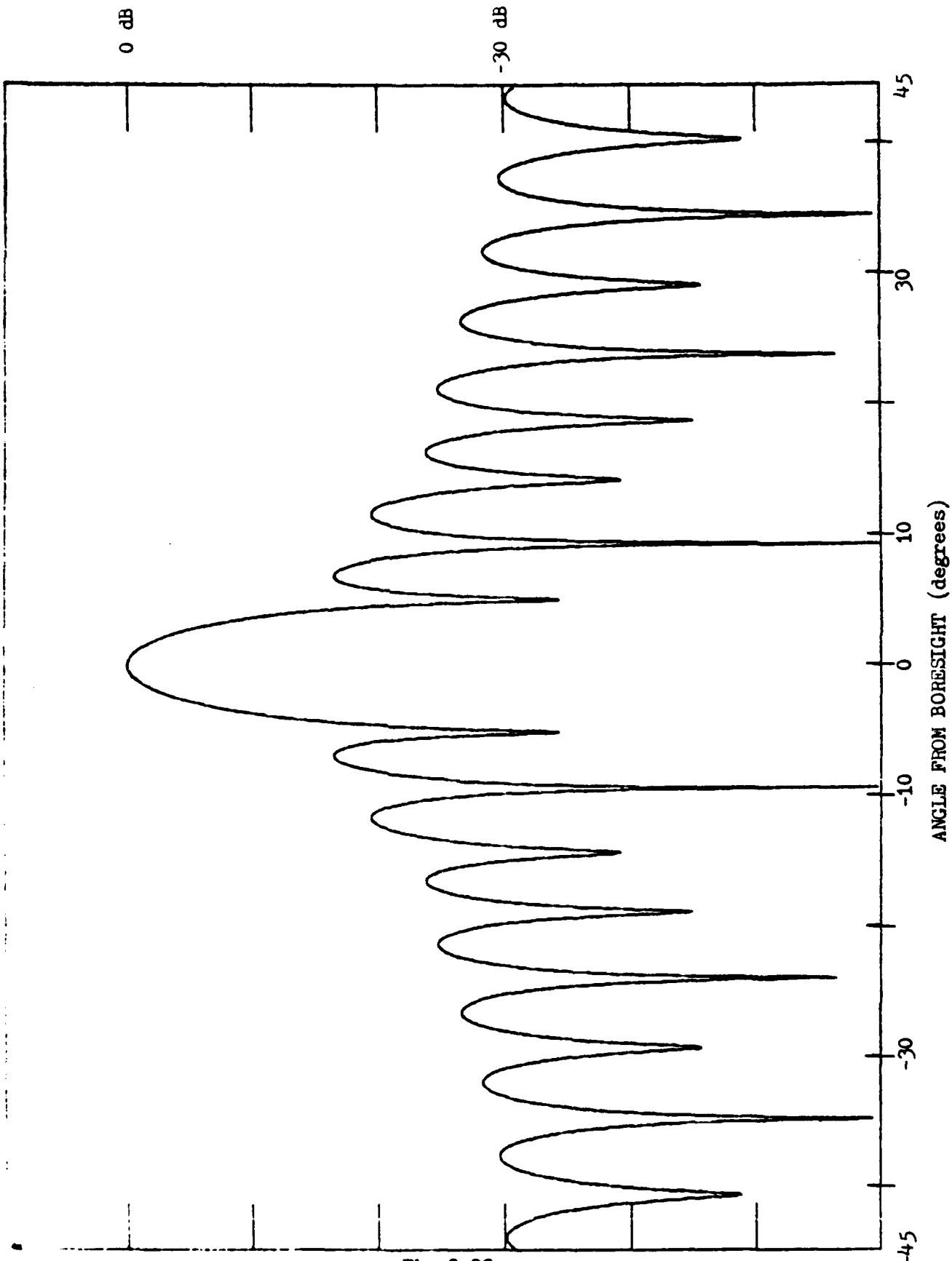

Fig 3-23.

dominant in determining null location. A comparison of patterns is in order. Figure 3-15 shows the pattern resulting from the analytic derivative distribution. Figure 3-16 shows the pattern of the messy distribution. The amplitude error has effected side-lobe levels and null depths but not null locations. The side-lobe level and null depth errors are noticeable, but not intolerable.

Figures 3-17 through 3-23 we correspond to Figures 3-10 through 3-16 for a spherical reflector with all the previously described dimensions reduced by a factor of ten. Comparing Figures 3-22 and 3-23 shows that null location has not been altered. Again, the effect of the amplitude error is limited to side-lobe level and null depth. Consequently, this work will continue to employ the technique of this section, even though the results are only qualitative, except for null location. Clearly, future work must refine the second derivative approximation.

IV Beamshaping

Reflector Equation

The simplest method for implementing a given antenna pattern applies geometrical optics to a known power pattern to get a reflector shape that generates the pattern (Ref 10: 497). The technique is crude, but might provide a first approximation (Ref 10: 497). If the reflector resulting from the method is physically unrealizeable, one cannot however, simply call the pattern unrealizeable. The method is not that conclusive. The reader should also note that, because the method is based on geometrical optics, only reflectors large compared to a wavelength should be considered.

Assuming that the desired power pattern is $P(y)$ between y_1 and y_2, one can generate a reflector as follows. Referring to figure 4-1 (Ref 10: 498), positive angles are clockwise from the horizontal and the distance from the feed point to the reflector surface for a given value of x is defined to be $r(x)$. The x is the angle from horizontal to the incident ray, while y is the angle from horizontal to the reflected ray. The y_1 and y_2 are the limits of the range over which one wished to specify $P(y)$; the pattern outside the range will be ignored, but the reader should be aware that diffraction effects will yield non-zero field. The pattern level will fall quickly outside the specified range as long as the size of the reflector meets geometrical optics criteria (Ref 10: 497). The x_1 and x_2 define the angular extent of the reflector. The geometry of figure 4-1, coupled with the law of reflection, leads to the equation defining the reflector contour (Ref 10: 498):

$$\frac{1}{r}\frac{dr}{dx} = \tan\frac{x - y}{2} \qquad (4\text{-}1)$$

Before one can integrate Eq (4-1), he must first find the relationship between y and x. This arises from power considerations. Geometrical optics demands that the power in a given tube of rays must remain constant (Ref 2: 404). Consequently, if no loss occurs at reflection, the power in the incident ray tube must equal that in the reflected ray tube (Ref 10: 499). Defining the incident power pattern from the feed as I(x) and considering incident and reflected ray tubes with angular width dx and dy respectively, energy conservation gives (Ref 10: 499):

$$I(x)\,dx = K\,P(y)\,dy \tag{4-2}$$

where the K is a constant of proportionality. The fact that the total power from the feed must equal the total reflected power determines the K from (Ref 10: 499):

$$\int_{x_1}^{x_2} I(u)\,du = K \int_{y_1}^{y_2} P(v)\,dv \tag{4-3}$$

To determine the relationship between y and x from Eq (4-2), one must consider that the power in any feed range x_1 to x will equal the power in some corresponding reflected range y_1 to y. Applying this information to Eq (4-2) yields (Ref 10: 499):

$$\int_{y1}^{y} P(u)\,du = \frac{1}{K} \int_{x_1}^{x} I(v)\,dv \tag{4-4}$$

Eq (4-4) defines y implicitly as a function of x. In order to simplify the calculations, I(x) = 1 was assumed, implying an isotropic feed over the range x_1 to x_2. Using this in Eqs (4-3) and (4-4) gives a simpler expression

for the right hand side of Eq (4-4):

$$\int_{y_1}^{y} P(u)\,du = \frac{x - x_1}{x_2 - x_1} \int_{y_1}^{y_2} P(v)\,dv \qquad (4\text{-}5)$$

One can think of Eq (4-5) as defining $g(y) = f(x)$. The y can be computed from this as $y = g^{-1}(f(x))$ which is y as a function of x. In general, y must be found through interpolation of numerical data, since the analytic integration of P(y) may not always be feasible.

To illustrate the use of this relationship, a simple example might prove useful. If one defines $P(y) = \csc^2(y)\cos(y)$ then is follows that:

$$\int_{y_1}^{y_2} P(u)\,du = \frac{1}{\sin(y_1)} - \frac{1}{\sin(y_2)} = P_r \qquad (4\text{-}6)$$

Similarly:

$$\int_{y_1}^{y} P(u)\,du = \frac{1}{\sin(y_1)} - \frac{1}{\sin(y)} \qquad (4\text{-}7)$$

Sticking Eqs(4-6) and (4-7) into Eq (4-5) yields an expression for y:

$$y = \sin^{-1}\left[\left(\frac{1}{\sin(y_1)} - P_r\left(\frac{x - x_1}{x_2 - x_1}\right)\right)^{-1}\right] \qquad (4\text{-}8)$$

This can be used in solving for r(x).

Eq (4-4) enables one to integrate Eq (4-1) directly. Doing so results in an expression for the radial distance from the feed to the reflector surface for a given angle x (Ref 10: 499):

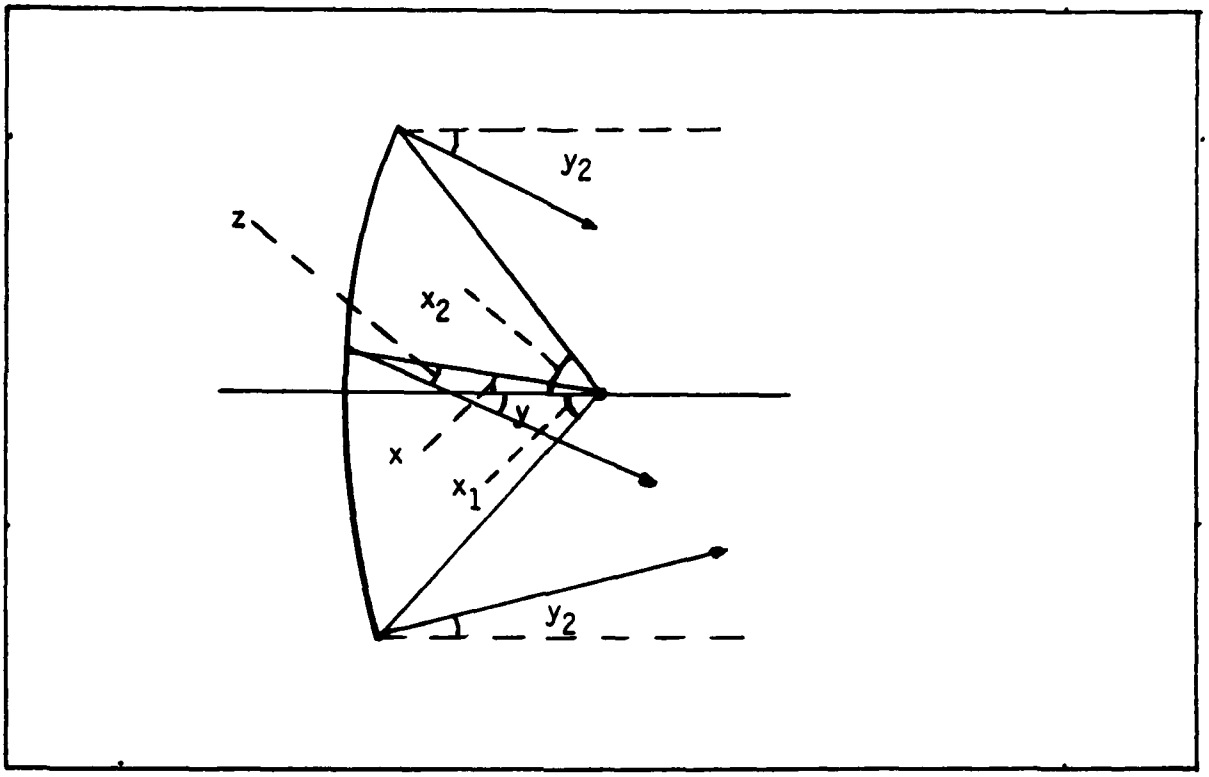

Fig 4-1. Geometry for Beamshaping

$$\ln \frac{r}{r_o} = \int_0^x \tan\left[\frac{u - y(u)}{2}\right] du \qquad (4\text{-}9)$$

This leads directly to:

$$r(x) = r_o \exp\left\{ \int_0^x \tan\left[\frac{u - y(u)}{2}\right] du \right\} \qquad (4\text{-}10)$$

The r_o is a scale factor which determines the absolute dimensions of the reflector. In choosing r_o, one must always remember that the contour was derived from geometrical optics principles and one's confidence in it should deteriorate as the size of the reflector decreases. Also, the technique ignores any phase considerations and is crude. It is really best applied to attempts to implement main-beam shapes, not patterns.

Implementation

As stated earlier, an isotropic feed simplifies calculations, so this was assumed. Therefore, Eq (4-5) applies. Furthermore, x_1 and x_2 were chosen as -60 degrees and +60 degrees respectively. This gives $x_2 - x_1 = 120^o$ and $(x - x_1)/(x_2 - x_1) = (3x + \pi)/(2\pi)$. Given this, the computerized application of beamshaping is simple:

1. Select y_1, y_2 , and $P(y)$.
2. Compute $P_r = \int_{y_1}^{y_2} P(u)\, du$.
3. Define $f(x) = P_r\, (3x + \pi)/(2\pi)$.
4. Tabulate $g(y) = \int_{y_1}^{y} P(u)\, du$ for y_1 to y_2.
5. Compute $y = g^{-1}(f(x))$ by interpolation whenever needed.
6. Tabulate $r(x)/r_o$ from Eq (4-10).
7. Compute r_o from chosen reflector diameter and choice for x_1 or x_2.
8. Scale $r(x)/r_o$ to get $r(x)$.

To illustrate beamshaping, a sin(x)/x example was computed. For this case, the expression for P(y) was:

$$P(y) = \left[\frac{\sin(\beta \frac{L}{2} \sin y)}{\beta \frac{L}{2} \sin y} \right]^2 \qquad (4\text{-}11)$$

where L was the diameter of the desired reflector, chosen to be 100 wavelengths. Figure 4-2 shows the result which is discernably parabolic.

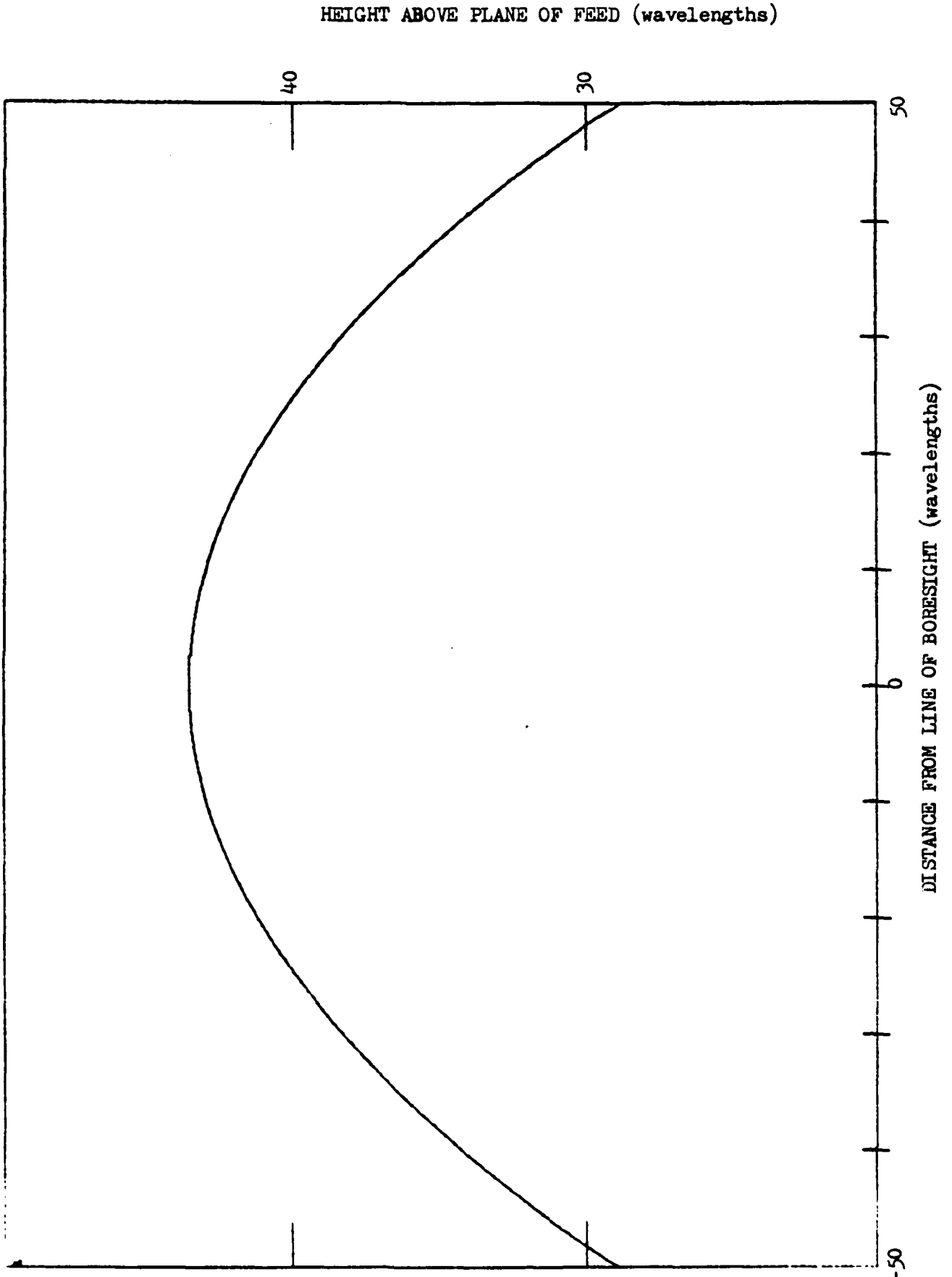
HEIGHT ABOVE PLANE OF FEED (wavelengths)
40
30
50
0
-50
DISTANCE FROM LINE OF BORESIGHT (wavelengths)

Fig 4-2.

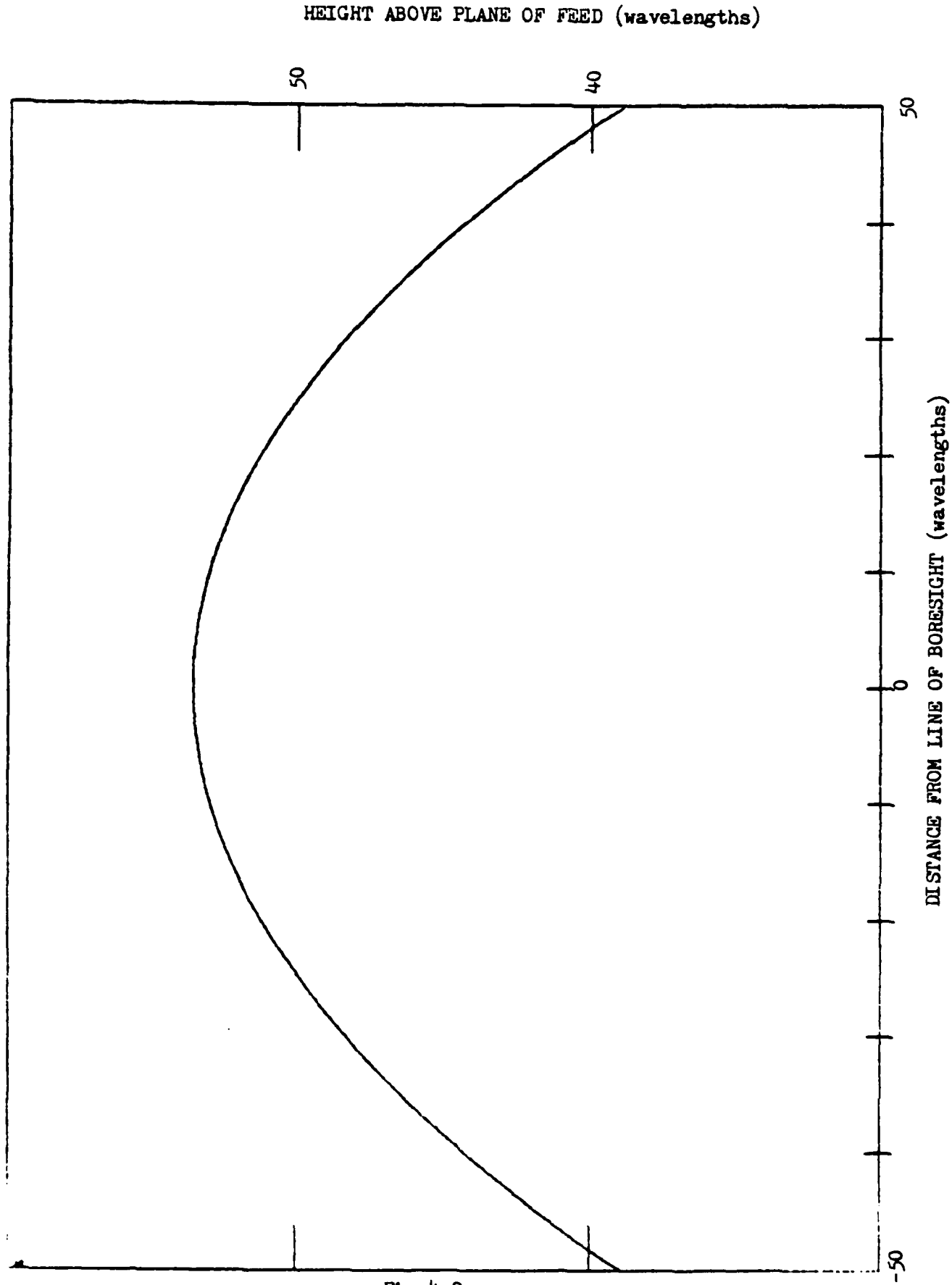
HEIGHT ABOVE PLANE OF FEED (wavelengths)
50
40
50
0
-50
DISTANCE FROM LINE OF BORESIGHT (wavelengths)

Fig 4-3.

Pattern Null Attempt

In order to find a nulled P(y) to use in the method of this section, the reader should refer to Eqs (1-20) and (1-22). These equations define the nulled pattern resulting from an Applebaum array of K elements. With uniform quiescent weighting, the quiescent pattern is a sin(Kx)/sin(x). For a continuous aperture with a uniform distribution on it, the pattern is a sin(x)/x. One might form a loose connection between the two cases and use the Sa(x) = sin(x)/x in place of the sin(Kx)/sin(x) in equation (1-20) when trying to find a nulled pattern for the case of apertures. Interpreting Kd as L and using Sa(x) instead of sin(Kx)/sin(x) in Eqs (1-20) and (1-22) yields:

$$P(y) = \left| Sa(\emptyset) - \exp(jz)\, Sa(\emptyset_j)\, Sa(z) \right|^2 \qquad (4\text{-}12)$$

where

$\emptyset = \beta \frac{L}{2} \sin y$

$\emptyset_j = \beta \frac{L}{2} \sin y_j$

$z = \beta \frac{L}{2} (\sin y - \sin y_j)$

y_j= angular location of desired null

The reflector resulting from this is shown in figure 4-3. The reader will note that the shape is the same as that for the sin(x)/x pattern shown in figure 4-2.

The beamshaping technique cannot adequately cover the nulling case, because it ignores all phase considerations. Its primary application is in the synthesis of reflector shapes which will produce a given main-beam configuration, such as the csc-squared beam discussed earlier. Pursuing it further is not recommended.

V Suggested Extensions and Summary

Refined Analysis

Before one can refine the analysis technique given in this work, he must first solve, or at least circumvent, the second derivative instability described in Section III and Appendix B. A possible fix might be to alter the computational perspective used in the program in Appendix D. Instead of calculating r_c as an intermediate step, one might do better by finding r_{cw} in one step:

$$r_{cw} = \frac{r_1}{1 + \frac{2\, f''(x_i)\, r_1}{(1 + (f'(x_i))^2)^{3/2} \cos d}} \qquad (5\text{-}1)$$

where r_c and r_{cw} are the physical radius of curvature of the reflector at x_i and the radius of curvature of the reflected wavefront respectively. The r_1 is the distance from the feed to the reflection point (x_i, y_i) and d is the angle of reflection with respect to the surface normal. Such a computational trick might smooth the results. The idea is due to Capt. Thomas Johnson, who was teaching at the Air Force Institute of Technology at the time of this writing.

Given that one finds a workable fix, he might seek an analysis technique which more faithfully reflects the actual fields and patterns. Much of the work discussed previously involved reflectors ten wavelengths across. One can justifiable question the accuracy of geometrical optics alone in such a case, since diffraction effects should be quite noticeable. Fig 3-18 shows a discontinuous aperture field which is common in a geometrical optics analysis. At ten wavelengths, however, one expects the field to vary much more smoothly. Generating the aperture field distribution with

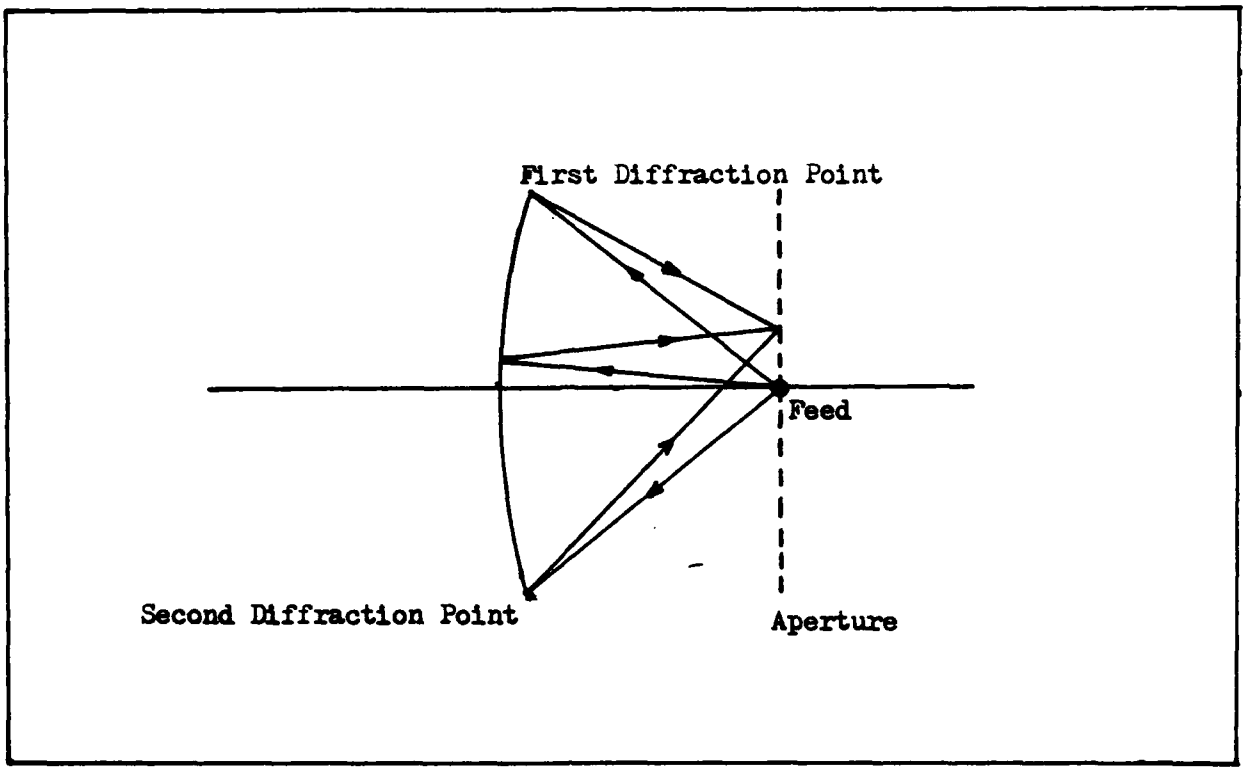

Fig 5-1. Simple GTD Geometry

a simple geometrical theory of diffraction (GTD) approach will do much for this problem. Such a technique could also be used to compute the far-field pattern; however, a GTD generated aperture field coupled with aperture integration would be more instructive in the nulling problem.

Figure 5-1 shows the simplest GTD model for the problem under consideration here. The total field at a point on the aperture is the sum of the contributions from all reflected rays and the two rays singly-diffracted from the edges (Ref 12: 484). The reflected rays are found by the methods of Section III. The calculation of the diffracted fields is discussed elsewhere (Ref 12: 458-477); a straightforward method specialized to the problem at hand can be found in Appendix C for the reader's convenience. Higher order effects decrease in significance with increasing reflector size, inclusion of these is a discretionary matter.

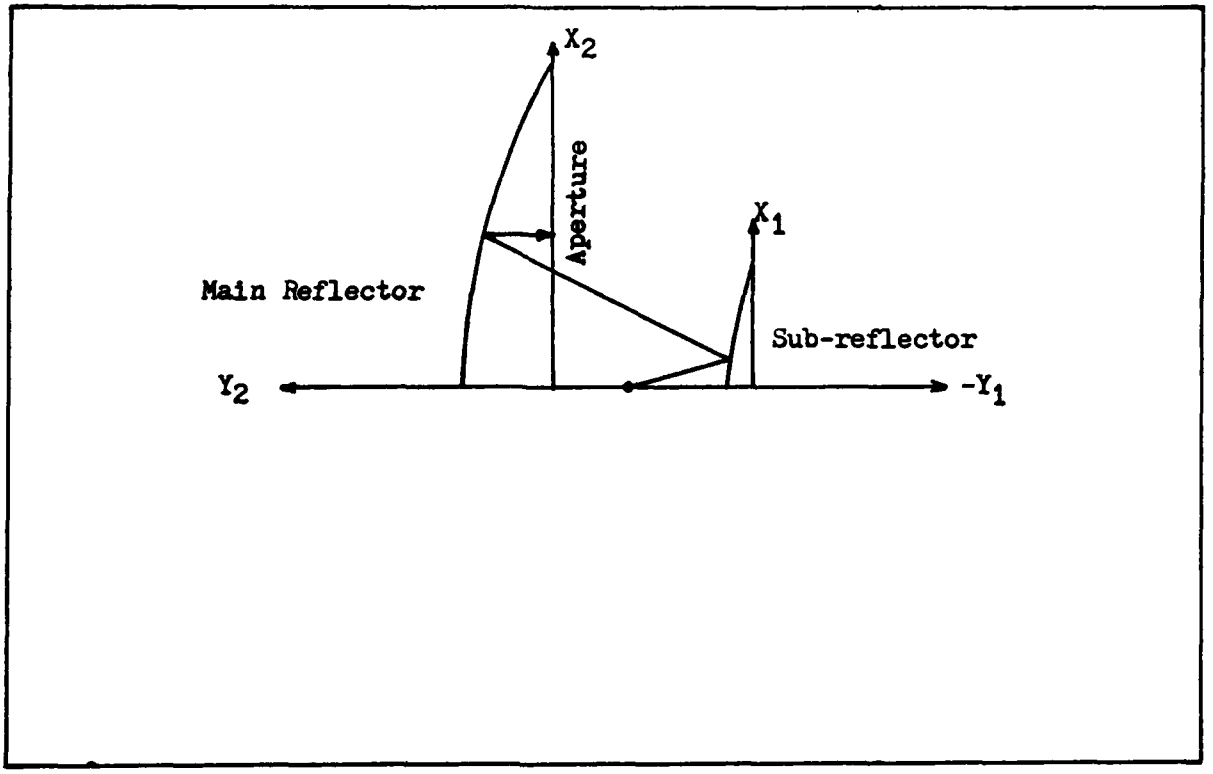

Fig 5-2. Galindo Dual Reflector

Suggestion for Implementing Distributions

The most promising technique for implementing the distributions of Section II is due to Galindo (Ref 2). The method employs the principles of geometrical optics to implement arbitrarily specified aperture amplitude and phase distributions with a dual reflector geometry as shown in figure 5-2 (Ref 2: 404). The problem eventually reduces to the numerical solution of a coupled pair of first order, non-linear, ordinary differential equations (Ref 2: 404). The development is intricate and the interested reader should look to Reference 2 for an explanation of the method. This method is designed for dual reflectors like that in figure 5-2; however, one might be able to apply the principles behind the analysis to a single reflector and develop a similar method, one that considers phase. Reference 8 presents a method based on Galindo's but computationally simpler; however,

its application to single reflectors does not look too promising.

Summary

Aperture integration provides a viable technique for considering pattern nulling with reflector antennas. It is directly analogous to the summation of element field contributions found in antenna array calculations. Consequently, the array weights given by Applebaum's adaptive array formulation can be used as discrete points in a continuous aperture distribution. Section II illustrated how these distributions resulted in nulled patterns.

In analyzing large reflectors with non-traditional contours, geometrical optics is quite useful. The usefulness of the method presented in Section III, however, is limited by the numerical instability of the second derivative approximation. The reader will note that the method performed better on the ten wavelength case than on the one hundred wavelength cases from a numerical standpoint. This improvement results from using the same number of discrete points in the ten wavelength cases as were used in the hundred wavelength cases, giving a smaller step size for the reflector grid. Unfortunately, as in most numerical analysis problems, further reducing the step size does not always give better results. Increasing the number of grid points in the ten wavelength examples in Section III in order to shrink the step size actually makes the problem worse. The fix given at the beginning of this section seems the best candidate for a solution. Given that the numerical problem can be removed, the ray-tracing/geometrical optics analysis could be useful in further work. Coupling it with a formulation of geometrical theory of diffraction can make it even more useful.

The beamshaping method presented in Section IV is already well known. It is easy to implement, but too simplistic for the problem under consideration.

The results are unacceptable when applied to pattern nulling, possibly because all phase considerations are ignored. The method was originally designed to synthesize main-beam shapes and is out of its depth in the nulling problem. Galindo's method should provide a good baseline for further studies. Other methods for dual off-set reflectors, also based on geometrical optics, may also prove useful.

Appendix A: Applebaum Control Equation Verification

Verifying the Applebaum control equation demands that one first find an expression for the signal-to-noise ratio and then show that the control law weights in fact maximize the S/N. As a first step, one computes the outputs v_s and v_n (Ref 1: 586):

$$v_s = \alpha \sum_{i=1}^{k} w_i s_i \tag{A-1}$$

$$v_n = \sum_{i=1}^{k} w_i n_i \tag{A-2}$$

If one defines weight vector $W = [w_1 \ . \ . \ . \ w_k]^T$ and noise vector $N = [n_1 \ . \ . \ . \ n_i]^T$ (Ref 1: 590) along with the signal vector defined in Section I, he can simplify the expressions:

$$v_s = \alpha W^T S \tag{A-3}$$

$$v_n = W^T N \tag{A-4}$$

The next step in determining the signal-to-noise ratio is computing the noise power in the output. This is given by (Ref 1: 586):

$$\begin{aligned} P_n &= E\,[|v_n|^2] \\ &= E\,[v_n^* v_n] \\ &= E\,[(W^T N)^*(W^T N)] \end{aligned} \tag{A-5}$$

Noting in Eq (A-5) that $W^TN = N^TW$, one can further write (Ref 1:586):

$$P_n = (W^T)*E[N*N^T]W \tag{A-6}$$

However, $E[N*N^T] = M$, the noise covariance matrix (Ref 1:586). This leads to the following equation for noise power:

$$P_n = (W^T)*MW \tag{A-7}$$

The matrix M is Hermitian and positive definite, so it can be diagonalized by a coordinate transformation (Ref 1: 586). If one calls the transformation matrix A, the signal and noise vectors in the transformed coordinates become:

$$\hat{S} = AS \tag{A-8}$$

$$\hat{N} = AN \tag{A-9}$$

To compute P_n under this transformation, one proceeds as follows:

$$v_n = \hat{W}^T\hat{N} \tag{A-10}$$

Substituting Eq (A-9) into Eq (A-10) results in:

$$\begin{aligned} v_n &= \hat{W}^TAN \\ &= (A^T\hat{W})^TN \end{aligned} \tag{A-11}$$

Comparing Eq (A-11) with Eq (A-4) implies (Ref 1: 587):

$$W = A^T\hat{W} \tag{A-12}$$

Employing the transformed vectors gives noise power as (Ref 1: 587):

$$P_n = (\hat{W}^T)*E[\hat{N}*\hat{N}^T]W \tag{A-13}$$

But matrix A decorrelates the noise components and equalizes the power of each (Ref 1: 587). The $\hat{M}$ can be written (Ref 1: 587):

$$\hat{M} = E[\hat{N}*\hat{N}^T] = P_n I_k \tag{A-14}$$

Choose $P_n = 1$ and $\hat{M} = I_k$. Thus, Eq (A-13) becomes (Ref 1: 587):

$$P_n = (\hat{W}^T)*\hat{W} \tag{A-15}$$

Substituting Eq (A-12) into Eq (A-7) gives:

$$P_n = (\hat{W}^T)*A*MA^T\hat{W} \tag{A-16}$$

Comparing with Eq (A-15) indicates (Ref 1: 587):

$$A*MA^T = I_k \tag{A-17}$$

$$M = (A^TA*)^{-1} \tag{A-18}$$

To verify the control law, one starts with the optimum weight vector for a system with equal and uncorrelated noise components (Ref 1: 587):

$$\hat{W}_o = \mu S* \tag{A-19}$$

where μ is arbitrary.

Under the transformation, v_s is given by (Ref 1: 587):

$$v_s = \alpha \hat{W}^T S \tag{A-20}$$

Applying the Schwarz Inequality to Eq (A-20) yields:

$$|v_s|^2 \leq |\alpha|^2[(\hat{W}^T)*\hat{W}][(\hat{S}^T)*\hat{S}] \tag{A-21}$$

Substituting Eq (A-15) into Eq (A-21) shows that:

$$\frac{P_s}{P_n} \leq |\alpha|^2[(\hat{S}^T)^*\hat{S}] \tag{A-22}$$

This determines an upper bound for signal-to-noise ratio. If one shows that Eq (A-19) produces this upper bound, then he demonstrates the Eq (A-19) is optimal (Ref 1: 587).

Putting Eq (A-19) into Eq (A-20) enables one to compute the signal power out (Ref 1: 587):

$$\begin{aligned} P_s &= |v_s|^2 \\ &= |\alpha\mu(\hat{S}^T)^*\hat{S}|^2 \\ &= |\alpha|^2|\mu|^2[(\hat{S}^T)^*\hat{S}]^2 \end{aligned} \tag{A-23}$$

The noise power comes from replacing $\hat{W}$ in Eq (A-15) with $\hat{W}_o$ in Eq (A-19) (Ref 1: 587):

$$\begin{aligned} P_n &= (\hat{W}^T)^*\hat{W} \\ &= \mu^*(\hat{S}^T)^*\mu\hat{S} \\ &= |\mu|^2[(\hat{S}^T)^*\hat{S}] \end{aligned} \tag{A-24}$$

Dividing Eq (A-23) by Eq (A-24) leads to:

$$\frac{P_s}{P_n} = |\alpha|^2[(\hat{S}^T)^*\hat{S}] \tag{A-25}$$

Consequently, Eq (A-19) is optimal. However, the untransformed array weights are needed, not the transformed weights $\hat{W}$.

Substituting Eq (A-19) into Eq (A-12) gives an expression for the actual weights (Ref 1: 587):

$$W_o = A^T\hat{W}_o$$

$$= A^T(\mu\hat{S}^*)$$

$$= \mu A^T A^* S^* \qquad \text{(A-26)}$$

One can infer from Eq (A-18) that $M^{-1} = A^T A^*$ so that Eq (A-26) becomes (Ref 1: 587):

$$W_o = \mu M^{-1} S^* \qquad \text{(A-27)}$$

This verifies the Applebaum control law to be:

$$MW_o = \mu S^* \qquad \text{(A-28)}$$

Appendix B: Second Derivative Approximation

The error in the amplitude distribution revealed by the spherical reflector example in Section III arises directly from inaccuracies in the approximate computation of the second derivative at the impact point on the reflector surface. The errors in amplitude are severe because the radius of curvature of the reflector depends on the second derivative. The equation for the surface of Figure 3-10 is:

$$f(x) = \sqrt{R^2 - x^2} - h_c \qquad \text{(B-1)}$$

where $R = 200$, $h_c = 150$. The second derivative is:

$$f''(x) = -\frac{R^2}{(R^2 - x^2)^{3/2}} \qquad \text{(B-2)}$$

On $-50 < x < 50$, the second derivative is bounded by $-0.00551 < f''(x) < -0.005$; so $f''(x)$ is always small in magnitude. Since $f''(x)$ is in the denominator of the expression for the radius of curvature, small errors in f'' can generate wild variations in r_c. The results in significant error in the wavefront radius of curvature calculated from Eq (3-7). This is the root source of the amplitude error.

Unfortunately, as stated on page 205 of Reference 3,"the process of differentiating is basically an unstable process." The following formulas were used (Ref 3: 206):

$$f_o'' = \frac{f_1 - 2f_o + f_{-1}}{h^2} + \text{terms of order } h^2 \qquad \text{(B-3a)}$$

$$f''_o = \frac{-f_2 + 16f_1 - 30f_o + 16f_{-1} - f_{-2}}{12h^2} + \text{terms of order } h^4 \qquad \text{(B-3b)}$$

$$f''_o = \frac{f_1 - f_{-1}}{h} \text{ applied twice} \qquad \text{(B-3c)}$$

Eqs (B-3a) and (B-3b) yielded meaningless results, while B-3c produced data that clustered around the distribution found from using Eq (B-2) to compute the second derivative.

Experimenting with double precision arithmetic might generate better results; however, this will probably not solve the problem in general. In the most general case, the reflector will be the result of some other numerical algorithm. Employing double precision will most likely yield only a long string of meaningless digits, since one cannot know the reflector surface to arbitrary precision. A simple experiment conducted in the course of this work showed no difference between single and double precision amplitude results for the 10-wavelength spherical reflector. In this experiment, the second derivative was calculated with double precision, but the numerator differences in the difference quotients of Eq (B-3c) resulted from single precision arithmetic. This reflected that, in general, one cannot know f_{-1} and f_1 to arbitrary precision. Since no improvement followed from this, one must conclude that errors in the numerator difference, magnified through division by the small h^2, produce the error. Only if algorithms which generate the reflector grid can supply very great precision, will double precision arithmetic prove useful.

Appendix C: Diffracted Rays

The edge diffracted field is given by (Ref 12: 472):

$$E_d(s) = - D E_i A(s) \exp(-j\beta s) \qquad \text{(C-1)}$$

where

s = distance from diffraction point to observation point.
E_i = incident field phasor at diffraction point.
A(s) = 1/ s (Spatial Attenuation Factor).
D = diffraction coefficient.

The s is computed by simple analytic geometry, since the points of diffraction and observation are both known. For isotropic feed, the $E_i = \exp(-j\beta r_1)/\sqrt{r_1}$ where r_1 is the distance from feed to diffraction point.

Calculation of D is somewhat more involved. Figure C-1 shows the geometry. Naturally, the diffracted ray in question is the one which intersects the aperture point under consideration. The angle $\emptyset$ must be computed based on the location of the aperture point with respect to the point of diffraction. The $\emptyset'$, however, depends only on the feed location and the edge location. The angles are measured with respect to the tangent line to the curve at the edge. Once the angles have been determined, one should compute (Ref 12: 473-475):

$$L = \frac{s\, r_1}{s + r_1} \qquad \text{(C-2a)}$$

$$N_+^+ = \frac{\pi + (\emptyset + \emptyset')}{4\pi} \quad \text{rounded} \qquad \text{(C-2b)}$$

$$N_-^+ = \frac{\pi + (\emptyset - \emptyset')}{4\pi} \quad \text{rounded} \qquad \text{(C-2c)}$$

$$N_+^- = \frac{-\pi + (\phi + \phi')}{4} \quad \text{rounded} \tag{C-2d}$$

$$N_-^- = \frac{-\pi + (\phi - \phi')}{4} \quad \text{rounded} \tag{C-2e}$$

The N's are integers found by rounding the given expressions to the nearest integer (Ref 12: 475). They are in turn used to compute (Ref 12: 474):

$$a^+(\phi + \phi') = 2\cos^2\left[\frac{4\pi N_+^+ - (\phi + \phi')}{2}\right] \tag{C-3a}$$

$$a^-(\phi + \phi') = 2\cos^2\left[\frac{4\pi N_+^- - (\phi + \phi')}{2}\right] \tag{C-3b}$$

$$a^+(\phi - \phi') = 2\cos^2\left[\frac{4\pi N_-^+ - (\phi - \phi')}{2}\right] \tag{C-3c}$$

$$a^-(\phi - \phi') = 2\cos^2\left[\frac{4\pi N_-^- - (\phi - \phi')}{2}\right] \tag{C-3d}$$

Defining the following is helpful (Ref 12: 474):

$$Q = -\exp(-j\pi/4)/(4\sqrt{2\pi\beta}) \tag{C-4a}$$

$$K_1 = \cot\left[\frac{\pi + (\phi - \phi')}{4}\right] \tag{C-4b}$$

$$K_2 = \cot\left[\frac{\pi - (\phi - \phi')}{4}\right] \tag{C-4c}$$

$$K_3 = \cot\left[\frac{\pi + (\phi + \phi')}{4}\right] \tag{C-4d}$$

$$K_4 = \cot \frac{\pi - (\phi + \phi')}{4} \qquad \text{(C-4e)}$$

Also, F(X) as follows is needed (Ref 12: 474):

$$F(X) = j2\left|\sqrt{X}\right| \exp(jX) \int_{\sqrt{X}}^{\infty} \exp(-jt^2)\, dt \qquad \text{(C-5)}$$

With all the preceeding definitions, one can calculate the diffraction coefficient (Ref 12: 474):

$$D = Q\left[K_1 F(\beta L a^+(\phi - \phi')) + K_2 F(\beta L a^-(\phi - \phi')) - K_3 F(\beta L a^+(\phi + \phi')) + K_4 F(\beta L a^-(\phi + \phi'))\right] \qquad \text{(C-6)}$$

The reader should note that Eq (C-6) applies only to the problem at hand, a straight edge with an incident field parallel to the edge. The reader should consult Reference 12 and available literature for any other problems.

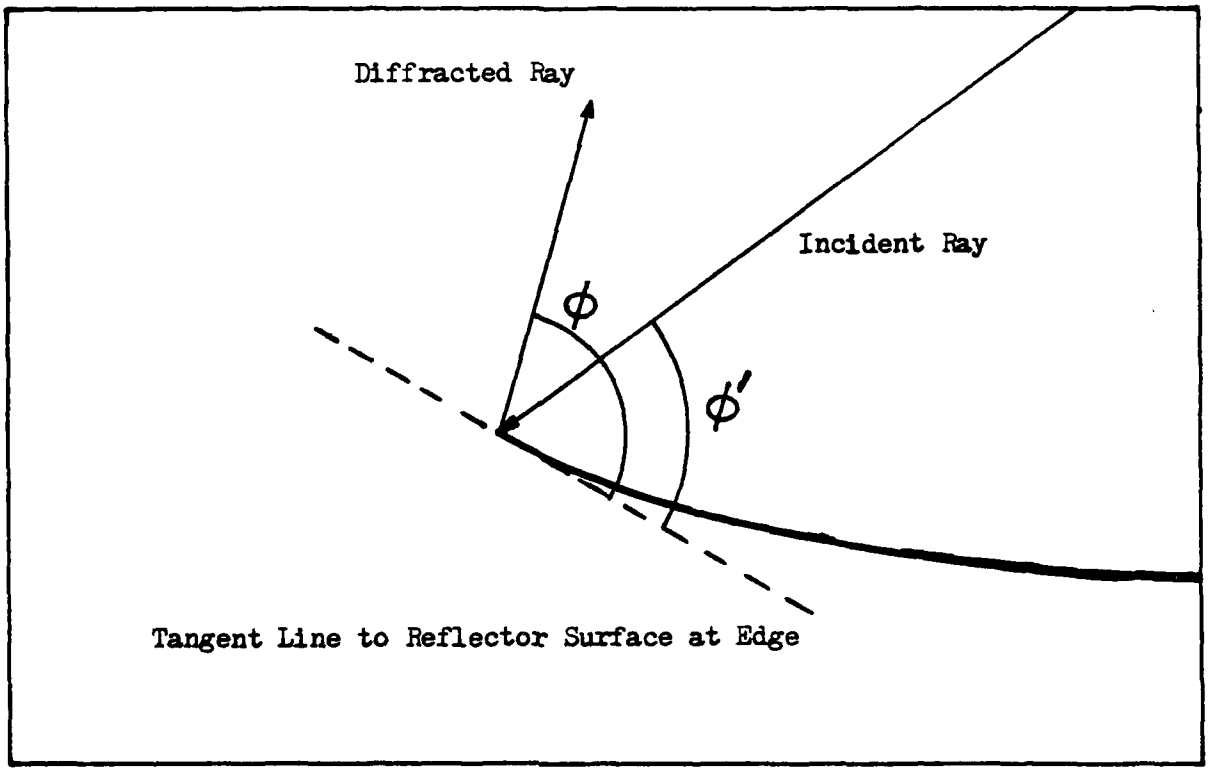

Fig C-1. Angles for Diffraction Coefficient

Appendix D: Programs

This appendix contains programs used in this work. The language is 77 standard Fortran. The purpose of each program or subroutine is noted in the listings themselves.

AD-A138 049 PATTERN NULLING BY REFLECTOR SHAPING(U) AIR FORCE INST 2/2
OF TECH WRIGHT-PATTERSON AFB OH SCHOOL OF ENGINEERING
D A HAVENS DEC 83 AFIT/GE/EE/83D-26

UNCLASSIFIED F/G 20/14 NL

END
FILMED
3-84
DTIC

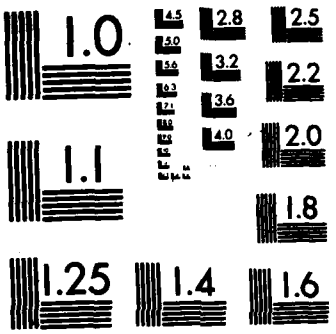

MICROCOPY RESOLUTION TEST CHART
NATIONAL BUREAU OF STANDARDS-1963-A

```
      Subroutine APTFLD(RZ,NGRID,TI,YA,NRAYS,EA,YEA,NAP)
*
*           APTFLD is the controlling routine for the ray tracing
*           method and will calculate an approximate aperture field.
*
*           RZ is the grid of reflector points, given as distance above
*           the aperture plane.
*
*           NGRID is the number of grid points.
*
*           TI and YA are working arrays. The NRAYS should be chosen as
*           some appreciable fraction of NGRID, say 1/4.
*
*           EA is the array of approximate aperture field values and
*           YEA is the array of aperture points.  The NAP is the number
*           of aperture points.
*
*           Inputs:  RZ,NGRID,NRAYS,NAP
*
      Real RZ(NGRID),TI(NRAYS),YA(NRAYS,6),YEA(NAP)
      Complex EA(NAP)
      Common /BOUNDS/ RFYMIN,RFYMAX,YEAMIN,YEAMAX
      Common /CNSTNT/ PI,BETA
      HG = (RFYMAX - RFYMIN)/FLOAT(NGRID-1)
      HA = (YEAMAX - YEAMIN)/FLOAT(NAP-1)
      Do 1 I=1,NAP
        YEA(I) = YEAMIN + HA*FLOAT(I-1)
        EA(I) = (0.0, 0.0)
    1 Continue
      TMIN = ATAN(RZ(NGRID)/RFYMAX)
      TMAX = PI - ATAN(ABS(RZ(1)/RFYMIN))
      DT = (TMAX - TMIN)/FLOAT(NRAYS-1)
      Do 2 I=1,NRAYS
        TI(I) = TMIN + DT*FLOAT(I-1)
        Call TRACE(HG,RFYMIN,RZ,NGRID,TI(I),
     1             YA(I,1),YA(I,2),YA(I,3),YA(I,4),YA(I,5),YA(I,6))
    2 Continue
      Do 7 I=1,NAP
        Q = YEA(I) - YA(1,1)
        If(ABS(Q).LT.1.0E-4)then
          Call FIELD(YA(1,1),YA(1,2),YA(1,3),YA(1,4),YA(1,5),YA(1,6),
     1               EA(I))
        Endif
        Do 6 K=2,NRAYS
          QQ = YEA(I) - YA(K,1)
          If(ABS(QQ).LT.1.0E-4)then
            Call FIELD(YA(K,1),YA(K,2),YA(K,3),YA(K,4),YA(K,5),YA(K,6)
     1                 EA(I))
            Go to 5
```

```
            Endif
            If((ABS(Q).LT.1.0E-4).OR.(ABS(QQ).LT.1.0E-4))Go to 5
            If(Q*QQ .GT. 0.0)Go to 5
            TLOW = TI(K-1)
            THIH = TI(K)
            Q1 = Q
            QQ1 = QQ
```



```
            Do 3 JJ=1,100
            TM = (TLOW + THIH)/2.0
            Call TRACE(HG,RFYMIN,RZ,NGRID,TM,YAPT,YI,ZI,THR,DZDY,D2ZDY2)
            QQQ = YEA(I) - YAPT
            If(ABS(QQQ) .LT. 1.0E-4) Go to 4
            If(Q1*QQQ .GT. 0.0)then
              TLOW = TM
              Q1 = QQQ
            Endif
            If(QQQ*QQ1 .GT. 0.0)then
              THIH = TM
              QQ1 = QQQ
            Endif
        3   Continue
        4   Call FIELD(YAPT,YI,ZI,THR,DZDY,D2ZDY2,EA(I))
        5   Q = QQ
        6 Continue
        7 Continue
          Return
          End

          Subroutine TRACE(H,YMIN,Z,NG,THETA,YAPT,YI,ZI,THR,DZDY,D2ZDY2)
*
*           TRACE does the actual ray tracing for given incident ray
*           angle with the horizontal.
*
*           H is the reflector grid spacing and YMIN is the lowest
*           point on the aperture.
*
*           Z is the reflector grid with size NG.
*
*           THETA is the angle that the incident ray makes with the
*           horizontal, measured counter-clockwise positive.
*
*           YAPT is the intersection point of the reflected ray with
*           the aperture plane.
*
*           YI and ZI specify the impact point of the incident ray.
*           THR, DZDY, D2ZDY2 are the angle of reflection with respect
```

```
*           to the surface normal, the first derivative, and the second
*           derivative respectively.
*
*           Inputs:  H,YMIN,Z,NG,THETA
*
      Real Z(NG),K
      Common /CNSTNT/ PI,BETA
      If(ABS(THETA - PI/2.0) .LT. 1.0E-4)then
        YI = 0.0
        ZI = Z((NG-1)/2+1)
        Call DERV((NG-1)/2+1,Z,NG,H,DZDY,D2ZDY2)
        Call BOUNCE(YI,ZI,DZDY,THETA,THR,YAPT)
        Return
      Endif
      K = TAN(THETA)
      YNM1 = YMIN
      GNM1 = K*YMIN - Z(1)
```



```
      If(ABS(GNM1) .LT. 1.0E-4) then
        YI = YMIN
        ZI = Z(1)
        Call DERV(1,Z,NG,H,DZDY,D2ZDY2)
        Call BOUNCE(YI,ZI,DZDY,THETA,THR,YAPT)
        Return
      Endif
      Do 5 N=2,NG
        YN = YNM1 + H
        GN = K*YN - Z(N)
        If(ABS(GN) .LT. 1.0E-4) then
          YI = YN
          ZI = Z(N)
          Call DERV(N,Z,NG,H,DZDY,D2ZDY2)
          Call BOUNCE(YI,ZI,DZDY,THETA,THR,YAPT)
          Return
        Endif
        If(GNM1*GN .GT. 0.0) Go to 4
        F = GN/(GN - GNM1)
        YI = YN*(1.0 - F) + F*YNM1
        ZI = Z(N)*(1.0 - F) + F*Z(N-1)
        Call DERV(N-1,Z,NG,H,DZNM1,D2ZNM1)
        Call DERV(N,Z,NG,H,DZDYN,D2ZN)
        DY = YI - YNM1
        DZDY = DZNM1 + D2ZNM1*DY
        D2ZDY2 = D2ZNM1 + (D2ZN - D2ZNM1)*DY/H
        Call BOUNCE(YI,ZI,DZDY,THETA,THR,YAPT)
        Return
    4   YNM1 = YN
```

```
        GNM1 = GN
    5 Continue
      End

      Subroutine BOUNCE(YI,ZI,DZDY,THETA,THR,YAPT)
*
*          BOUNCE serves TRACE.  The YI,ZI,THETA,DZDY are inputs.
*
      Common /CNSTNT/ PI,BETA
      If(ABS(DZDY) .LT. 1.0E-6) then
        PHI = PI/2.0
        Go to 1
      Endif
      If(DZDY .LT. 0.0) then
        PHI = ATAN(1.0/ABS(DZDY))
        Go to 1
      Endif
      PHI = PI - ATAN(1.0/DZDY)
    1 PSI = 2.0*PHI - THETA
      THR = ABS(PHI - THETA)
      If(ABS(PSI - PI/2.0) .LT. 1.0E-4) then
        YAPT = YI
        Return
      Endif
      If(PSI .LT. PI/2.0) then
        YAPT = YI - ZI/TAN(PSI)
        Return
```



```
      Endif
      YAPT = YI + ZI/TAN(PI-PSI)
      Return
      End

      Subroutine FIELD(YAPT,YI,ZI,THR,DZDY,D2ZDY2,EAPER)
*
*          FIELD calculates the contribution of the reflected ray
*          to the aperture field.
*
*          YAPT,YI,ZI,THR,DZDY,D2ZDY2 are inputs.  They are the
*          intersection of reflected ray with aperture, impact
*          point, angle of reflection with respect to surface
*          normal at impact point, and first and second derivatives
*          at impact point respectively.
*
      Complex EAPER
      Real L
      Common /CNSTNT/ PI,BETA
```

```
      DY = YAPT - YI
      RHO = SQRT(YI*YI + ZI*ZI)
      RHOA = SQRT(ZI*ZI + DY*DY)
      L = RHO + RHOA
      PHI = -BETA*L
      A = 1.0/SQRT(RHO)
      If(ABS(D2ZDY2) .LT. 1.0E-6)then
        A = A*SQRT(RHO/(RHO + RHOA))
        Go to 1
      Endif
      RC = (1.0 + DZDY*DZDY)**1.5/D2ZDY2
      W = ABS(1.0/RHO + 2.0/(RC*COS(THR)))
      If(W .LT. 1.0E-5)Go to 1
      RCW = 1.0/W
      If(D2ZDY2 .GT. 0.0) A = A*SQRT(RCW/(RCW + RHOA))
      If(D2ZDY2 .LT. 0.0) then
        If(ABS(RCW - RHOA) .LT. 1.0E-5)Go to 1
        If(RHOA .LT. RCW) A = A*SQRT(RCW/(RCW - RHOA))
        If(RHOA .GT. RCW) then
          A = A*SQRT(RCW/(RHOA - RCW))
          PHI = PHI + PI/2.0
        Endif
      Endif
    1 EAPER = EAPER + A*CEXP(CMPLX(0.0,PHI))
      Return
      End

      Subroutine DERV(N,Z,NG,H,DZDY,D2ZDY2)
*
*          DERV simply approximates the derivatives of the reflector
*          grid at grid points using established numerical
*          differentiation formulas.
*
*          N is the point in question, while Z is the reflector grid
*          NG is its dimension. H is the spacing.  These are all input.
*
      Real Z(NG)
```



```
      If(N .EQ. 1) then
        DZDY = FR2(Z(N),Z(N+1),Z(N+2),H)
        DZDY1 = C2(Z(N),Z(N+2),H)
        DZDY2 = C2(Z(N+1),Z(N+3),H)
        D2ZDY2 = FR2(DZDY,DZDY1,DZDY2,H)
        Return
      Endif
      If(N .EQ. NG) then
        DZDY = FR2(-Z(N),-Z(N-1),-Z(N-2),H)
```

```
      DZDYM1 = C2(Z(N-2),Z(N),H)
      DZDYM2 = C2(Z(N-3),Z(N-1),H)
      D2ZDY2 = FR2(-DZDY,-DZDYM1,-DZDYM2,H)
      Return
    Endif
    If((N .EQ. 2).OR.(N .EQ. NG-1 )then
      DZDY = C2(Z(N-1),Z(N+1),H)
      If(N .EQ. 2)then
        DZDYM1 = FR2(Z(N-1),Z(N),Z(N+1),H)
        DZDY1 = C2(Z(N),Z(N+2),H)
        D2ZDY2 = C2(DZDYM1,DZDY1,H)
      Else If(N .EQ. NG-1)then
        DZDYM1 = C2(Z(N-2),Z(N),H)
        DZDY1 = FR2(-Z(N+1),-Z(N),-Z(N-1),H)
        D2ZDY2 = C2(DZDYM1,DZDY1,H)
      Endif
      Return
    Endif
    DZDY = C2(Z(N-1),Z(N+1),H)
    DZDYM1 = C2(Z(N-2),Z(N),H)
    DZDY1 = C2(Z(N),Z(N+2),H)
    D2ZDY2 = C2(DZDYM1,DZDY1,H)
    Return
    End

    Function FR2(X0,X1,X2,H)
    FR2 = (-3.0*X0 + 4.0*X1 - X2)/(2.0*H)
    Return
    End

    Function C2(XM1,X1,H)
    C2 = (X1 - XM1)/(2.0*H)
    Return
    End
```

```
      Subroutine APTINT(E,P,X,NA,F,THETA,NP,YMIN,YMAX,TMIN,TMAX)
*
*           APTINT computes the far field for a given aperture
*           distribution.
*
*           E and P are the amplitude and phase respectively of the
*           aperture distribution. Input
*
*           X is a complex scratch array.
*
*           NA is the dimension of the E,P,X.
*
*           F is the pattern that results.
*
*           THETA is the angle from boresight associated with the
*           corresponding F value.
*
*           YMIN and YMAX are the dimensions of the aperture.
*
*           TMIN and TMAX give the range of angle for which the patter
*           will be calculated.
*
      Real E(NA),P(NA),F(NP),THETA(NP),MAX
      Complex X(NA),Q
      Common /PIBETA/ PI,BETA
      H = (YMAX - YMIN)/FLOAT(NA-1)
      DTHETA = (TMAX - TMIN)/FLOAT(NP-1)
      Do 2 I=1,NP
        THETA(I) = TMIN + DTHETA*FLOAT(I-1)
        STH = SIN(THETA(I))
        Do 1 J=1,NA
          Y = YMIN + H*FLOAT(J-1)
          X(J) = E(J)*CEXP(CMPLX(0.0,BETA*Y*STH + P(J)))
    1   Continue
        Call SRL(X,NA,YMIN,YMAX,Q)
        F(I) = CABS(Q)
    2 Continue
      MAX = F(1)
      Do 3 I=1,NP
        If(F(I) .GT. MAX)MAX = F(I)
    3 Continue
      Do 4 I=1,NP
        F(I) = F(I)/MAX
        THETA(I) = THETA(I)*(180.0/PI)
    4 Continue
      Return
      End

      Subroutine SRL(F,N,XMIN,XMAX,Q)
*
```

```
*           Simpson's Rule integration routine associated with AMPINT.
*
      Complex F(N),Q
      H = (XMAX - XMIN)/FLOAT(N-1)
      L = N - 2
      If(((N-1)/2)*2 .NE. (N-1))L = L - 3
```



```
      Q = (0.0,0.0)
      Do 1 I=1,L,2
        Q = Q + (F(I) + 4.0*F(I+1) + F(I+2))
    1 Continue
      Q = H*Q/3.0
      If(L .EQ. N-2)Return
      Q = Q + 3.0*H*(F(N-3)+3.0*F(N-2)+3.0*F(N-1)+F(N))/8.0
      Return
      End
```

```
      Program CNVRT
*
*          This program converts the rho versus psi data from the
*          beamshaping formulas into a equi-spaced x-y format.
*
      Real RHO(--dimension of rho--),PSI(--dimension of psi--)
      Open(1,File='name of input file')
      Open(2,File='name of output file')
      NP = --number of input data points--
      NG = --number of output data points--
      YMIN = --lower limit of aperture--
      YMAX = --upper limit of aperture--
      HG = (YMAX - YMIN)/FLOAT(NG-1)
      Rewind 1
      Do 100 K=1,NP
        Read(1,5) PSI(K),RHO(K)
  100 Continue
      Do 6 I=1,NG
        Y = YMIN + HG*FLOAT(I-1)
        Q = Y - RHO(1)*SIN(PSI(1))
        If(ABS(Q) .LT. 1.0E-5)then
          P = PSI(1)
          R = RHO(1)
          Go to 4
        Endif
        Do 3 J=2,NP
          QQ = Y - RHO(J)*SIN(PSI(J))
          If(ABS(QQ) .LT. 1.0E-5)then
            P = PSI(J)
            R = RHO(J)
            Go to 4
          Endif
          If(Q*QQ .GT. 0.0)Go to 2
          DRDP = (RHO(J) - RHO(J-1))/(PSI(J) - PSI(J-1))
          Q1 = Q
          Q2 = QQ
          P1 = PSI(J-1)
          P2 = PSI(J)
    1     P = (P1 + P2)/2.0
          R = RHO(J-1) + DRDP*(P - PSI(J-1))
          X = Y - R*SIN(P)
          If(ABS(X) .LT. 1.0E-5)Go to 4
          If(Q1*X .GT. 0.0)then
            Q1 = X
            P1 = P
            Go to 1
          Endif
          Q2 = X
          P2 = P
          Go to 1
```

```
2       Q = QQ
3     Continue
4     Z = R*COS(P)
      Write(2,5) Y,Z
5     Format(2F12.5)
6   Continue
```



```
      Stop
      End
```

Bibliography

1. Applebaum, Sidney P. "Adaptive Arrays," IEEE Transactions on Antennas and Propogation, AP-24: 585-598 (September 1976).

2. Galindo, Victor. "Design of Dual-Reflector Antennas with Arbitrary Phase and Amplitude Distributions," IEEE Transactions on Antennas and Propogation, AP-12: 403-408 (July 1964).

3. Gerald, Curtis F. Applied Numerical Analysis (Second Edition). Reading, MA: Addison-Wesley Publishing Company, 1978.

4. Kauffman, J. F., William F. Croswell, and Leand J. Jowers. "Analysis of the Radiation Patterns of Reflector Antennas," IEEE Transactions on Antennas and Propogation, AP-24: 53-65 (January 1976).

5. Lang, Jeffrey H., John R. Gersh, and David H. Staelin. "Electrostatically Controlled Wire-Mesh Antenna," Electronics Letters, 14: 655-656 (September 1978).

6. Lang, J. H. and David H. Staelin. "Electrostatically-Controlled Large-Aperture Reflecting Satellite Antennas, Proceedings of the IEEE Conference on Decision and Control, 1980: 750-754.

7. Lang, J. H. and David H. Staelin. " Electrostatically Figured Reflecting Membrane Antennas for Satellites," IEEE Transactions on Automatic Control, AC-27: 666-670 (June 1982).

8. Narasimhan, M. S., V. Anantharam, and K. M. Prasad. "A Note on the Shaping of Dual Reflector Antennas," IEEE Transactions on Antennas and Propogation, AP-29: 551-552 (May 1981).

9. Rusch, W. V. T. and P. D. Potter. Analysis of Reflector Antennas. New York: Academic Press, 1970.

10. Silver, Samuel, ED. Microwave Antenna Theory and Design. New York: McGraw-Hill Book Company, 1949.

11. Sletten, Carlyle J., F. S. Holt, and S. B. Herskovitz. "Wide-Angle Lenses and Image Collapsing Subreflectors for Nontracking Solar Collectors," Applied Optics, 19: 1449 (May 1980).

12. Stutzman, Warren L. and Gary A. Thiele. Antenna Theory and Design. New York: John Wiley & Sons, 1981.

VITA

Second Lieutenant Douglas A. Havens was born on 4 June 1960 in New York, New York. After graduating high school in Joppa, Maryland in 1978, he attended Lehigh University in Bethlehem, Pennsylvania. He graduated with a Bachelor of Science degree in computer engineering in 1982. He was commissioned in the USAF Reserve through the ROTC and entered the Air Force Institute of Technology in June of 1982.

Permanent Address: 1006 Erwin Dr.
Joppa, MD 21085

UNCLASSIFIED

SECURITY CLASSIFICATION OF THIS PAGE

AD-A132049

REPORT DOCUMENTATION PAGE

1a. REPORT SECURITY CLASSIFICATION: Unclassified	1b. RESTRICTIVE MARKINGS
2a. SECURITY CLASSIFICATION AUTHORITY	3. DISTRIBUTION/AVAILABILITY OF REPORT: Approved for Public Release; Distribution Unlimited
2b. DECLASSIFICATION/DOWNGRADING SCHEDULE	
4. PERFORMING ORGANIZATION REPORT NUMBER(S): AFIT/GE/EE/83D-26	5. MONITORING ORGANIZATION REPORT NUMBER(S)
6a. NAME OF PERFORMING ORGANIZATION: School of Engineering; 6b. OFFICE SYMBOL (If applicable): AFIT/EN	7a. NAME OF MONITORING ORGANIZATION
6c. ADDRESS (City, State and ZIP Code): Air Force Institute of Technology, Wright-Patterson AFB, OH 45433	7b. ADDRESS (City, State and ZIP Code)
8a. NAME OF FUNDING/SPONSORING ORGANIZATION: Rome Air Development Center; 8b. OFFICE SYMBOL (If applicable): RADC/EECS	9. PROCUREMENT INSTRUMENT IDENTIFICATION NUMBER
8c. ADDRESS (City, State and ZIP Code): Hanscom AFB, MA	10. SOURCE OF FUNDING NOS. — PROGRAM ELEMENT NO. / PROJECT NO. / TASK NO. / WORK UNIT NO.
11. TITLE (Include Security Classification): PATTERN NULLING BY REFLECTOR SHAPING	
12. PERSONAL AUTHOR(S): Douglas A. Havens	
13a. TYPE OF REPORT: MS Thesis; 13b. TIME COVERED: FROM _____ TO _____	14. DATE OF REPORT (Yr., Mo., Day): DECEMBER 1983; 15. PAGE COUNT: 106
16. SUPPLEMENTARY NOTATION	

17. COSATI CODES		
FIELD	GROUP	SUB. GR.
20	03	
20	14	

18. SUBJECT TERMS (Continue on reverse if necessary and identify by block number): Electromagnetism; Electromagnetic Wave Reflections

19. ABSTRACT (Continue on reverse if necessary and identify by block number)

Thesis Advisor: Andrew J. Terzuoli

Approved for public release: IAW AFR 190-17.
7 Feb 84
LYNN E. WOLAVER
Dean for Research and Professional Development
Air Force Institute of Technology (AIC)
Wright-Patterson AFB OH 45433

20. DISTRIBUTION/AVAILABILITY OF ABSTRACT: UNCLASSIFIED/UNLIMITED ☒ SAME AS RPT. ☐ DTIC USERS ☐	21. ABSTRACT SECURITY CLASSIFICATION: Unclassified
22a. NAME OF RESPONSIBLE INDIVIDUAL: Andrew J. Terzuoli, Ph. D.	22b. TELEPHONE NUMBER (Include Area Code): (513)-255-3576; 22c. OFFICE SYMBOL: AFIT/EN

DD FORM 1473, 83 APR — EDITION OF 1 JAN 73 IS OBSOLETE.

UNCLASSIFIED

SECURITY CLASSIFICATION OF THIS PAGE

This work explores the application of Applebaum adaptive array concepts to antennas with a continuous aperture. The array weights were found to work well as discrete points in an aperture distribution which produced nulled radiation patterns through aperture integration. In order to analyze arbitrarily shaped reflectors, a ray tracing scheme coupled with geometrical optics was constructed to calculate aperture fields from reflectors defined by discrete grids. Finding a reflector for a nulled pattern with well established beamshaping techniques failed. Other methods were suggested for future work.

END

FILMED

3-84

DTIC